

Biochemical modulation of microtubule dynamic instability

Claire H. Edrington

Department of Biology
McGill University
Montreal, Quebec, Canada

April 2023

A thesis submitted to McGill University in partial fulfillment of the requirements of the degree
of Doctor of Philosophy

© Claire H. Edrington, 2023

Abstract

Microtubules are an essential component of the cytoskeleton. These long slender tubes made of α/β -tubulin dimers are involved in cell division, migration and differentiation. They are able to perform such a wide variety of tasks because of their dynamic instability, i.e. their intrinsic ability to switch between phases of growth and shrinkage. Indeed, the microtubule cytoskeleton is constantly getting broken down and rebuilt. Precise spatiotemporal regulation of microtubule growth, shrinkage, lifetime, and nucleation is therefore essential for cell survival. In this thesis, I will discuss two ways in which microtubule dynamics can be modulated, through the physical and biochemical properties of their environment. First, it was recently shown that microtubule dynamics are sensitive to cytoplasm concentration *in vivo*. Surprisingly, increasing cytoplasm concentration slowed microtubule growth and shrinkage rates, in contrast to the expected effect from increased macromolecular crowding. I reconstituted the slower rates *in vitro* by increasing viscosity with a small viscogen, glycerol. Typically, slower growth rates correlate with decreased microtubule lifetimes. However, I observed the opposite, that viscosity increases microtubule lifetime despite slowing growth rates. Interestingly, the size of a viscogen determines the spatial scale of the reaction it influences. I therefore varied viscogen size to probe the spatial scale of the conformational changes in tubulin being slowed by viscosity. A small increase in viscogen size from 3Å (glycerol) to 4Å (trehalose) was sufficient to decrease the effect on microtubule lifetimes. This suggests that the structural transition in tubulin that leads to catastrophe is on the order of 3 Å. The structural transitions that underlie dynamic instability are not only influenced by the viscosity of their environment, but also by a wide array of MAPs. By combining two MAPs with opposing functions, a nucleator (DCX) and a catastrophe factor (EB3), I observed non-additive effects on microtubule nucleation and lifetime. This suggests that the two MAPs, though they share

a binding site, recognize different structural elements within that binding site. In addition, this provides evidence that nascent microtubules are structurally distinct from mature growing ends, even in the presence of templates. Together, this thesis provides two tools with which to separate parameters of microtubule dynamics that are typically thought of as linked. In doing so, my work contributes to our understanding of the fundamental structural transitions underlying microtubule dynamic instability.

Résumé

Les microtubules sont une composante essentielle du cytosquelette. Ces longs tubes fait de dimères d' α/β -tubuline sont impliqués dans la division cellulaire, la migration et la différenciation. Les microtubules peuvent accomplir une grande variété de tâches grâce à leur instabilité dynamique, c'est-à-dire leur capacité de passer entre des phases de polymérisation et de dépolymérisation. En effet, le réseau de microtubules est constamment déconstruit et reconstruit. Une régulation précise au niveau spatiotemporelle de l'élongation, du rétrécissement et de la transition entre ces phases est donc essentielle à la survie de la cellule. Dans cette thèse, je discuterai ma caractérisation *in vitro* de deux techniques de modulation de la dynamique des microtubules, soit par les propriétés physiques ou biochimiques de leur environnement. Il a récemment été démontré que la dynamique des microtubules est sensible à la concentration du cytoplasme *in vivo*. Étonnamment, une augmentation de la concentration du cytoplasme a ralenti la vitesse de polymérisation et de dépolymérisation des microtubules, contrairement à l'effet attendu par une augmentation de l'encombrement macromoléculaire. J'ai reconstitué les vitesses ralenties *in vitro* en augmentant la viscosité du tampon grâce à un petit viscosogène, le glycérol. Typiquement, les vitesses de polymérisations plus lentes sont corrélées avec une plus haute fréquence de transitions à la dépolymérisation, qu'on appelle catastrophes. Par contre, j'observe le contraire : la viscosité diminue la fréquence de catastrophes malgré la polymérisation plus lente. Il est important de noter que la taille d'un viscosogène détermine l'échelle spatiale de la réaction qu'il influence. J'ai donc fait varier la taille du viscosogène pour déterminer l'échelle spatiale du changement de conformation dans la tubuline qui est ralenti par la viscosité. Une légère augmentation de la taille du viscosogène de 3Å (glycérol) à 4Å (tréhalose) était suffisante pour diminuer l'effet sur la fréquence de catastrophes. Cela suggère que la transition structurelle dans

la tubuline qui mène à une catastrophe suite à l'hydrolyse du GTP est à l'ordre de 3Å. Les changements de conformation dans la tubuline qui sont à la base de l'instabilité dynamique sont non seulement influencés par la viscosité de leur environnement, mais aussi par un vaste éventail de protéines associées aux microtubules (MAPs). En combinant deux MAPs aux fonctions opposées, un facteur de nucléation (la doublecortine) et un facteur de catastrophes (la end-binding protein 3), j'ai observé des effets non-additifs sur la nucléation et les catastrophes. Cela suggère que, malgré le fait que ces deux MAPs partagent un site de liaison, ils reconnaissent différents éléments structurels dans ce site de liaison. De plus, ces résultats suggèrent que les microtubules naissants sont structurellement différents des microtubules matures en croissance. En somme, cette thèse souligne deux outils qui peuvent séparer des paramètres de l'instabilité dynamique qui sont normalement considérés liés. Mon travail contribue donc à notre compréhension des transitions structurelles fondamentales qui sont à la base de l'instabilité dynamique.

Acknowledgements

If I ever read anything boring, I can be sure it wasn't written by my supervisor, Dr. Gary Brouhard. His infectious obsession for microtubules translates into clear, effective science communication, and just plain good writing. I would like to thank Gary for accepting me into a world of perplexing polymers and supporting me through a wild experimental exploration which included much trial and error. On that note, I would also like to thank my supervisory committee, Dr. Stephanie Weber and Dr. Anthony Mittermaier, who provided helpful discussion and always had fun questions during every meeting since my very first steps as a graduate student.

This thesis would have been very different had I not met our collaborators Dr. Arthur Molines and Dr. Fred Chang at my first Gordon Research Conference in 2019. Thank you, Arthur, for reigniting my curiosity during the “unprecedented times” that followed that conference and reminding me how fun it is to do experiments.

To the members of the Brouhard Lab and Bechstedt Lab past and present: I will always remember being in a cold room with good friends at 2 am, with everything smelling vaguely of brains. A special thank you to Dr. Sami Chaaban, Dr. Hadrien Mary, and Thomas McAlear, who taught me everything I needed when I first joined the lab and helped me solve a million problems through the years.

Thank you as well to all the folks on the second floor of Bellini for the smiles and the hellos in the hallway, for the reagents I may have borrowed, and for the lunchtime laughs. You all made it a joy to come into work.

Finally, I want to thank my friends and family for supporting and encouraging me through graduate school, especially Matias for being my daily cheerleader.

Contribution of Authors

The work described in Chapter 2 is currently being prepared as a manuscript for publication. It is a continuation of collaborative work published in Molines et al., 2022. The experiments described in Chapter 2 were designed in collaboration with my supervisor, Dr. Gary Brouhard, and our collaborators, Dr. Arthur Molines and Dr. Fred Chang from the University of California San Francisco. In February 2022, Dr. Molines came for a short visit to our lab here in Montreal, during which time I trained Dr. Molines in the use of our microscopes and together we performed the experiments and analyzed data described in Figure 2.2-2.5, and Figure 2.10. After his visit, I completed the dataset for Figures 2.2-2.5. I performed all additional experiments and analysis described in Figures 2.6-2.15.

The experiments described in Chapter 3 were designed in collaboration with my supervisor, Dr. Gary Brouhard. All experimental manipulations, data analysis, and figure preparation were carried out by me.

Chapters 1 and 4 constitute a literature review and a discussion of results from Chapters 2 and 3 in the context of the current understanding of dynamic instability. They do not contain original data, but rather a discussion of work referenced throughout the text.

Contributions to Original Knowledge

This work shows, for the first time, the effects of viscosity on *all* parameters of dynamic instability (growth, shrinkage, lifetime, nucleation, and rescue). The measurements of the changes in these parameters in response to different viscosogens shows for the first time that microtubule shrinkage rates are slowed by viscosogens of all sizes. Furthermore, this work contributes to the growing body of evidence that microtubule lifetimes are not necessarily correlated with GTP-cap size. In addition, these results suggest that microtubule catastrophes are limited by small conformational changes in tubulin, as opposed to large changes at the level of movement of full protofilaments. The effects of the small viscosogen glycerol on microtubule growth and shrinkage rates specifically has been published in Molines et al. 2022. The full characterization of all parameters of dynamic instability in response to three different viscosogens will be included in a manuscript currently under preparation for submission for publication.

In addition, I have characterized microtubule dynamics in the presence of DCX and EB3 together for the first time. My work shows that combining this nucleator and this catastrophe factor results in non-additive effects and suggests that small nucleation intermediates have a different conformation from mature growing ends. This work contributes to our understanding of the interactions between MAPs and the conformations of tubulin within the microtubule.

Table of Contents

Abstract.....	2
Résumé.....	4
Acknowledgements.....	6
Contribution of Authors.....	7
Contributions to Original Knowledge.....	8
Table of Contents.....	9
List of Figures.....	12
List of Tables.....	13
List of Abbreviations.....	14
1 An introduction to microtubules and dynamic instability.....	15
1.1 Introduction.....	15
1.2 Dynamic instability.....	16
1.3 The GTP-cap model.....	18
1.4 Microtubule growth.....	20
1.4.1 Describing microtubule growth with a one-step model.....	20
1.4.1 Describing microtubule growth with a two-step model.....	23
1.5 The structure of a microtubule end.....	27
1.5.1 Tubulin can adopt a curved or a straight conformation.....	27
1.5.1 Tubulin can adopt an expanded or a compacted conformation.....	29
1.6 Catastrophes: from growth to shrinkage.....	33
1.6.1 Catastrophes are a multi-step process.....	33
1.6.1 Defects in the microtubule lattice.....	34
1.6.2 Rescues: from shrinkage to growth.....	34
1.7 Structural plasticity in the microtubule lattice.....	35
1.8 Nucleation.....	36
1.8.1 Spontaneous nucleation.....	37
1.8.2 Templated nucleation.....	38
1.8.3 Microtubule nucleation without a minimal nucleus.....	38
1.9 Controlling microtubule nucleation.....	40
1.9.1 Inhibiting nucleation by promoting catastrophe.....	40

1.9.2	Promoting nucleation by inhibiting catastrophe	41
1.9.3	Promoting nucleation by outrunning catastrophe	41
1.10	Conclusion.....	42
2	Dynamic instability is modulated by the viscosity of the environment	44
2.1	Introduction	44
2.1.1	Modulating the physical properties of the environment to study biochemical reactions ⁴⁵	
2.1.2	Modulating viscosity to study conformational changes in proteins.....	47
2.2	Results	50
2.2.1	Growth rates are sensitive to viscosity	51
2.2.2	Shrinkage rates are sensitive to viscosity.....	54
2.2.3	Lifetimes and rescue frequency are sensitive to viscogen size.....	56
2.2.4	Estimating the size of the GTP cap with EB.....	61
2.2.5	Viscosity promotes templated nucleation	65
2.2.6	Spontaneous nucleation is sensitive to viscogen size	69
2.2.7	Glycerol stabilizes microtubules in the absence of tubulin	73
2.3	Discussion	75
2.4	Methods.....	78
2.4.1	Tubulin purification	78
2.4.2	Microtubule growth reconstitution assay.....	78
2.4.3	Viscosity measurements.....	80
2.4.4	Interference reflection microscopy	80
2.4.5	Analysis of microtubule dynamics.....	80
2.4.6	Microtubule pelleting assay	81
2.4.7	Buffer exchange	81
2.4.8	EB3-GFP purification	81
2.4.9	EB comet imaging and analysis.....	82
2.4.10	Analysis of EB comets.....	83
3	The combined effects of DCX and EB3 on dynamic instability	84
3.1	Introduction	84
3.1.1	XMAP215 and the two-step model for microtubule growth	84
3.1.2	EBs and the GTP-cap.....	86
3.1.3	Combining XMAP215 and EB revealed allostery in the lattice	88
3.1.4	DCX and the nucleotide-independent end structure	90
3.1.5	Combining EB and DCX to untangle nucleation and catastrophe.....	91

3.2	Results	94
3.2.1	EB promotes catastrophes and suppresses nucleation	94
3.2.2	DCX suppresses catastrophes and promotes nucleation.....	97
3.2.3	EB3 reduces microtubule lifetimes even in the presence of DCX.....	99
3.2.4	DCX accelerates microtubule nucleation, even in the presence of EB3.....	102
3.2.5	DCX and EB3 promote rescues together	103
3.2.6	DCX and EB3 slow shrinkage rates.....	105
3.2.7	DCX and EB3 increase growth rates	108
3.3	Discussion	110
3.4	Methods.....	112
3.4.1	Protein purification	112
3.4.2	Reconstitution of microtubule dynamics in vitro.....	113
3.4.3	IRM imaging of dynamic microtubules	113
4	Discussion.....	114
4.1	Introduction	114
4.2	Catastrophes are preceded by small conformational changes in tubulin	116
4.3	Nucleation intermediates are different from growing ends.....	119
4.4	The importance of stabilizing curved tubulin intermediates	121
4.5	Lifetimes can be uncoupled from the GTP-cap size	124
4.6	Microtubules are sensitive to their environment	126
4.7	Outlook.....	128
	References.....	132

List of Figures

Figure 1.1 Microtubules are intrinsically dynamic.....	17
Figure 1.2 Microtubule growth rates increase with tubulin concentration.....	21
Figure 1.3 The two-step model involves an intermediate state.....	25
Figure 1.4 The conformational changes underlying dynamic instability are not yet clear.....	32
Figure 2.1 Microtubule dynamics reconstituted in vitro.....	51
Figure 2.2 Microtubule dynamics are sensitive to viscosity and viscogen size.....	52
Figure 2.3 Microtubule growth rates are modulated by viscogens of different sizes.....	53
Figure 2.4 Microtubule shrinkage rates are slowed by all three viscogens.....	55
Figure 2.5 Microtubule lifetimes are modulated by viscogens of different sizes.....	58
Figure 2.6 Rescue frequency is sensitive to viscogen size.....	60
Figure 2.7 EB3-GFP binds to the ends of growing microtubules in a characteristic comet shape.	62
Figure 2.8 Average Comet profiles in the presence of viscogens.....	63
Figure 2.9 EB comet intensity increases with microtubule growth rate.....	64
Figure 2.10 Small viscogens increase the probability of templated nucleation.....	66
Figure 2.11 The lag time to templated nucleation is sensitive to viscosity and viscogen size.....	68
Figure 2.12 Pelleting assay for measuring spontaneous nucleation.....	70
Figure 2.13 Glycerol lowers the critical concentration for spontaneous nucleation.....	71
Figure 2.14 Glycerol significantly lowers the critical concentration for spontaneous nucleation.....	72
Figure 2.15 Glycerol slows shrinkage even in the absence of tubulin.....	74
Figure 2.16 Workflow for EB comet analysis.....	83
Figure 3.1 EB3 shortens lifetimes and suppresses templated nucleation.....	96
Figure 3.2 DCX extends lifetimes and reduces nucleation times.....	98
Figure 3.3 Combining DCX and EB3 changes microtubule dynamics.....	100
Figure 3.4 EB3 concentration determines lifetimes.....	101
Figure 3.5 Nucleation time is determined by the concentration of DCX.....	103
Figure 3.6 DCX and EB3 promote rescue together.....	105
Figure 3.7 Shrinkage rates are slowed by DCX and EB3.....	107
Figure 3.8 DCX and EB3 increase microtubule growth rates.....	109

List of Tables

Table 1 Comparison of the properties of DCX and EB.....93

List of Abbreviations

γ-TuRC	γ -Tubulin Ring Complex
BSA	Bovine Serum Albumin
CLASP	Cytoplasmic Linker-Associated Protein
CPAP	Centrosomal-P4.1-Associated Protein
DCX	Doublecortin
EB	Ending-Binding
EB1	End-Binding Protein 1
EB3	End-Binding Protein 3
EM	Electron Microscopy
GDP	Guanosine Diphosphate
GMPCPP	Guanylyl-(A, B)-Methylene-Diphosphonate
GTP	Guanosine Triphosphate
GTPγS	Guanosine 5'-O-[Γ -Thio]Triphosphate
IRM	Interference Reflection Microscopy
MAP	Microtubule Associated Protein
PEG	Polyethylene Glycol
pf	Protofilament
TAMRA	Tetramethylrhodamine
TIRF	Total Internal Reflection Fluorescence
TOG	Tumor Overexpression Gene
XMAP215	Xenopus Microtubule Associated Protein 215

1 An introduction to microtubules and dynamic instability

1.1 Introduction

Self-assembly of large biomolecular structures is essential for many of the functions of eukaryotic cells. The cytoskeleton in particular is a prime example of how regulated assembly and disassembly of large polymer networks leads to a variety of cellular morphologies and behaviors. Composed of microtubules, actin filaments, and intermediate filaments, the cytoskeleton provides cells with structural support, the ability to migrate, and the ability to divide.

Microtubules are a particularly interesting component of the cytoskeleton because, unlike other polymers, microtubules are intrinsically dynamic (T. Mitchison & Kirschner, 1984b). To form a microtubule, dimers of α/β -tubulin associate head to tail to form protofilaments which associate laterally to form a hollow tube. For most polymers, the energetic barrier to polymer formation, i.e. to nucleation, is overcome by subunit concentrations above a certain threshold. In other words, once the subunit concentration passes the threshold, the polymer will elongate. Only when the subunit concentration is reduced can the polymers shrink. However, microtubules are no ordinary polymer. At consistent tubulin concentrations, microtubules switch between periods of growth and periods of shrinkage (Jonasson et al., 2019; T. Mitchison & Kirschner, 1984b). This spontaneous switching behavior between growth and shrinkage is termed “dynamic instability” and is an intrinsic property of microtubules. Dynamic instability was proposed in 1984 (T. Mitchison & Kirschner, 1984b), first observed in 1986 (Horio & Hotani, 1986), and the first characterization of this dynamic behavior soon followed (Walker et al., 1988).

Thirty-nine years later, we still do not have a robust biochemical model to explain the mechanisms underlying dynamic instability. In this thesis, I will discuss my work using physical

and biochemical tools to modulate the different phases of dynamic instability: growth, shrinkage, nucleation, catastrophe, and rescue. Chapter 1 will provide a brief overview of our current framework for understanding dynamic instability. Next, Chapter 2 will showcase the use of viscosity and viscogen size as a tool for determining the size scale of conformational changes occurring in tubulin during catastrophe. Chapter 3 will take a biochemical turn, exploring the relationship between catastrophe and nucleation by combining two MAPs, a nucleator and a catastrophe factor. Using *in vitro* reconstitutions of microtubule dynamics, I have uncoupled catastrophe rates from growth rates, and nucleation from catastrophe. This demonstrates that though the parameters of dynamic instability are tightly linked, and do have some common structural features, each phase may have unique particularities that can be modulated by cells to tightly control microtubule network organization throughout the cell cycle.

1.2 Dynamic instability

Microtubules can switch between growth and shrinkage because of the GTPase activity of tubulin (T. Mitchison & Kirschner, 1984b). When in its GTP state, tubulin can bind to the end of a growing microtubule and get incorporated into the polymer lattice. Sometime after the tubulin dimer is incorporated, it hydrolyzes its bound GTP. The delay between tubulin addition to the end and GTP hydrolysis creates a microtubule that is mostly made of GDP-tubulin, with a region rich in GTP-tubulin at the end. This GTP-rich region is known as the “GTP-cap” (Carlier & Pantaloni, 1981). In the textbook picture, the GTP-cap stabilizes the microtubule; loss of the GTP-cap causes the switch from growth to shrinkage, called “catastrophe” (Figure 1.1). Generally, faster microtubule growth is associated with lower catastrophe frequencies (Walker et al., 1988). This is

because faster growth means more tubulin dimers are able to add to the growing end before GTP is hydrolyzed, resulting in a larger GTP-cap.

How did we come to this model for thinking about dynamic instability? In the following sections, I will describe the features of dynamic instability in more detail. In addition, I will be highlighting the studies that lead us to our current collective understanding of the mechanochemical cycles undergone by tubulin that fuel this dynamic behavior.

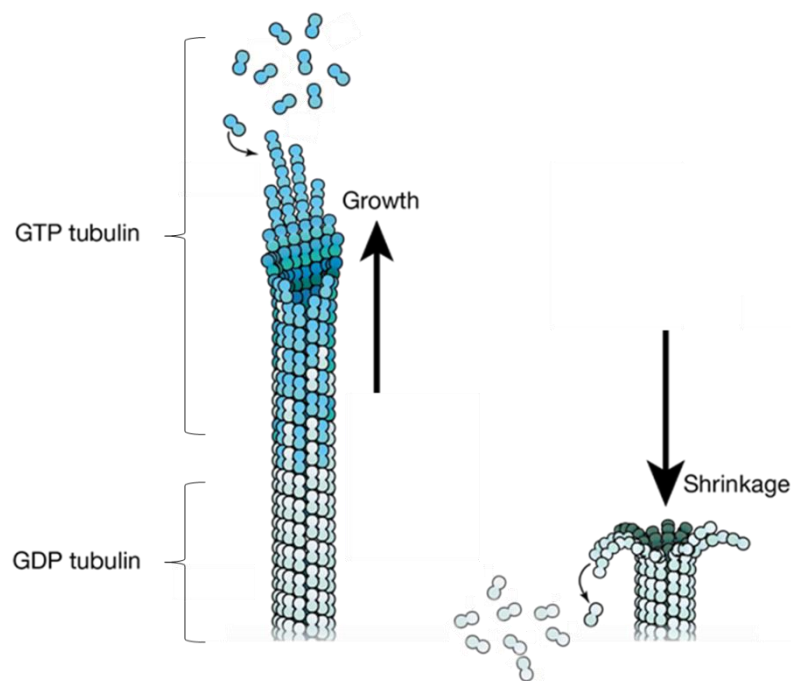


Figure 1.1 Microtubules are intrinsically dynamic.

Schematic representation of a dynamic microtubule. Dimers of α/β -tubulin bind to the end of a growing microtubule in the GTP state. After incorporation into the microtubule, tubulin hydrolyzes its GTP. The delay between tubulin binding and GTP hydrolysis creates a region rich in GTP at the end of the growing microtubule, and a mostly GDP lattice. When the GTP cap is lost, microtubules shrink rapidly due to the lateral separation of protofilaments which curl outwards and peel apart, releasing GDP tubulin.

1.3 The GTP-cap model

The notion that tubulin is a GTPase came soon after the discovery of tubulin itself (Borisy & Taylor, 1967), and the confirmation that tubulin (at the time known as “colchicine binding protein”) was indeed the subunit of microtubules (Weisenberg et al., 1968). Tubulin dimers were shown to bind to GTP at a one-to-one ratio (Weisenberg et al., 1968), and to hydrolyze GTP *after* polymerization, not before (David-Pfeuty et al., 1977). Was GTP hydrolysis required for polymerization? This question was answered with the help of a non-hydrolysable analogue of GTP, GMPPNP. Microtubules polymerized readily with GMPPNP, showing that hydrolysis was not required for polymerization (Weisenberg & Deery, 1976). These microtubules not only polymerized with GMPPNP, but they were hyperstable. They did not undergo catastrophes, even if tubulin was washed out. Later, Marie France Carlier and Dominique Pantaloni measured the rate of GTP hydrolysis at different tubulin concentrations. They found that, while tubulin assembly rates increased with tubulin concentration, the rate of GTP hydrolysis remained constant (Carlier & Pantaloni, 1981).

Together, these observations established the foundations for the GTP-cap model: 1) GTP-tubulin can polymerize, 2) GTP hydrolysis occurs *after* tubulin polymerization, and 3) GTP-analogue-microtubules are stable. However, it was very unclear why microtubules would need a GTP-rich region at the growing end, the assumption being that microtubules were like any regular polymer, growing and shrinking depending on the concentration of subunits. Carlier and Pantaloni speculated about “the involvement of a conformational change in the assembly process” (Carlier & Pantaloni, 1981). However, the role of such a conformational change was unknown. Perhaps GTP hydrolysis triggered a conformational change in tubulin. Alternatively, a conformational change in tubulin could induce GTP hydrolysis, providing additional stability to the polymer.

The GTP-cap model was famously put to the test by Tim Mitchison and Marc Kirschner in 1984. As with many bulk biochemistry experiments of the time, they monitored microtubule growth by measuring polymer mass over time by absorbance. As more microtubules nucleated and grew, absorbance signal went up (T. Mitchison & Kirschner, 1984b). In an earlier experiment they had noticed strange trends in their measurements of polymer length in snapshots of populations of microtubules. Within the same population, it seemed that both growing and shrinking microtubules could coexist, suggesting some instability in the polymer (T. Mitchison & Kirschner, 1984a).

To test whether removing the GTP cap would result in microtubule disassembly, they passed their solution of polymerizing microtubules through a thin needle, using shear force to break apart the microtubules. For an equilibrium polymer, breaking the polymers into smaller polymers would not change the total polymer mass. For microtubules, the shearing resulted in a rapid decrease in absorbance signal, indicating the microtubules had not only broken, but depolymerized, followed by a quick recovery of the signal as microtubules regrew. By breaking these microtubules, Mitchison and Kirschner had removed their GTP-caps, exposing the unstable GDP lattice which quickly depolymerized. Thus, they proposed that microtubules were intrinsically dynamic, coining the term “dynamic instability” to refer to this ability to go from growth to shrinkage even at constant tubulin concentrations.

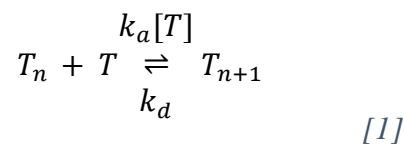
Dynamic instability and the GTP-cap model were therefore proposed before anyone could directly observe dynamic microtubules in action. It wasn't until 1986 that individual microtubules could be monitored over time (Horio & Hotani, 1986). From electron microscopy snapshots of populations of microtubules growing at steady state, Mitchison and Kirschner interpreted a progressive decrease in the number of longer polymers over time as a sign of the coexistence of growing and shrinking polymers in the same population. The advancement of “real-time video

recording” with dark-field microscopy showed that a single microtubule could repeatedly switch between phases of growth and shrinkage (Horio & Hotani, 1986). Two years later came the first direct measurement of the rate constants describing each phase of dynamic instability: growth, shrinkage, catastrophe, rescue, and nucleation (Walker et al., 1988). With this new information, the field could now build biochemical models to describe and predict microtubule behavior in different conditions.

1.4 Microtubule growth

1.4.1 Describing microtubule growth with a one-step model

Bulk polymerization experiments and electron microscopy snapshots had established a linear relationship between microtubule growth rate and tubulin concentration (T. Mitchison & Kirschner, 1984b). Because of this linear relationship, microtubule growth could be described by a simple model of polymer growth (Oosawa & Asakura, 1975). In such a model, microtubules (or any polymer) can be described as a 1D polymer of n tubulin subunits (T_n) which grows by the addition of single tubulin subunits (T) to form a longer polymer (T_{n+1}).



In this reaction, tubulin is added onto a microtubule end at a rate determined by a second-order association rate constant, k_a , dependent on the concentration of tubulin ($[T]$). In the reverse reaction, tubulin can be removed from the end of a microtubule at a rate determined by the first-order dissociation rate constant, k_d , independent of tubulin concentration. The net growth of the

polymer (v_g), or net change in length, more generally, is therefore a result of associations and dissociations of tubulin at the tip, and can be described by the following:

$$v_g = k_a[T] - k_d \quad [2]$$

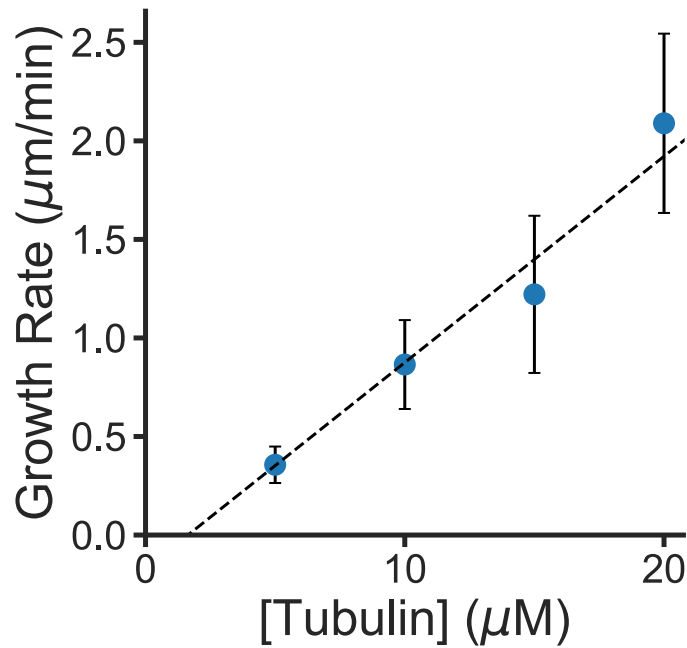


Figure 1.2 Microtubule growth rates increase with tubulin concentration.

Example of growth rates measured at different tubulin concentrations. Data represent means \pm standard deviation from $n = 75\text{-}355$ growth events measured from at least 3 experimental replicates for each condition. Growth rates increase linearly with tubulin concentration. The slope of the line of best fit corresponds to the association rate constant. The association rate constant measured here is $3.1 \mu\text{M}^{-1} \text{s}^{-1}$.

An example dataset is shown in Figure 1.2, demonstrating the linear relationship between microtubule growth rate and tubulin concentration. With this equation, Walker et al. calculated the association and dissociation rate constants based on their experimentally measured growth rates at different tubulin concentrations (Walker et al., 1988). They measured a k_a of $8.9 \mu\text{M}^{-1} \text{s}^{-1}$ for

microtubule plus ends, the first value of k_a from direct quantification of individual dynamic microtubules. Depending on the experimental method used, and the origin of the purified tubulin, the k_a generally falls within 2-10 $\mu\text{M}^{-1} \text{s}^{-1}$ (reviewed in Desai & Mitchison, 1997). Microtubules can have a range of protofilament numbers *in vivo*, but microtubules polymerized *in vitro* typically have 13 protofilaments (Chaaban & Brouhard, 2017). Taking this 13-protofilament architecture into account, this rate constant becomes 0.2-0.8 $\mu\text{M}^{-1} \text{s}^{-1}$ for each individual protofilament. How does the rate constant for microtubule growth compare to other biochemical reactions?

In 1992, Scott Northrup and Harold Erickson calculated the “generic upper limit” for the rate constant of a diffusion limited reaction between two proteins: 0.5-5 $\mu\text{M}^{-1} \text{s}^{-1}$ (Northrup & Erickson, 1992). This range came from Northrup and Erickson’s computational models and corresponded well with known values of rate constants at the time for reactions like the tetramerization of hemoglobin (0.4-0.6 $\mu\text{M}^{-1} \text{s}^{-1}$) (Ip et al., 1976; Kellett & Gutfreund, 1970) or the binding of certain antibodies with antigens like hemoglobin, cytochrome *c*, and others (0.6-4 $\mu\text{M}^{-1} \text{s}^{-1}$) (Noble et al., 1969; Ward et al., 1989). Slower protein associations would likely be the result of energy barriers in addition to diffusion, while faster associations would reflect strong attractive forces driving complex formation. Insulin dimerization, for example, is one of these fast reactions with an association rate constant of 100 $\mu\text{M}^{-1} \text{s}^{-1}$ (Koren & Hammes, 1976).

In other words, at under 1 $\mu\text{M}^{-1} \text{s}^{-1}$ for each protofilament, microtubule growth is on the slow end of “typical” diffusion-limited reactions, suggesting it is not diffusion-limited. In comparison, the growth of actin filaments, another important cytoskeletal component, is determined by a rate constant of 2-8 $\mu\text{M}^{-1} \text{s}^{-1}$ (Pollard & Cooper, 1986). Like some of the reactions mentioned above, actin filament growth is a diffusion limited process (Drenckhahn & Pollard, 1986). This was determined by growing actin filaments in buffers of different viscosities

containing small viscosogens like glycerol, sucrose, or ethylene glycol. Increasing solution viscosity decreased actin growth rates, and thus lowered the association rate constant. Extrapolating from their data, Detlev Drenckhahn and Thomas Pollard determined that the association rate constant for actin tended towards infinity as viscosity approached zero. Therefore, the main barrier to actin filament growth is arrival of actin to the end of a growing filament. Actin filament growth can therefore be accurately described by a one-step model for polymerization as described above in equations 1 and 2. As the concentration of actin increases, the chances of an actin monomer diffusing to the end of a filament increases, and the rate of filament growth increases. Is microtubule growth a diffusion limited process like actin filament growth?

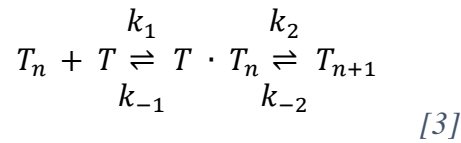
In 1997, David Odde calculated the theoretical maximum growth rate of microtubules (Odde, 1997). At 10 μM tubulin, given a tubulin diffusivity of $5.9 \times 10^{-12} \text{ m}^2 \text{ s}^{-1}$ (Salmon et al., 1984), the maximum microtubule growth rate would be 65 $\mu\text{m}/\text{min}$, or 135 subunits/sec for each protofilament. However, with a rate constant of 0.2-0.8 $\mu\text{M}^{-1} \text{ s}^{-1}$ for each individual protofilament, microtubule growth rates ranged between 1-2 $\mu\text{m}/\text{min}$ at 10 μM tubulin (Drechsel et al., 1992; Walker et al., 1988). The discrepancy between the predicted maximal growth rate and the observed growth rates suggested that the number of tubulin dimers diffusing to the end of a growing microtubule is much higher than the number of tubulin dimers that become incorporated into the microtubule. In other words, diffusion must not be the rate-limiting step of microtubule growth. Thus, there must be other steps in the process which is unaccounted for in a simple one-step model.

1.4.1 Describing microtubule growth with a two-step model

The one-step model for microtubule growth needed to be expanded in order to explain the effects of a microtubule polymerase, XMAP215. XMAP215 was the fastest known polymerase at the time, accelerating microtubule growth rates by 5-fold (Brouhard et al., 2008; Gard &

Kirschner, 1987). In the one-step model framework, the effect of XMAP215 corresponds to an increase of the measured association rate constant from 0.3 to 1.5 $\mu\text{M}^{-1} \text{s}^{-1}$. Even in the presence of XMAP215, microtubule growth rates thus remained slow compared to the maximum theoretical value (Odde, 1997) and remained in the range of diffusion-limited protein interactions (Northrup & Erickson, 1992).

Strikingly, XMAP215 not only accelerated microtubule growth, but it also accelerated the shrinkage rates of GMPCPP microtubules in the absence of free tubulin (Brouhard et al., 2008). Accelerating both the forward and the reverse reaction is typical feature of catalysts that lower the free energy of an intermediate in a reaction. Thus, XMAP215 was determined to be a catalyst of microtubule growth. Therefore, microtubule growth must involve an intermediate which is stabilized by XMAP215. The one-step model needed to be expanded to include such an intermediate:



In the two-step model, as before, microtubules made up of n tubulin subunits (T_n) grow by the binding of individual tubulins (T) to elongate the polymer by one subunit (T_{n+1}). Before the new tubulin is fully incorporated into the growing microtubule, the tubulin-microtubule complex adopt an intermediate state, often described as a “loosely bound” state (Brouhard et al., 2008; Wieczorek et al., 2015; Zanic et al., 2013). The two events in this model are therefore 1) arrival of tubulin to the growing end, forming the intermediate tubulin-microtubule complex $T \cdot T_n$, and 2) isomerization of tubulin that allows its incorporation into the lattice.

According to the one-step model, as the tubulin concentration is increased, so is the growth rate. In this simple model, there is no upper limit to microtubule growth. However, most biochemical reactions reach a maximal rate at a given substrate concentration. The two-step model does indeed predict a saturation of growth rates, where the maximum rate is determined by k_2 , the rate constant for the isomerization of tubulin. In other words, the two-step model predicts that the rate-limiting step of microtubule growth is not the arrival of subunits to the growing end, as is the case for actin, but rather, the isomerization that allows tubulin to become incorporated into the lattice.

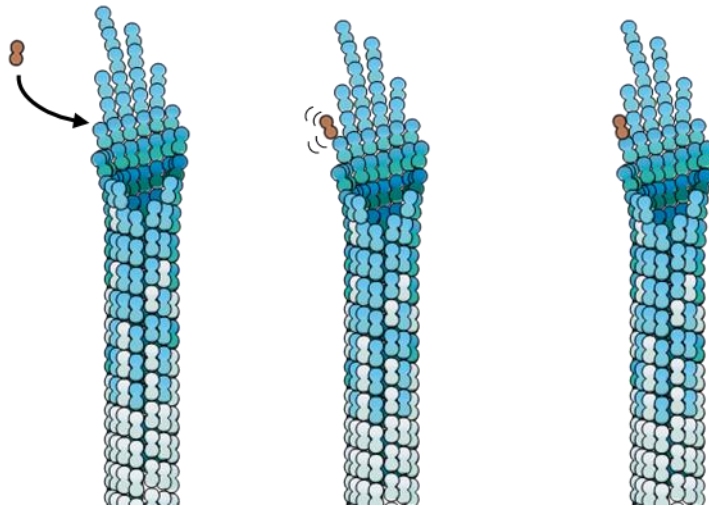


Figure 1.3 *The two-step model involves an intermediate state.*

Schematic representation of the two-step model. Incoming tubulin is loosely bound to the growing microtubule end before undergoing an isomerization, allowing it to incorporate into the lattice. Microtubule growth therefore has two steps: 1) arrival of tubulin to the growing end and 2) isomerization of tubulin for incorporation into the microtubule.

Based on this two-step model, Wieczorek et al. sought to determine experimentally whether microtubule growth was diffusion limited or reaction limited (Wieczorek et al., 2013). To do this, they measured the effects of viscosity on microtubule growth, similar to the experiments on actin carried out by Drenckhahn and Pollard (Drenckhahn & Pollard, 1986). When viscosity

was increased with small molecules like glycerol or ethylene glycol, microtubule growth rates were reduced (Wieczorek et al., 2013). As was the case with actin, the association rate constant tended to infinity as the data was extrapolated to a viscosity of zero. These experiments with small viscosogens indicated that tubulin binding to a microtubule end is a diffusion limited process.

When viscosity was increased with large macromolecules like PEG or BSA, microtubule growth rates were accelerated (Wieczorek et al., 2013). An increase in polymerization rates in the presence of macromolecular crowders was also observed for actin (Drenckhahn & Pollard, 1986). To test the limits of microtubule growth *in vitro*, Wieczorek et al. combined macromolecular crowders with MAPs to increase growth rates even further. The polymerase XMAP215 had been shown to act synergistically with the end-binding protein EB1 to increase growth rates (Zanic et al., 2013). Interestingly, microtubule growth rates saturated around 20 $\mu\text{m}/\text{min}$ even when tubulin concentration was increased in the presence of XMAP215 and EB1 (Wieczorek et al., 2013). When macromolecular crowders were added in addition to XMAP215 and EB1, microtubule growth rates still saturated, albeit at faster rates (around 40 $\mu\text{m}/\text{min}$). These experiments demonstrated that the two-step model's predicted saturation of growth rates could be recapitulated *in vitro*. In addition, the saturation of microtubule growth rates in the presence of polymerases and crowders showed that the upper limit of microtubule growth rates is determined by the isomerization step, and not by diffusion.

So, is microtubule growth diffusion limited or reaction limited? The answer is both. Tubulin binding to the end of a growing microtubule is a diffusion limited process, while tubulin isomerization and incorporation into the microtubule lattice is independent of tubulin diffusion rates. When the rate of isomerization is fast relative to the rate of tubulin arrival at the tip (e.g. at low tubulin concentrations), then microtubule growth rates are diffusion limited. When the rate of

isomerization is slow compared to the rate of diffusion, the microtubule growth rates are reaction limited. The two-step model therefore provides a more detailed framework for thinking of tubulin addition to the end of a growing microtubule compared to the one-step model.

The structural basis of the isomerization step is still an active topic of debate in the field. At the very least, there is consensus around the fact that there is a structural mismatch between tubulin in solution and tubulin in a microtubule lattice (Brouhard & Rice, 2014). Some conformational changes must necessarily occur in tubulin to adapt to a lattice organization, but the details are not yet clear. In addition, the GTPase activity of tubulin further complicates things: what are the structural differences between GTP-tubulin and GDP-tubulin that lead to catastrophe? The two-step model fails to answer questions like this. To explain dynamic instability, our concept of a microtubule must expand beyond a simple model of single tubulin dimers binding to a single type of binding site. We must consider the structure of the growing microtubule end: an arrangement of multiple protofilaments of varying lengths that will eventually separate laterally to peel apart following catastrophe.

1.5 The structure of a microtubule end

1.5.1 Tubulin can adopt a curved or a straight conformation

In 1991, cryo-EM images of shrinking microtubules showed protofilaments peeling apart and curling outwards, in a “ram’s horn” appearance, as well as curled “oligomeric disassembly products” (Mandelkow et al., 1991). In contrast, growing microtubules had straight ends, with protofilaments of varying lengths, creating tapered end structures. This data provided evidence for a model where polymerization-competent tubulin (i.e. GTP tubulin) has a “straight” conformation,

allowing assembly of a tube. GTP hydrolysis creates strain in the microtubule lattice because of GDP tubulin's preferred "curved" conformation (Howard & Timasheff, 1986; Melki et al., 1989). When the stabilizing cap is lost, the GDP tubulin is free to curl outwards, and the microtubule shrinks rapidly. For many years, this was the canonical model for microtubule growth—straight GTP-tubulin assembles into a tube, and curved GDP-tubulin produces strain to quickly disassemble the tube. Later X-ray crystallography structures of tubulin dimers bound to Rb3, a destabilizing factor in the stathmin family, provided details about the curved structure of GDP tubulin (Gigant et al., 2000; Ravelli et al., 2004). Notably, GDP tubulin had a characteristic bend at the intradimer interface of about 12° , compared to the structure of straight tubulin captured in zinc-induced sheets by cryo-EM (Nogales et al., 1998). While it was accepted early on that GDP tubulin preferentially adopts a curved conformation, the conformation of GTP tubulin was not so clear. A few years following the publication of the first images of the growing microtubule end (Mandelkow et al., 1991), new cryo-EM images of growing microtubule ends showed tapered sheet-like structures that curved slightly (Chretien et al., 1995), suggesting GTP tubulin may be curved. Small angle X-ray scattering data showed that both GTP and GDP-tubulin adopted identical curved conformations in solution (Rice et al., 2008). It took a few years to obtain direct structural data to confirm these two observations.

Following the cryo-EM images and small angle X-ray scattering data suggesting GTP-tubulin was curved in solution, a combination of structural and biochemical data provided additional evidence. In the span of a few years, many X-ray crystallography structures of GTP-tubulin showed a characteristic 12° kink in the tubulin dimer, just like in GDP-tubulin (Ayaz et al., 2012; Nawrotek et al., 2011; Pecqueur et al., 2012). In each of these structures, tubulin was bound to a protein (specifically stathmin/Rb3, DARPin, and a TOG domain). There was therefore

a possibility that the observed curvature was a result of these proteins binding, and not an intrinsic property of tubulin in the GTP form. However, several biochemistry experiments showed that none of these proteins had any preference for GDP or GTP-tubulin (Ayaz et al., 2012; Honnappa et al., 2003; Shearwin et al., 1994). Experiments with small molecule ligands showed similar results, that tubulin binding was unaffected by the nucleotide state. No one could detect tubulin straightening as a result of GTP binding. It is now widely accepted that GTP tubulin is curved, and must straighten to form lateral contacts *during* polymerization, not before (Brouhard & Rice, 2014, 2014). Some of the most recent structural data using recombinant *drosophila* tubulin supports this notion as well (Wagstaff et al., 2022).

1.5.1 Tubulin can adopt an expanded or a compacted conformation

In order to understand dynamic instability, the field had to understand the difference between GTP-tubulin and GDP-tubulin. If both dimers were curved in solution, how did their structures compare within a microtubule? The first 3D reconstruction of a microtubule from averaging of cryo-EM images came in 1999 from Eva Nogales, who had previously solved the structure of tubulin by crystallography (Nogales, 1999; Nogales et al., 1998). Before a 3D reconstruction was possible, analysis of cryo-EM images showed differences between GDP microtubules and GMPCPP microtubules (to mimic the GTP state). These images showed tubulin in GMPCPP microtubules was “expanded” longitudinally compared to tubulin in GDP microtubules (Hyman et al., 1995). This finding was confirmed following the cryo-EM “resolution revolution” in which 3D reconstructions of microtubules could reach below 5 Å, providing near atomic-level detail in some cases. These higher resolution structures of microtubules showed that tubulin dimers in a GMPCPP microtubule were 84 Å long, while tubulin dimers in GDP microtubules were 82 Å long, suggesting that GTP hydrolysis lead to a 2 Å “compaction” in the

tubulin dimers of the lattice (Alushin et al., 2014). The original reconstructions required microtubules to be decorated with kinesin motor domains to distinguish α and β tubulin in initial alignments (Alushin et al., 2014). Higher-resolution structures allowed a more detailed comparison of the different nucleotide states (R. Zhang et al., 2015), and later the observed compaction was confirmed in the absence of any decorating proteins (R. Zhang et al., 2018).

These higher-resolution structures revealed in more detail the differences between GMPCPP and GDP tubulin. Firstly, that compaction is a result of rearrangements in α -tubulin causing an overall 2 Å shift in the longitudinal direction. Secondly, these rearrangements involve a rotation of the α -tubulin relative to β -tubulin, creating a twist in the tubulin dimer of around 1 Å. This dimer twist results in changes to the overall “supertwist” of protofilaments along the microtubule, a feature that depends both on protofilament number and on lateral contact angles. Compaction also increases the surface area of intradimer interactions by over 250 Å², which is predicted to strengthen the longitudinal contacts (Manka & Moores, 2018). Meanwhile, the twisting and rearrangement of the α -tubulin would create uneven compression on either side of the dimer, moving some lateral contact points 1-2 Å away from their original position, thus weakening lateral contacts (Manka & Moores, 2018; R. Zhang et al., 2018).

The matter is not yet closed however, as the accuracy of GMPCPP as a GTP mimic has been put into question. X-ray fiber diffraction experiments carried out on microtubules with a longer list of GTP analogues suggest an alternative mechanism (Estévez-Gallego et al., 2020). They observed that GMPCPP expanded lattices while other GTP analogues did not. The model of tubulin compaction as a result of GTP hydrolysis could therefore be founded on an artefact of a lattice-expanding nucleotide. Estévez-Gallego et al. suggested that GMPCPP is closer in structure to the hydrolysis intermediate GDP-Pi than to GTP. If this is the case, then tubulin would bind to

a microtubule in a compacted GTP state, expand during hydrolysis to release the phosphate, then return to a compacted state after phosphate release. Ideally, to confirm one model or another, we would be able to reconstruct a GTP lattice without the use of nucleotide analogues that can have confounding effects.

Recently, some new methods have provided structural data on microtubules that do not require the use of nucleotide analogues. For example, advances in the purification of recombinant mammalian tubulin have enabled the generation of tubulin mutants with impaired or inhibited GTP hydrolysis (Roostalu et al., 2020). By cryo-EM, microtubules made from mutant catalytically inactive tubulin are expanded and twisted compared to GDP wild type microtubules (LaFrance et al., 2022). For the first time, the field has access to structures of mammalian tubulin truly containing GTP, and not an analogue. In addition, tubulin from non-mammalian organisms like *C. elegans* and yeast produced microtubules with expanded lattices in the GDP state, suggesting compaction may not be required for dynamic instability (Chaaban et al., 2018; Howes et al., 2017; von Loeffelholz et al., 2017).

In short, things have gotten complicated. The idea that GTP hydrolysis changes the conformation of tubulin in various ways (compaction, twisting, curving) means that the growing microtubule end is a much more complex structure than originally thought. Though such a complex structure cannot be contained in a simple model, the idea that GTP hydrolysis induces *some* conformational changes in tubulin that produce strain in the lattice by modulating longitudinal and lateral contact strength provides a framework to explain the mechanochemical basis of dynamic instability. However, the field has not settled on which conformational changes are specific to GTP hydrolysis, in what order they occur, which are rate-limiting, etc. In addition, though we are

starting to gather a list of conformational changes that could produce strain in the lattice, we do not fully understand how strain is released during catastrophe (Figure 1.4).

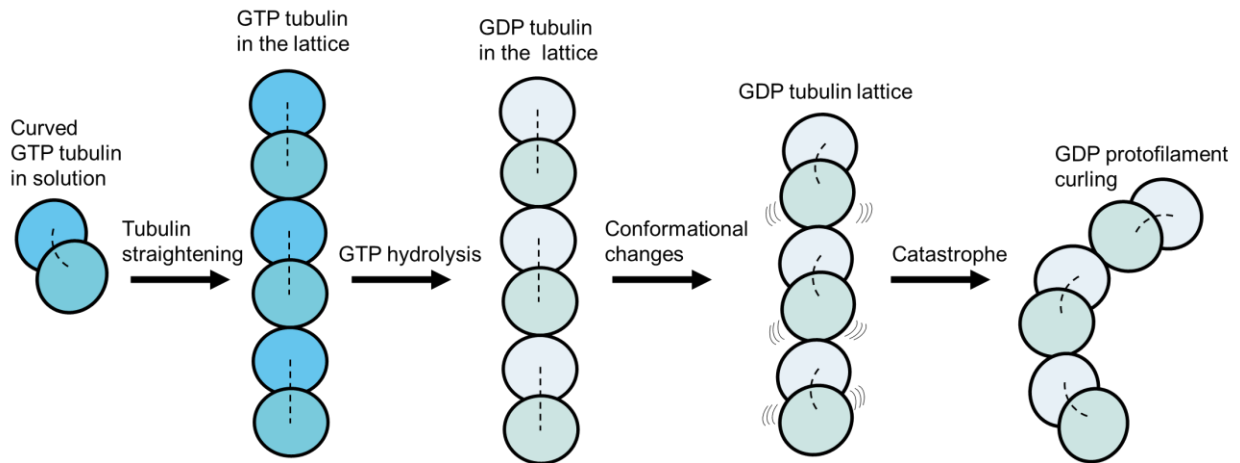


Figure 1.4 The conformational changes underlying dynamic instability are not yet clear.

Schematic representation of some of the steps in the tubulin conformation cycle. Curved GTP-tubulin must straighten to become incorporated into the microtubule. Following GTP hydrolysis, tubulin undergoes conformational changes including small compactions and twisting, especially in the α -subunit. The exact conformational changes leading to catastrophe are unknown, but once catastrophe does occur, GDP-tubulin protofilaments break their lateral contacts, curl outwards from the microtubule axis, and peel apart.

There is still no consensus as to the structure of a growing microtubule end. Early cryo-EM showed long tapered sheets at the ends of growing microtubules (Chretien et al., 1995), but some more recent tomography showed instead flared ends, with each protofilament growing independently (McIntosh et al., 2018). The importance of lateral contacts in microtubule growth is highlighted in recent computational models that replicate experimental growth data (Cleary et al., 2022; Cleary & Hancock, 2021), supporting a tapered end model. It still is not clear however how exactly the structure of the microtubule end changes during growth leading up to catastrophe.

1.6 Catastrophes: from growth to shrinkage

1.6.1 Catastrophes are a multi-step process

Simply put, a catastrophe occurs as a result of loss of the GTP cap, exposing GDP tubulin at the end of a microtubule (T. Mitchison & Kirschner, 1984a). New evidence for this mechanism came from experiments using EB1, a microtubule end-binding protein that tracks growing microtubule ends in a characteristic comet shaped signal. EB1 binds with higher affinity to microtubules made with GTP analogues than to GDP microtubules (Maurer et al., 2011; Zanic et al., 2009), so it is considered as a readout for the GTP cap size. In the moments right before catastrophe, EB1 signal decreases by 80%, indicating a loss in its binding site, i.e. a loss of the GTP cap, right before catastrophe.

As discussed above, the GTP hydrolysis reaction was shown to be independent of tubulin concentration or microtubule growth rate (Carlier & Pantaloni, 1981). The rate of GTP hydrolysis in the microtubule is therefore determined by a first-order rate constant. For many years catastrophes themselves were assumed to be a single step process. This assumption was supported by and largely based on early measurements of catastrophe frequency (Walker et al., 1988, 1991), implying that microtubule lifetimes (or time to catastrophe) are exponentially distributed. In such a model, catastrophes are stochastic processes that can occur any time in the growth phase. However, later work showed that the distribution of microtubule lifetimes was not exponential, but rather followed a γ -distribution (Gardner, Zanic, et al., 2011; Janson et al., 2003; Odde et al., 1995). This γ distribution of microtubule lifetimes indicates that catastrophe is a multi-step process: many events need to occur before a catastrophe ensues. The more time a microtubule spends growing, the more likely it is to catastrophe. Microtubules therefore undergo some kind of

aging process, where destabilizing “events” accumulate and eventually result in catastrophe. The exact nature of the multiple steps leading to catastrophe is still up to debate.

1.6.1 Defects in the microtubule lattice

One hypothesis about the destabilizing events leading to catastrophe is that the growing end may accumulate structural defects as the microtubule ages. Fluorescence microscopy measurements of the tapering of protofilaments at growing ends showed that faster growing microtubules had longer end tapers, and that tapers elongated over the life of a microtubule (Coombes et al., 2013; Gardner, Charlebois, et al., 2011). This work suggested that, as microtubules age, the length of the taper increases, meaning that the variance in protofilament length at the end increases. This extended taper or increased protofilament length variance would result in a higher probability of defects as the microtubule grew (one example of a defect would be a change in the protofilament number in the middle of the lattice). Eventually the microtubule (or perhaps more specifically the GTP cap) would accumulate enough defects that the lattice becomes unstable. At that point, GTP tubulin addition at the end would not suffice to maintain the integrity of the tip, and catastrophe would follow (Coombes et al., 2013). Though there has been investigation as to the nature and effect of lattice defects in microtubules, the structural features of these defects are not well defined (Aumeier et al., 2016; Mohan et al., 2013; Rai et al., 2019, 2021; Schaedel et al., 2019; Triclin et al., 2021).

1.6.2 Rescues: from shrinkage to growth

Sites of damage or defects in the microtubule lattice have been proposed to confer overall stability to microtubules by promoting rescues, the switch from shrinkage back to growth (Aumeier et al., 2016; Fees & Moore, 2019; Rai et al., 2019; Schaedel et al., 2019). It has been suggested that repair of defects by the incorporation of GTP-tubulin into the lattice could produce

“GTP islands” in the lattice (Dimitrov et al., 2008; Tropini et al., 2012). Because of their GTP-induced conformation, these islands would stop a shrinking microtubule in its tracks and promote the transition back to growth (Bollinger et al., 2020). Work with microtubule-targeting agents provided further evidence that defects in the microtubule such as transitions in protofilament number could have long-lasting effects on rescue frequency (Mohan et al., 2013; Rai et al., 2019, 2021). Indeed, multiple rounds of rescues can be observed at these sites, suggesting that some rescues occur as a result of a long-term property within part of the lattice. Alternatively, some rescues can also be caused by a disruption of the shrinking microtubule end (Fees & Moore, 2019). MAPs or cations can have this effect, reversing shrinkage by uncoupling the mechanical strain of the rapidly depolymerizing protofilament from its neighbors. Whatever their underlying mechanism, rescues continue to puzzle the field, and the search continues for the exact structural features within the lattice that confer stability or promote catastrophe.

1.7 Structural plasticity in the microtubule lattice

Recent advances in cryo-EM structure refinement algorithms have allowed very detailed analysis of microtubule lattices, and of the plasticity of these structures (Debs et al., 2020). It is now possible to observe things like kinks in the lattice, multiple seams, and other deviations from helical symmetry (Debs et al., 2020; LaFrance et al., 2022). This observation does raise questions about the effects of such deviations that could be considered defects. Are they a normal part of dynamic instability in that they accumulate and contribute to the occurrence of catastrophes or are lattice defects completely separate from the destabilizing events happening in or around the GTP cap? Work with taxane-induced defects suggest that protofilament number transitions could have long-range effects in the microtubule lattice, changing the growth rate and catastrophe frequency

of the lattice sections following the defect (Rai et al., 2019, 2021). A defect could generate a lattice with even more accumulated strain, thereby becoming more sensitive to the events leading to catastrophe.

The structural plasticity of microtubules makes it difficult for biochemists to elaborate kinetic equations to describe dynamic instability (Kueh & Mitchison, 2009). Tubulin can adopt a range of conformations in solution and within the microtubule. Small adjustments in individual tubulin dimers like a 12° bend or a 2 \AA compaction can lead to large scale changes in the structure of the microtubule. A protofilament curling outwards during shrinkage, for example, can deviate $> 10 \text{ nm}$ relative to the center axis of the microtubule (Mandelkow et al., 1991; McIntosh et al., 2018). Twisting of the α -tubulin subunit relative to the β -tubulin subunit on the order of 1 \AA can accumulate over the length of the microtubule lattice, changing the overall skew of protofilaments relative to the microtubule axis (LaFrance et al., 2022). Together, the small changes within individual tubulin dimers result in μm level changes to microtubule lengths in short periods of time. If we are to understand which conformational changes in tubulin are at the heart of dynamic instability, we must first and foremost understand the spatial scale that is relevant at key transition points like catastrophe. In Chapter 2, I will describe the use of viscosity as a tool to determine relevant spatial scales in the conformational changes in tubulin leading to catastrophe.

1.8 Nucleation

The structural plasticity of microtubules makes it challenging to understand how a microtubule is formed in the first place. In the case of simple polymers, nucleation is relatively

easy to understand. Because of the complexity of the microtubule polymer, microtubule nucleation remains one of the most poorly understood phases of dynamic instability.

1.8.1 Spontaneous nucleation

Nucleation of equilibrium polymers can be described by simple kinetic models. Free subunits face an energetic barrier to come together to form a polymer. In the formation of filaments like actin or sickle-cell hemoglobin, the energetic barrier to nucleation is overcome upon formation of a “minimal nucleus” (Erickson & Pantaloni, 1981; Oosawa & Asakura, 1975; Oosawa & Kasai, 1962). The minimal nucleus is defined as the first stable intermediate in the nucleation pathway (or the last stable one, in some publications). Over time, subunits may associate and dissociate. The formation of these early unstable oligomers becomes increasingly unfavorable as they grow in size until the formation of the stable minimal nucleus. All subsequent additions to the minimal nucleus are favorable, allowing polymer elongation (Erickson & Pantaloni, 1981; Flyvbjerg et al., 1996; Fyngson et al., 1994; Voter & Erickson, 1984). Since the main barrier to nucleation is the formation of this minimal nucleus, then increasing subunit concentration should increase the probability of nucleation significantly.

However, just as is the case for growth, microtubule nucleation proved more complex than what could be described by simple kinetic models. Turbidity experiments monitoring microtubule formation suggested that the minimal tubulin nucleus was made of 7 dimers (Voter & Erickson, 1984). In other words, once a tubulin oligomer reached 7 dimers in size, microtubules could carry on growing. However, the 7-dimer nucleus was proposed based on an analysis assuming a single-step nucleation process. Re-analysis of the same data with multi-step models suggested that the sought-after minimal nucleus was closer to 15 dimers in size (Flyvbjerg et al., 1996; Kuchnir Fyngson et al., 1995). A minimal nucleus of 12-15 dimers was a compelling idea, since it matched

with the number of protofilaments in typical microtubules (Erickson, 1974; Tilney et al., 1973). In addition, a 12-15 dimer would match the number of tubulin binding sites on the textbook microtubule nucleator in cells, the γ -Tubulin Ring Complex (γ -TuRC) (Keating & Borisy, 2000; Zheng et al., 1995).

1.8.2 Templated nucleation

In cells, microtubules are nucleated at the centrosome by γ -TuRCs. These ring-shaped complexes have the same shape as a microtubule, and so should provide the perfect template onto which tubulin can assemble. However, in *in vitro* experiments, tubulin assembly onto γ -TuRCs faces an energetic barrier that growing microtubule ends do not (Wieczorek et al., 2015). At low tubulin concentrations, microtubules cannot nucleate from templates like γ -TuRCs or blunt stabilized “seed” microtubules. A microtubule already actively growing at a high concentration of tubulin can however continue to grow even when the tubulin concentration is lowered below this nucleation threshold. This suggests that an oligomer made of 13 laterally associated tubulin dimers is not an adequate minimal nucleus, since growth from such a structure remains unfavorable.

It seems therefore that γ -TuRCs are not the perfect nucleators the textbooks can make them out to be. Rather, they behave as templates onto which additional factors like XMAP215 and TPX2 can help overcome the energetic barrier to assembling a growing microtubule (Flor-Parra et al., 2018; Petry et al., 2013; Popov et al., 2002; Thawani et al., 2018; Verma & Maresca, 2019).

1.8.3 Microtubule nucleation without a minimal nucleus

The shape of the γ -TuRC may be one reason for its limits as a nucleator. It was thought that pre-stabilizing weaker lateral contacts would be the key to efficient nucleation of new microtubules, but it seems that this lateral stabilization is insufficient. Blunt templates like γ -TuRCs can only offer longitudinal contacts to incoming tubulin dimers. However, this is only one

of the three ways tubulin dimers can bind: to longitudinal binding sites, to lateral binding sites, and to “cozy corners”, presenting both a lateral and a longitudinal contact (Erickson & Pantaloni, 1981; Mickolajczyk et al., 2019). Tubulin dimers are proposed to have a higher affinity for corner sites, since they can make both a lateral and longitudinal contacts in them. Corner sites provide an explanation for measurements of long dwell times of tubulin dimers binding to growing microtubule ends (Mickolajczyk et al., 2019), and are the basis of a recent model for microtubule nucleation (Rice et al., 2021).

The model proposed by Rice et al. is one where microtubules form by the stepwise addition of lateral or longitudinal layers to rectangular sheet-like structures, i.e. by accretion. Corner sites are key in this mode, where each lateral or longitudinal layer fills quickly because of the generation of new corner sites. In contrast to a minimal nucleus model where polymerization is unfavorable until an oligomer of critical size is reached, in this accretion model, oligomer growth accelerates with each layer addition until steady-state microtubule growth is achieved. This accretion model for microtubule formation could explain why nucleation from blunt templates like γ -TuRCs remains unfavorable, since it requires the formation of a new layer, beginning with a singleton tubulin dimer making one longitudinal contact before a second can come along and help stabilize it.

Whichever model is used to interpret the data, it is clear that microtubule nucleation faces a kinetic barrier. Though simulations may differ in the precise way energetic penalties are modeled, one thing is clear, that curved GTP-tubulin dimers may be able to form small, curved oligomers, but eventually these oligomers must straighten to form a hollow tube, and that straightening is energetically costly. Similar questions can be asked about microtubule growth and nucleation:

what are the small-scale conformational changes that allow single tubulin dimers to straighten and become part of a microtubule?

1.9 Controlling microtubule nucleation

Microtubule nucleation is a kinetically unfavorable multi-step process (Rice et al., 2021; Roostalu & Surrey, 2017; Wieczorek et al., 2015). Firstly, the formation of a persistently growing end is limited by the structural mismatch between curved soluble tubulin dimers and straight tubulin dimers in a microtubule lattice. Secondly, early intermediates in the nucleation pathway are destabilized by GTP hydrolysis which causes the catastrophe of these small unstable oligomers. Microtubule nucleation can therefore be facilitated or inhibited by inhibiting or slowing GTP hydrolysis, inhibiting or slowing the curving of GDP tubulin dimers, facilitating tubulin straightening, or “outrunning” tubulin disassembly by increasing association rates. Conversely, nucleation can be inhibited by preventing straightening of GTP tubulin, accelerating GTP hydrolysis, or otherwise slowing tubulin association and accelerating dissociation events.

1.9.1 Inhibiting nucleation by promoting catastrophe

Wieczorek et al. showed that catastrophes contributed to the large energy barrier to nucleation by slowing nucleation with different catastrophe factors (Wieczorek et al., 2015). They used two MAPs for this: 1) MCAK, a microtubule depolymerase in the kinesin-13 family, and 2) EB1, an end-binding protein that accelerates GTP hydrolysis. In both cases, nucleation was slowed while catastrophe was accelerated. These observations showed that nucleation can be slowed by the acceleration of microtubule catastrophe, either by pushing tubulin in the GTP cap towards a

curved conformation to induce depolymerization (Helenius et al., 2006), or by accelerating GTP-hydrolysis and promoting a more unstable GDP-like conformation of tubulin (Maurer et al., 2014).

1.9.2 Promoting nucleation by inhibiting catastrophe

Conversely, nucleation is accelerated when catastrophes are inhibited. This was demonstrated with the slowly-hydrolysable GTP analogue, GMPCPP (Hyman et al., 1992). Microtubules polymerized with GMPCPP grow at similar rates as GTP microtubules, but they are hyperstable—they do not undergo dynamic instability. GMPCPP significantly promotes the spontaneous nucleation (Hyman et al., 1992) as well as templated nucleation (Wieczorek et al., 2015), showing that GTP hydrolysis contributes to the barrier to nucleation.

1.9.3 Promoting nucleation by outrunning catastrophe

Microtubule nucleation is a race between the formation of small tubulin assemblies and the dissociation of such assemblies. Therefore, nucleation can be facilitated by accelerating tubulin association rates, promoting tubulin additions before oligomers have time to disassemble. MAPs that promote tubulin association, like the polymerase XMAP215, can therefore accelerate nucleation. Indeed, XMAP215 was shown to decrease the time required for nucleation from templates *in vitro* (Wieczorek et al., 2015).

Overall, many experiments suggest a tight link between nucleation and catastrophe. However, since we still do not understand the conformational changes in tubulin that lead to catastrophe, nor those that must occur during nucleation, we cannot fully understand the relationship between these two transitions. In Chapter 3, I will discuss my work exploring the connection between nucleation and catastrophe using MAPs with opposing effects on dynamics. As I will discuss, the study of MAPs has expanded our knowledge of the intrinsic properties of

microtubules themselves and shed light on some of the underlying mechanisms of dynamic instability.

1.10 Conclusion

Thirty-nine years after dynamic instability was proposed, there has been substantial progress in characterizing this fundamental behavior of microtubules and developing biochemical models to describe and predict complex biopolymer behaviors. Thanks to advances in microscopy techniques, we can now precisely measure net growth and shrinkage rates of microtubules and obtain detailed distributions of catastrophe frequency and nucleation lag times. The use of total internal reflection fluorescence (TIRF) and interference reflection microscopy (IRM) in particular have provided precise measurements of small fluctuations in growth rates, allowing the characterization of the highly varied behavior of individual microtubule ends during growth to a level of detail that is lost when measuring net rates of a population (Cleary et al., 2022; Gardner, Charlebois, et al., 2011; Mahserejian et al., 2022). Meanwhile, improvements in recombinant protein purification have opened up the possibility to purify specific tubulin isotypes and mutants, allowing structure-function studies on mammalian tubulin that were not possible previously (Roostalu et al., 2020). In addition, with the continued advancement in cryo-EM technology and reconstruction algorithms, we can now reconstruct details of individual protofilaments, instead of a helical average (Debs et al., 2020).

The combination of all these advancements puts the field in a place where specific tubulin mutants can be purified, their dynamics quantified by TIRF or IRM microscopy, and their structure reconstructed by cryo-EM (LaFrance et al., 2022) to answer longstanding questions. Altogether,

the microtubule field continues to work towards bringing this complex polymer into a rigorous and quantitative biochemical framework.

In this thesis I will discuss my own work on microtubule dynamic instability through physical and biochemical means. It is by modulating the parameters of dynamic instability that we hope to gain an understanding of the underlying conformational cycles of tubulin. In Chapter 2, I will discuss my work on the conformational changes in tubulin important in moments of transition during dynamic instability. To this end, I modulated viscosity using viscogens of different sizes to probe the relevant size scales of these conformational changes. In Chapter 3, I will discuss a second project on dynamic instability, this time combining MAPs of opposing effects to uncouple nucleation from catastrophe. Lastly, in Chapter 4, I will discuss my results in the current context of microtubule research, comparing and contrasting my findings with recently published data. Overall, my work, like that of many others, demonstrates how the structural plasticity of tubulin contributes to the complexity of microtubule behavior. Thorough characterization of the conformational transitions in tubulin is essential to understanding how cells regulate their microtubule networks throughout the cell cycle.

2 Dynamic instability is modulated by the viscosity of the environment

2.1 Introduction

Much of our current understanding of dynamic instability is informed by cryo-EM and crystal structures of tubulin in different nucleotide, drug, or protein binding states. A variety of structural and biochemical data has shown that GTP-tubulin is curved in solution and must therefore straighten to be incorporated into a growing microtubule (Ayaz et al., 2012; Nawrotek et al., 2011; Pecqueur et al., 2012; Rice et al., 2008; Wagstaff et al., 2022). In addition, with the resolution revolution of cryo-EM came confirmation of early observations that GDP-tubulin in microtubules adopts a compacted state relative to GTP-like tubulin (Alushin et al., 2014; Hyman et al., 1995; R. Zhang et al., 2015, 2018). The compaction following GTP hydrolysis involves movements in the α -subunit of tubulin on the size scale of 1-2 Å, including longitudinal rearrangements and a twisting motion (Manka & Moores, 2018). GTP hydrolysis is therefore thought to produce strain in the lattice because of the differences between the lateral and longitudinal contacts made by GTP-tubulin and GDP-tubulin. As such, when the stabilizing GTP-cap is lost, the weakened lateral contacts made by GDP-tubulin are broken by the bending of GDP-tubulin and ultimately the curling and separation of individual protofilaments.

The detail with which we can compare GTP-like tubulin to GDP-tubulin lattices is one of the great advantages of high-resolution data generated by techniques like cryo-EM. However, this type of data only provides frozen snapshots of very dynamic processes. For example, though we know in near-atomic detail the differences between the expanded and the compacted

conformations of tubulin, we know very little about the transitions between these conformational states. Thus, structural methods must be combined with dynamic experiments in order to paint a full picture of dynamic instability.

2.1.1 Modulating the physical properties of the environment to study biochemical reactions

One way to probe dynamic conformational changes in biomolecules is through modulation of the physical properties of their environment like temperature, viscosity, and crowding. One of the first examples of such a technique that we learn about in early biochemistry courses is denaturation experiments. By progressively heating up a sample, we can measure the temperature at which the protein of interest denatures (i.e. the melting temperature). The higher the melting temperature, the more energy required to unfold the protein, thus, the more stable the protein is.

Below a protein's denaturation point, increasing the temperature of a solution can modify the rates of biochemical reactions. In 2018, Chaaban et al. took advantage of this concept to understand the fast dynamics of *C. elegans* microtubules (Chaaban et al., 2018). For both bovine and *C. elegans* tubulin, increasing the temperature increased microtubule growth rates. However, the effect of temperature on the association rate constant was more pronounced for bovine tubulin, meaning that the energy barrier for association of *C. elegans* tubulin was lower. Combining this observation with their high-resolution cryo-EM structure as well as molecular dynamics simulations, they concluded that *C. elegans* microtubules grow faster than bovine microtubules because of the of a pre-ordering of the loops that form lateral contacts during polymerization (Chaaban et al., 2018). This study is a prime example of how the combination of physical manipulations of biochemical reaction rates combined with high-resolution structural data can provide detailed insight into mechanisms of microtubule dynamics.

Physical properties of the environment can modulate the rates of biochemical reactions and provide insights into the underlying mechanisms. Modulating viscosity to determine the diffusion limit of a reaction is another classic example of this. Measuring the diffusion limit of a reaction is important because if the reaction actually occurs faster than the theoretical limit based on diffusion, there might be something else going on (e.g. strong attractive forces increasing the reaction rate) (Berg & von Hippel, 1985). Conversely, if the reaction occurs much slower than the theoretical diffusion limit, the reaction may be limited by an additional step. As mentioned in Chapter 1, Drenckhahn & Pollard used the relationship between filament growth and viscosity to determine whether actin filament growth was a diffusion limited process. Since small viscosogens slowed actin filament growth, and the growth rates tended to infinity as viscosity approached zero, actin filament growth was determined to be diffusion limited (Drenckhahn & Pollard, 1986). Similar experiments were carried out to determine whether the same could be said for microtubules. Indeed, arrival of tubulin to the growing microtubule end was determined to be diffusion limited as well (Wieczorek et al., 2013). However, increasing viscosity with large molecules that contribute to macromolecular crowding provided additional insight into the nature of microtubule growth.

For both actin filaments and microtubules, increasing viscosity with large macromolecular crowders like BSA and Dextran increased growth rates (Drenckhahn & Pollard, 1986; Wieczorek et al., 2013). Macromolecular crowding can indeed promote the formation of other types of assemblies like aggregates or condensates as well, due to excluded volume effects that increase the effective subunit concentration by reducing the volume available for subunits to explore (McGuffee & Elcock, 2010a; T. J. Mitchison, 2019). Interestingly, as discussed in Chapter 1, though microtubule growth rates were increased in the presence of macromolecular crowders, they

saturated, even in the presence of polymerizing enzymes (Wieczorek et al., 2013). The saturation of microtubule growth rates showed that microtubule growth involved an intermediate step which limits growth when arrival of tubulin dimers to the growing end is fast. Thus, the physical properties of the environment can be used to modulate biochemical reaction rates, shedding light on underlying mechanisms.

Molines et al. showed that the physical properties of the environment, or of cytoplasm more specifically, can have important impacts on reaction rates in cells, using microtubule dynamics as a model (Molines et al., 2022). They used osmotic shocks to grow or shrink fission yeast cells, effectively concentrating or diluting the cytoplasm within. As cytoplasm concentration was increased, one might have expected microtubule growth rates to increase as well. However, they observed the opposite: increasing cytoplasm concentration slowed microtubule growth, as well as microtubule shrinkage. Since they measured slower diffusion of tubulin and of GEMs, they hypothesized that increasing cytoplasm concentration may be slowing microtubule growth and shrinkage because of an increase in cytoplasm viscosity. This slow-down of microtubule growth and shrinkage was then recapitulated *in vitro* by increasing viscosity with the small viscogen glycerol, confirming that microtubules were slowed by increased cytoplasm viscosity (Drenckhahn & Pollard, 1986; Wieczorek et al., 2013).

2.1.2 Modulating viscosity to study conformational changes in proteins

Biochemical reaction rates can be modulated by the viscosity of their environment. At the size scale of proteins, we can think of viscosity as the friction experienced by a molecule moving through solution. As reviewed in Hagen, 2010, conformational changes involved in biochemical reactions can be dampened by friction with the surrounding solvent (Hagen, 2010). Importantly, the friction experienced by a molecule depends on its relative size compared to the molecules in

the solvent. Thus, the relationship between reaction rate and viscosity therefore depends on the relative size of the viscogen and the structural elements in motion during the reaction. In other words, viscogens of different sizes will differentially affect the solvent friction experienced by the parts of the protein in motion during conformational changes (Hagen, 2010; Sekhar et al., 2012, 2013; Yedgar et al., 1995).

Therefore, the dependence of a reaction rate on viscogen size can be used to estimate the size scale of a conformational change occurring during the reaction in question. For example, Sekhar et al. used the relationship between viscogen size and reaction rate to characterize the conformational changes in the four-helix FF domain from human HYPB/FBP11 (Sekhar et al., 2013), a protein shown to interact with huntingtin (Allen et al., 2002; Passani et al., 2000). Using an array of molecules of different sizes, they constructed a “molecular ruler” by measuring the relationship between the rate of interconversion between conformational states and viscosity for viscogens of different sizes. Thus, they determined that the transition of the FF domain from its native state to its intermediate state occurs via movements of small secondary structures on the order of 4 Å, rather than the simultaneous rearrangement of large clusters of residues (Sekhar et al., 2013, 2014).

We reasoned that viscogens of different sizes could be used as probes for all kinds of biochemical reactions, including microtubule dynamic instability. Therefore, we sought to determine the relevant size scales for all the phases of dynamic instability: growth, shrinkage, catastrophe, rescue, and nucleation. Structural data shows that tubulin undergoes a variety of conformational changes ranging from compaction to curvature to protofilament peeling. However, we currently do not understand the transitions between the different tubulin conformations. For example, some models suggest that protofilament straightening during growth is a major

determinant of catastrophe frequency (Alexandrova et al., 2022), but we do not have strong experimental data to support or rule out the importance of protofilament straightening. Importantly, the straightening of protofilaments occurs on a larger size scale (> 10 nm) than other conformational changes in tubulin like longitudinal compaction (2 \AA). Therefore, viscosogens of different sizes can be used as a tool to determine which is the relevant size scale for reactions like catastrophe.

To probe the size scale of the conformational changes occurring in tubulin throughout dynamic instability, we used three viscosogens of different sizes. The smallest, glycerol, with a hydrodynamic radius of around 3 \AA (Schultz & Solomon, 1961), is commonly used in tubulin purifications, and is often used as a small viscosogen in solvent friction studies of protein folding (Dupuis et al., 2018; Hagen, 2010; Yedgar et al., 1995). In the mid-range, we chose trehalose, a $\sim 4 \text{ \AA}$ sugar similar in structure to sucrose (Olsson & Swenson, 2020; Schultz & Solomon, 1961). Finally, on the larger end, we used BSA, a globular protein with a hydrodynamic radius of around 40 \AA (X. Zhang et al., 2015) (on the order of the size of an “average” protein (Milo & Phillips, 2015)) often used as a macromolecular crowder in *in vitro* (Ellis, 2001; McGuffee & Elcock, 2010a; Munishkina et al., 2004; Nettesheim et al., 2020; Shahid et al., 2017). We used these three viscosogens to determine the relationship between viscosity and viscosogen size on the rates of the reactions involved in each phase of dynamic instability.

We found that, even though glycerol and trehalose are close in size, they have very different effects on microtubule dynamics. Specifically, glycerol suppresses microtubule catastrophe and promotes rescues far more than trehalose, despite both slowing growth and shrinkage rates. This difference suggests that catastrophes are limited by a small conformational change in tubulin on the size scale of 3 \AA . This work demonstrates that a) the physical properties of the environment

can have significant effects on microtubule dynamics and b) transitions in dynamic instability are determined by small conformational changes in tubulin rather than large movements of whole protofilaments.

2.2 Results

To determine the effects of viscogen size on microtubule dynamics, we created reaction buffers of matching viscosities between 1.0 cP and 2.2. cP by increasing the concentration of glycerol, trehalose, or BSA. The viscosities of the reaction buffers were measured by a MEMS-based micro-sample viscometer. In these reaction buffers, we reconstituted microtubule dynamics using a single molecule assay (Gell et al., 2010). We used internal reflection microscopy (IRM) to visualize dynamic microtubules growing from stable GMPCPP seed microtubules adhered to a glass coverslip (Figure 2.1 A-B) (Mahamdeh et al., 2018; Mahamdeh & Howard, 2019). In order to quantify dynamic instability, timelapse movies of dynamic microtubules were converted into kymographs for analysis of individual microtubules (Figure 2.1C). From these kymographs, we quantified the rates of microtubule growth and shrinkage, as well as the microtubule lifetimes, rescue frequency and time required to nucleate. This workflow enabled us to determine how viscosity, and viscogen size, influence each phase of dynamic instability (Figure 2.2).

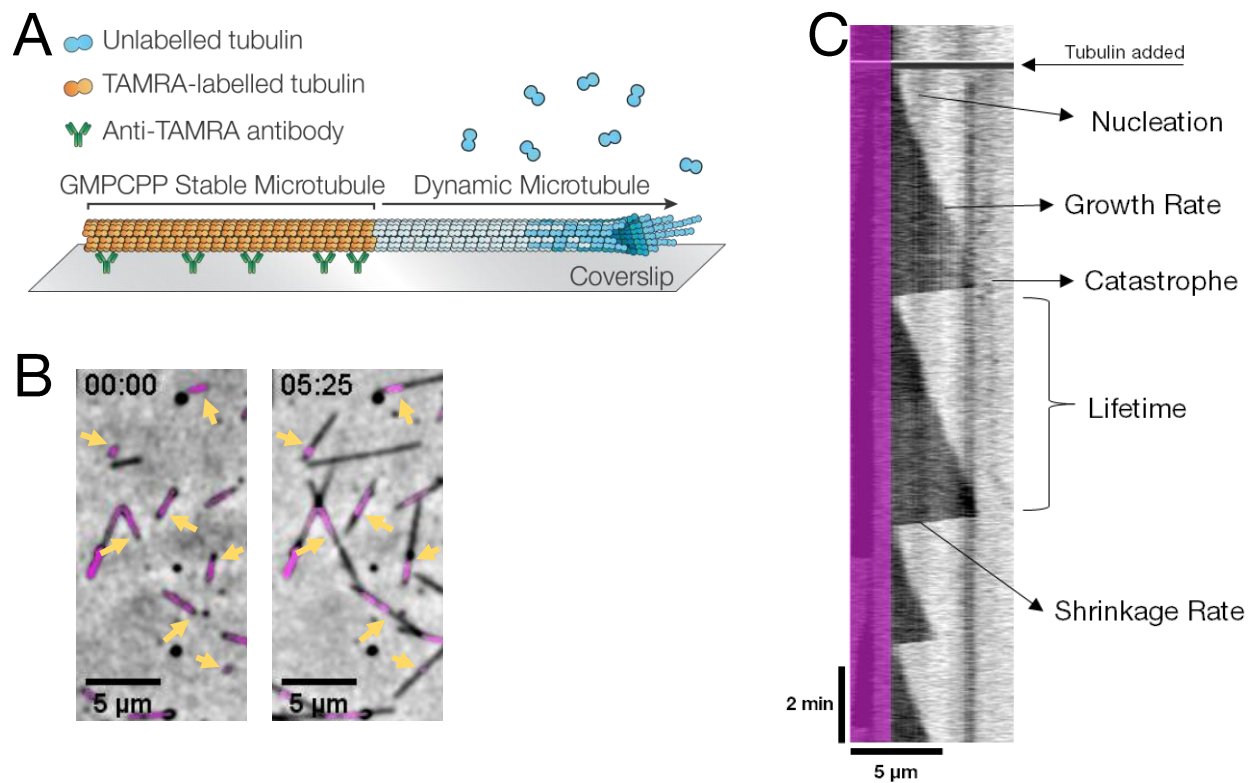


Figure 2.1 *Microtubule dynamics reconstituted in vitro*

A. Schematic representation of the *in vitro* reconstitution of microtubule dynamics. Stable TAMRA-labelled GMPCPP seeds are adhered to a cleaned glass coverslip by anti-TAMRA antibodies on the surface. Unlabeled tubulin is introduced and polymerizes onto the stabilized seed to form a dynamic microtubule. B. Representative field of view of a typical experiment. Stable GMPCPP seeds are adhered to the coverslip (pseudo-colored in magenta). With time, dynamic microtubules (black extensions) grow from the seeds. C. Representative kymograph used to quantify the dynamics of microtubules observed by IRM as in B. The dynamic microtubule (yellow arrows pointing out black extensions) grows from the stable seed (pseudo-colored in magenta), undergoing repeated rounds of growth, catastrophe, and shrinkage.

2.2.1 Growth rates are sensitive to viscosity

Previous work has shown that small viscosogens like glycerol decrease microtubule growth rates (Molines et al., 2022; Wieczorek et al., 2013). Consistent with these earlier measurements, when we increased viscosity from 1.0 cP to 2.2 cP with glycerol, microtubule growth rates were

slowed from $0.87 \pm 0.23 \mu\text{m}/\text{min}$ (mean \pm SD, $n = 355$) to $0.52 \pm 0.16 \mu\text{m}/\text{min}$ (mean \pm SD, $n = 25$, $p < 0.0001$, one-way ANOVA Dunnett's multiple comparison test) (Figure 2.2 and 2.3). Increasing viscosity with the slightly larger viscogen, trehalose, had a similar effect, slowing growth to $0.31 \pm 0.06 \mu\text{m}/\text{min}$ (mean \pm SD, $n = 33$, $p < 0.0001$). In contrast, increasing viscosity with the largest of our viscogens, BSA, increased growth rates to $0.95 \pm 0.19 \mu\text{m}/\text{min}$ (mean \pm SD, $n = 360$, $p < 0.0001$). This is consistent with previous data showing that large macromolecular crowders can accelerate microtubule growth, as crowding effects counteract the viscous effects by increasing the effective concentration of tubulin through excluded volume effects (Wieczorek et al., 2013).

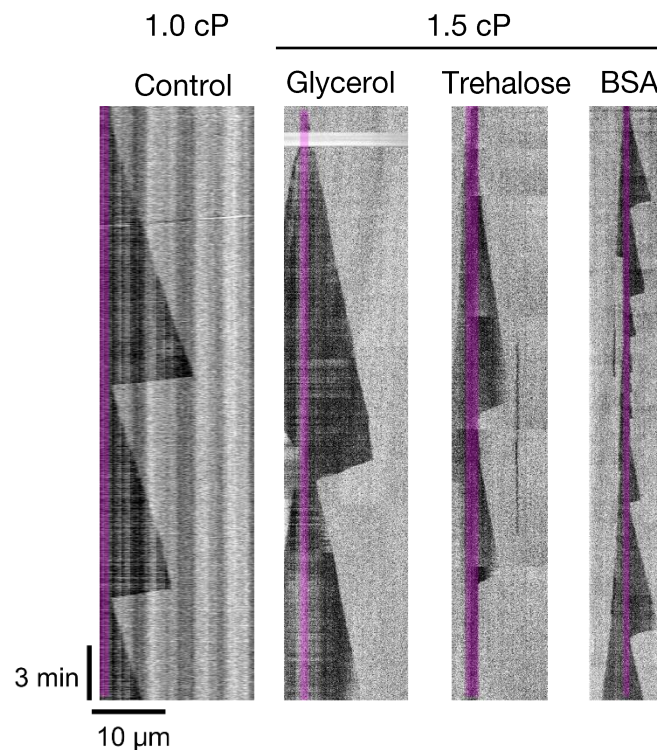


Figure 2.2 *Microtubule dynamics are sensitive to viscosity and viscogen size*

Representative kymographs of microtubules growing at $10 \mu\text{M}$ tubulin from stable GMPCPP seeds (pseudocolored in magenta) at the indicated viscosity in the absence (control) or presence of the indicated viscogen. Microtubules were visualized by IRM.

Consistent with previous work, we observed small viscogens slowing microtubule growth (Figure 2.2 and 2.3). The simplest interpretation of this result is that increased viscosity slows the diffusion of tubulin in the solution. By slowing diffusion, increased viscosity decreases the likelihood of a collision between soluble tubulin and the microtubule, thereby slowing net growth. In contrast, the crowding effects of large macromolecules like BSA counteract this slowing, resulting in overall increased growth rates. These results are also consistent with work done on actin, showing that small viscogens reduce filament growth rates and large crowders accelerate them (Drenckhahn & Pollard, 1986).

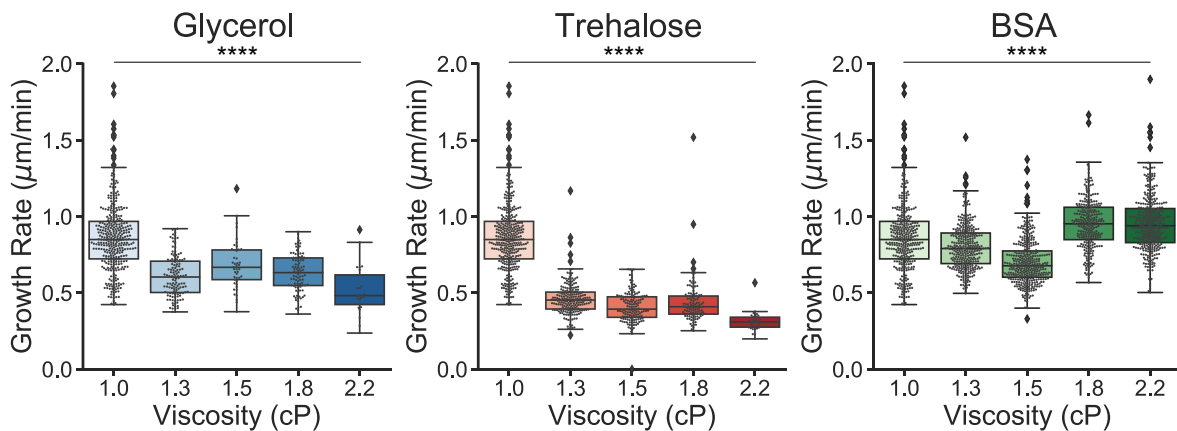


Figure 2.3 Microtubule growth rates are modulated by viscogens of different sizes

Growth rates of microtubules grown from 10 µM tubulin at increasing viscosities. In each case, the lowest viscosity (1.0 cP) represents the control buffer with no viscogen added. Data represents $n = 25\text{-}361$ growth events pooled from at least 2 experiments for each condition. Control data (1.0 cP) is the same in each plot. Individual data points are overlaid on the box plots. Boxplots show the median and interquartile range, with whiskers indicating the maximum and minimum values based on the interquartile range, and outlier values indicated by diamond data points. For each viscogen, a one-way unpaired Brown-Forythe ANOVA test followed by a Dunnett's post-hoc multiple comparisons test was used to compare the means of each group to control (****, $p \leq 0.0001$).

2.2.2 Shrinkage rates are sensitive to viscosity

As discussed above, there has been some previous work on the effects of viscosity on microtubule growth rates. In contrast, to the best of our knowledge, there has been no measurement of the effect of viscosity on microtubule shrinkage rates (other than our work published in (Molines et al., 2022)). Visualizing the microtubules by IRM allowed us to image at high enough frame rates to capture the rapid shrinkage rates and take long acquisitions to capture longer growth events without subjecting our samples to photodamage. We were therefore able to measure microtubule shrinkage rates at increasing viscosities and compare the effects of viscogens of different sizes. In all cases, increasing viscosity slowed microtubule shrinkage rates (Figure 2.2 and Figure 2.4). In control conditions, at a viscosity of 1.0 cP, microtubules shrunk with an average rate of $30.0 \pm 10.5 \mu\text{m}/\text{min}$ (mean \pm SD, $n = 75$). When viscosity was increased to 1.8 cP, the shrinkage rates were reduced to $12.2 \pm 14.1 \mu\text{m}/\text{min}$ (mean \pm SD, $n = 17$, $p < 0.0001$, one-way ANOVA and Tukey's multiple comparison test) by glycerol, $6.1 \pm 3.2 \mu\text{m}/\text{min}$ by trehalose (mean \pm SD, $n = 21$, $p < 0.0001$), and $15.7 \pm 8.0 \mu\text{m}/\text{min}$ by BSA (mean \pm SD, $n = 328$, $p < 0.0001$).

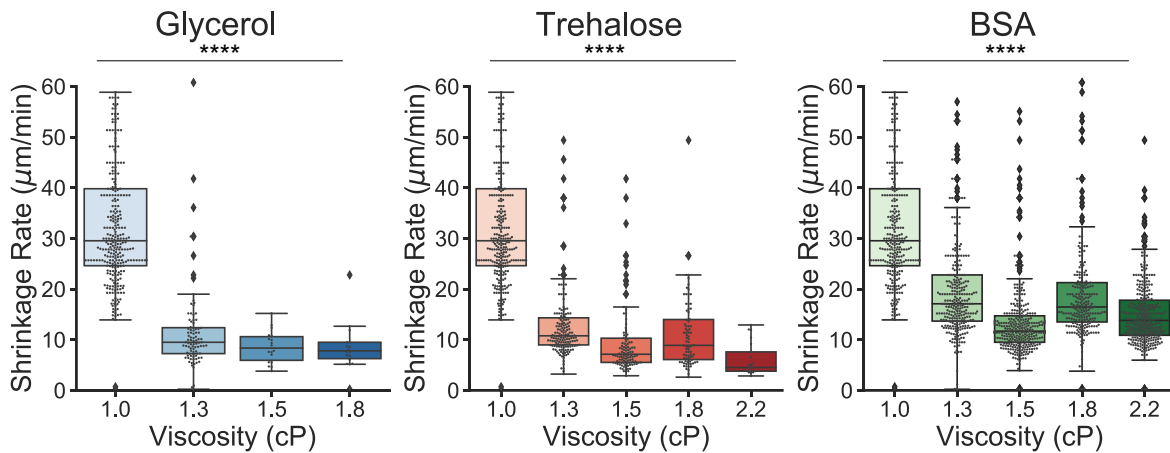


Figure 2.4 *Microtubule shrinkage rates are slowed by all three viscogens*

Shrinkage rates of microtubules grown from 10 µM unlabeled bovine tubulin as measured by IRM. Data represents n = 18-341 shrinkage events pooled from at least 3 experiments per condition. Control data (1.0 cP) is the same in each plot. Individual data points are overlaid on the box plots. Boxplots show the median and interquartile range, with whiskers indicating the maximum and minimum values based on the interquartile range, and outlier values are indicated by diamond data points. For each viscogen, a one-way unpaired ANOVA test followed by a Tukey's post-hoc multiple comparisons test was used to compare the means of each group to control (**** p ≤ 0.0001).

That shrinkage rates are slowed by viscosity suggests that each viscogen can slow the outward curling of tubulin dimers at the end of a shrinking microtubules, the tubulin dissociation rate from these shrinking ends, and/or the separation and curling of protofilaments. Since all three viscogens had a similar effect, it is likely that the relevant conformational change that determines shrinkage rates is large, as it is slowed by both small viscogens (glycerol) and large ones (BSA). Shrinkage rates may therefore be determined by the rate of movement of full protofilaments, peeling and curling outwards. Alternatively, since a simple thermodynamic model can predict slow dissociation of tubulin must accompany slow association of tubulin (Molines et al., 2022), shrinkage rates could also be determined by the rate of tubulin dissociation from shrinking

protofilaments. If this is the case, it would mean that crowding effects from BSA only accelerate association rate constants, and not dissociation rate constants, which are slowed by the increase in viscosity. Since glycerol and trehalose do not significantly increase the level of macromolecular crowding at the concentrations used, these small viscosogens would slow both the association and dissociation rate constants for tubulin binding to a microtubule end, explaining why they slow both growth and shrinkage rates.

2.2.3 Lifetimes and rescue frequency are sensitive to viscogen size

Since the small viscosogens glycerol and trehalose slowed microtubule growth, one might expect these microtubules to catastrophe more often and thus have shorter lifetimes. Generally, as microtubule growth rates increase and “outrun” GTP hydrolysis, the GTP cap can become longer. Longer GTP caps and faster microtubule growth are associated with longer lifetimes, with longer caps conferring additional stability to the growing microtubule (Figure 1.2) (Duellberg, Cade, Holmes, et al., 2016; Walker et al., 1988). With this in mind, one might expect slower-growing microtubules to have shorter lifetimes, as is the case with microtubules grown at low tubulin concentrations that catastrophe often. However, we observed the opposite trend. When increasing viscosity from 1.0 cP to 2.2 cP, the smaller viscosogens, glycerol and trehalose, both increased microtubule lifetimes from 4.9 ± 3.4 min (mean \pm SD, n=154) to 15.9 ± 5.5 min (mean \pm SD, n=39, $p < 0.0001$, Brown-Forsythe ANOVA and Dunnett multiple comparison test) and 8.4 ± 5.6 min (mean \pm SD, n = 77, $p < 0.0001$), respectively (Figure 2.5) even though they slowed microtubule growth rates (Figure 2.3). The larger viscogen, BSA, shortened lifetimes to 3.3 ± 2.5 min (mean \pm SD, n = 227, $p = 0.0002$), even though it accelerated microtubule growth (Figure 2.3). Interestingly, microtubule lifetimes were not only sensitive to changes in viscosity, but they were also sensitive to viscogen size. Surprisingly, though glycerol and trehalose both had similar

effects on growth rates, glycerol had a significantly stronger effect on lifetimes than trehalose. These results suggest that catastrophe is preceded by a small conformational change in tubulin that is significantly slowed by glycerol, but much less so by trehalose, and not by BSA.

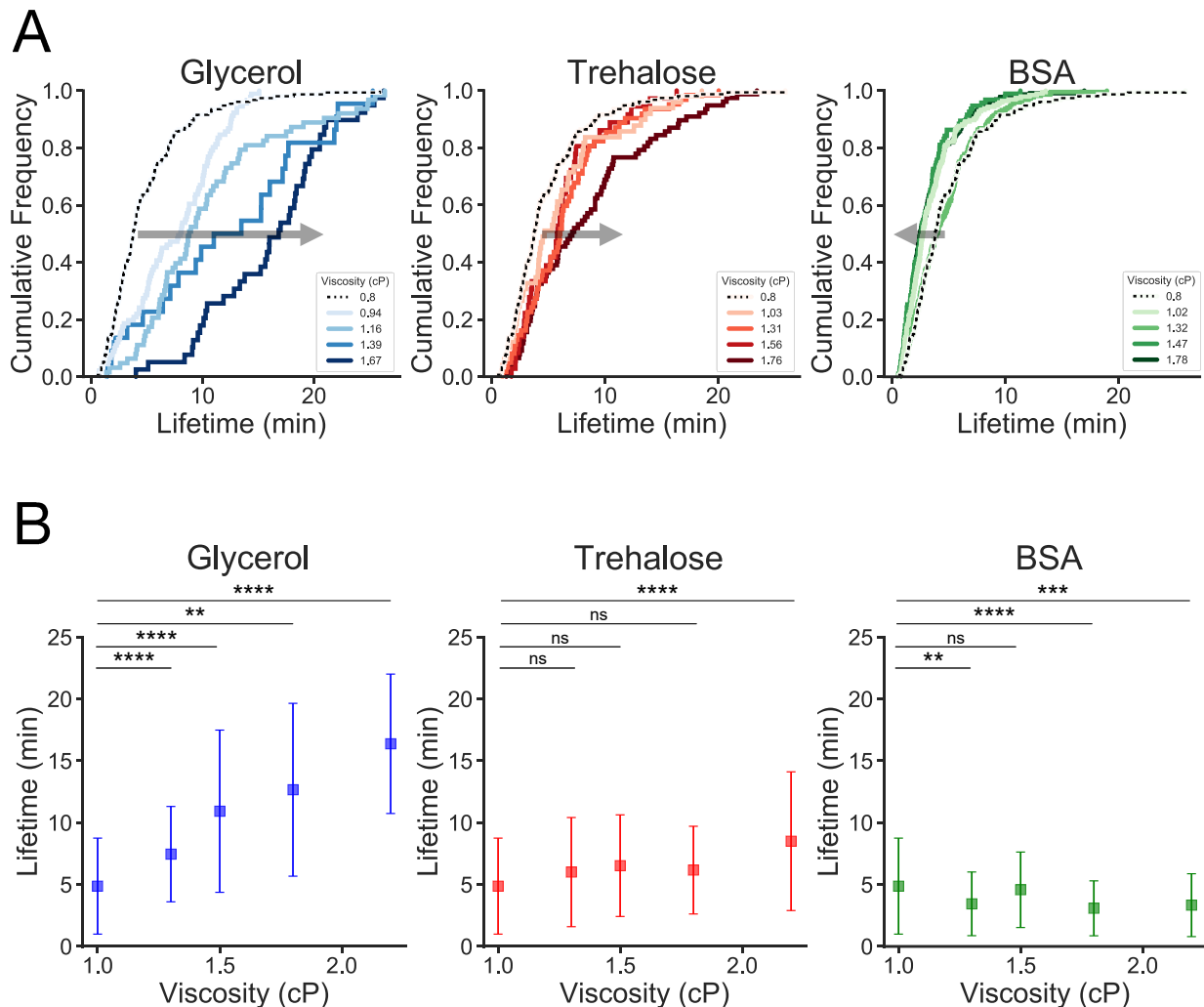


Figure 2.5 Microtubule lifetimes are modulated by viscogens of different sizes

A. Cumulative distributions of microtubule lifetimes at increasing viscosities at 5 μ M tubulin. With three different viscogens. Glycerol shifted the distribution of lifetimes to the right, towards longer lifetimes. Trehalose shifted the distribution to the right also, but to a lesser extent. BSA shifted the distribution slightly to the left, towards shorter lifetimes. B. Mean lifetimes at increasing viscosities with three different viscogens. Glycerol increased the mean microtubule lifetime, while trehalose does so only slightly, and BSA slightly reduced the mean microtubule lifetimes. Data represent means \pm standard deviation of $n = 26$ -227 growth events pooled from at least 2 experiments per condition. For each viscogen, a one-way unpaired Brown-Forsythe ANOVA test followed by a Dunnett's post-hoc multiple comparisons test was used to compare the means of each group to control (**** $p \leq 0.0001$, *** $p \leq 0.001$, ** $p \leq 0.01$, * $p \leq 0.05$, ns $p > 0.05$).

Since there was such a stark difference between the three viscogens in terms of their effect on reducing the frequency of transitions from growth to shrinkage, we measured their effects on the opposite transition, rescues (Figure 6). Measuring the number of rescues per unit of time or per unit of microtubule length shrunk, there is a clear difference between the viscogens here as well. For example, in control conditions, at 1.0 cP, we observe 0.002 ± 0.002 rescues per μm shrunk (mean \pm SD, $n = 4$). Increased viscosity to 1.8 cP with glycerol increases the rescue frequency to 0.45 ± 0.14 rescues/ μm (mean \pm SD, $n = 3$, $p = 0.0001$, one-way ANOVA and Tukey's multiple comparisons test). In contrast, increasing viscosity to 1.8 cP with trehalose or BSA only increased the rescue frequency to 0.016 ± 0.018 (mean \pm SD, $n = 3$, $p = 0.9023$) and 0.015 ± 0.003 rescues/ μm (mean \pm SD, $n = 3$, $p = 0.0796$), respectively (a statistically insignificant change in both cases).

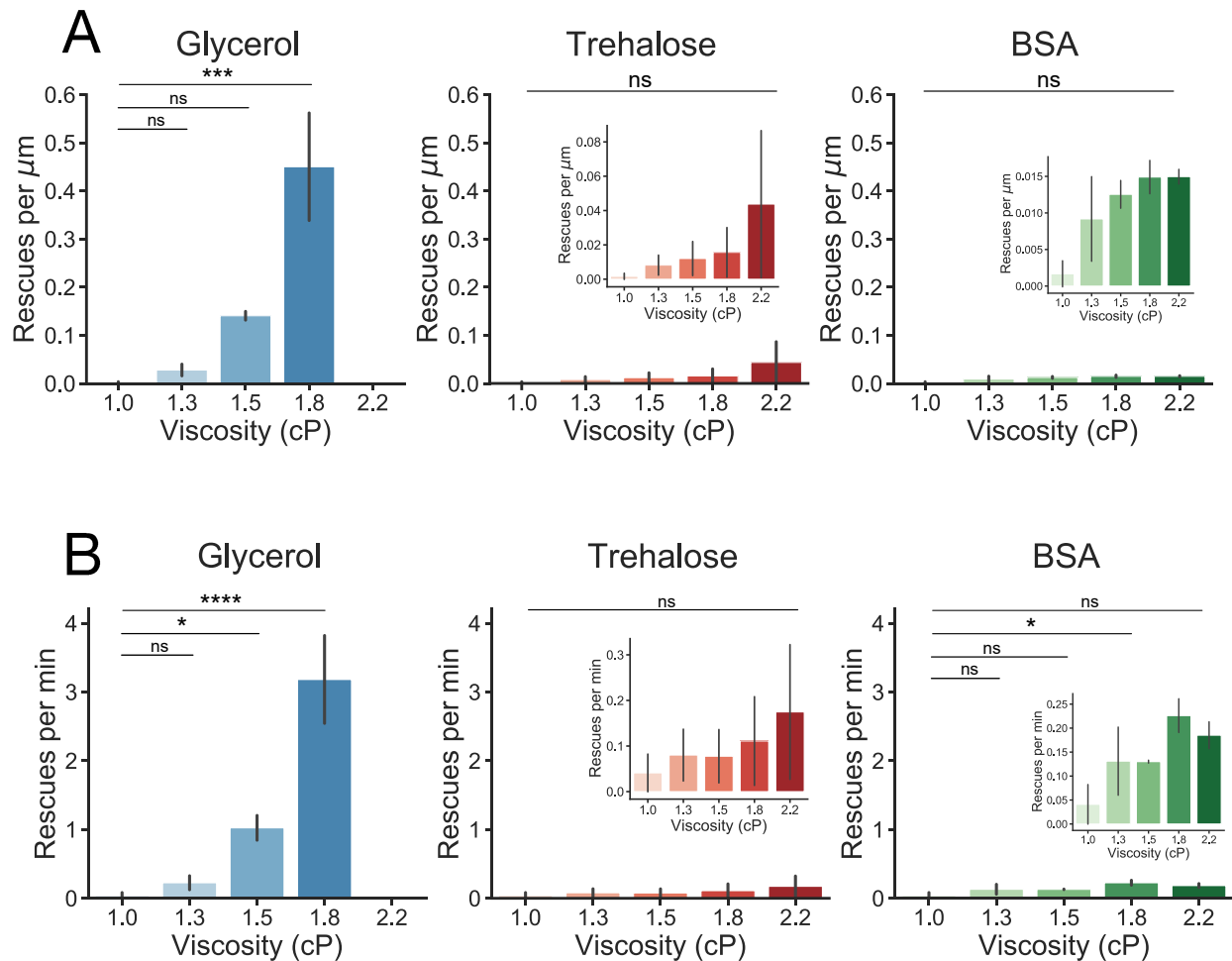


Figure 2.6 Rescue frequency is sensitive to viscogen size

A. Number of rescue events observed per μm length shrunk at increasing viscosities with three viscogens for microtubules grown at $10 \mu\text{M}$ tubulin. B. Number of rescues observed per minute spent shrinking at increasing viscosities with three viscogens for microtubules grown at $10 \mu\text{M}$ tubulin. Data represent rescue events observed in 18-341 shrinkage events from at least 3 experiments for each condition. A and B, for each viscogen, a one-way unpaired ANOVA test followed by a Tukey's post-hoc multiple comparisons test was used to compare the means of each group to control (**** $p \leq 0.0001$, *** $p \leq 0.001$, ** $p \leq 0.01$, * $p \leq 0.05$, ns $p > 0.05$).

Overall, glycerol is far more effective than trehalose or BSA at promoting microtubule growth through longer lifetimes and more frequent rescues. Presumably, glycerol is therefore more effective at stabilizing or promoting a conformation of tubulin at the microtubule end that leads to continued growth. Interestingly, though trehalose similarly slows growth and shrinkage rates, it has comparatively little effect on overall microtubule stability, only modestly increasing lifetimes and rescue frequency. Despite their similar size, why is glycerol so much better at preventing catastrophes and promoting rescues compared to trehalose?

2.2.4 Estimating the size of the GTP cap with EB

If glycerol is so effective at preventing catastrophe and extending microtubule lifetime, it must be stabilizing the microtubule end somehow to compensate for the slower tubulin association rate. One hypothesis is that this stabilization could occur by slowing GTP hydrolysis, resulting in larger GTP-caps despite the slower growth rates. To test this hypothesis, we needed a way to estimate the size of the GTP caps in our experiments. We therefore turned to the end-binding protein EB3. EBs are known to track growing microtubule ends, binding in a characteristic “comet” shape (Figure 2.7). Since EBs bind more strongly to microtubules made with GTP analogues than to GDP microtubules, EBs are considered to bind the GTP-cap, so the size of EB1 or EB3 comets is used as an indirect measurement of GTP cap size (Maurer et al., 2012, 2014; Roostalu et al., 2020; Zanic et al., 2009).

If glycerol prevents catastrophe by slowing GTP hydrolysis, we would expect to see larger EB comets (indicative of larger GTP caps) in the presence of glycerol. By that same logic, trehalose should also produce comets of slightly larger size since it slightly increases microtubule lifetimes. On the opposite end, BSA should create smaller comets since it shortens microtubule lifetimes.

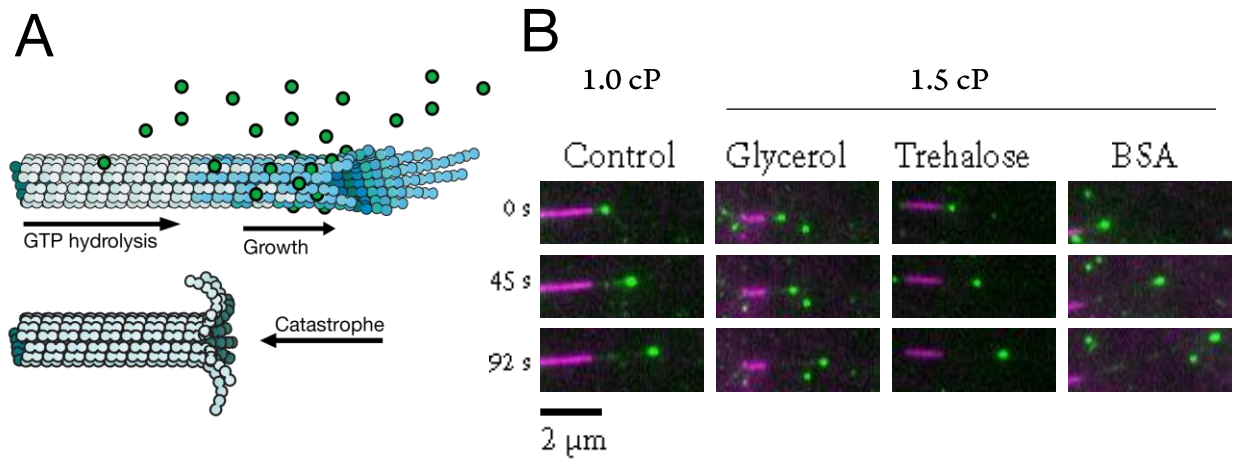


Figure 2.7 EB3-GFP binds to the ends of growing microtubules in a characteristic comet shape.

A. Schematic representation of EBs binding to the end of a growing microtubule, but not a shrinking microtubule. B. Representative images of EB3-GFP binding to the ends of microtubules growing in control buffer (1.0 cP) or in the presence of viscosogens (1.5 cP). Images are a composite of the signals from the TAMRA-labeled seeds (magenta) and EB3-GFP signal (green) at the ends of the dynamic microtubules, imaged by TIRF microscopy.

We therefore added EB3-GFP to our *in vitro* reconstitutions and used total internal reflection fluorescence (TIRF) microscopy to measure the effect of viscosogen size on EB3 comets. We measured the EB3-GFP binding profile along individual growing microtubules and aligned these profiles to generate an average comet (which mostly remained a diffraction limited spot in these experimental conditions). We then compared the total comet intensity between microtubules grown in control conditions, at 1.0 cP, and microtubules grown at a viscosity increased to 1.5 cP either with glycerol, trehalose, or BSA. In order to control for differences in microtubule growth rate at different viscosities, we imaged EB3 comets on microtubules grown in a range of tubulin concentrations. This way, we could also determine whether viscosity changes the relationship between growth and GTP cap size.

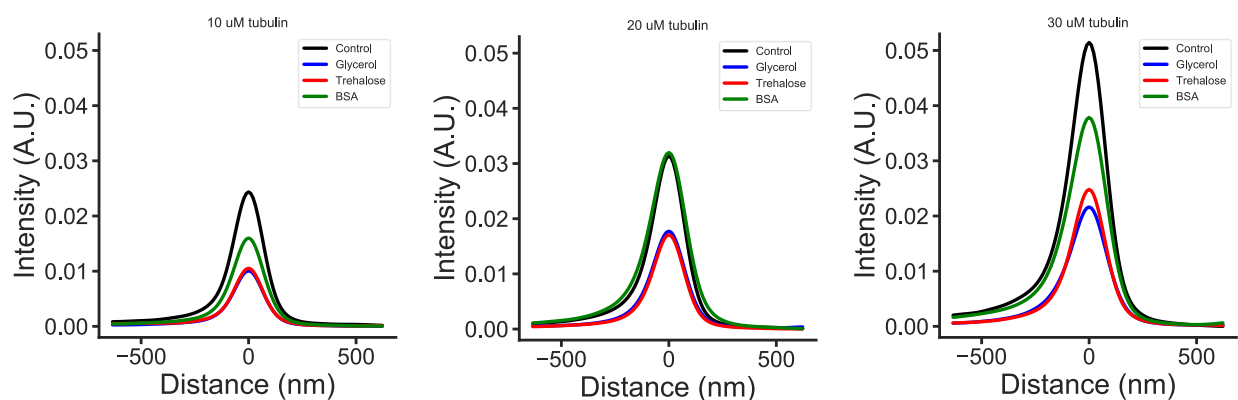


Figure 2.8 Average Comet profiles in the presence of viscogens

Comets were imaged by TIRF microscopy, rotated, and aligned at their peak intensity. An average profile was generated from at least 25 comets for each condition, as described in Figure 2.7.

In contrast to our prediction, at any given tubulin concentration tested, glycerol and trehalose did not increase comet size. Instead, all three viscogens lowered the total comet intensity, indicating that glycerol and trehalose do not increase lifetimes by enlarging GTP caps (Figure 2.8). To separate changes in comet intensity from changes in microtubule growth rate, we plotted total comet intensity as a function of microtubule growth rate. This way, we could clearly compare control microtubules grown at 1.0 cP to those grown in the presence of viscogens at 1.5 cP, without confounding differences in growth rates (Figure 2.9). Again, EB3 comets were significantly dimmer in the presence of glycerol, trehalose, or BSA, even when controlling for growth rate (as confirmed by a one-way ANOVA and Dunnett's multiple comparisons test on the results of a linear regression for each viscogen, glycerol $p \leq 0.001$, trehalose $p \leq 0.01$, and BSA $p \leq 0.001$). These results clearly indicate that EB3 comet intensity is correlated with growth rate, not with lifetimes. It is therefore unlikely that glycerol and trehalose increase microtubule lifetimes by increasing GTP-cap size.

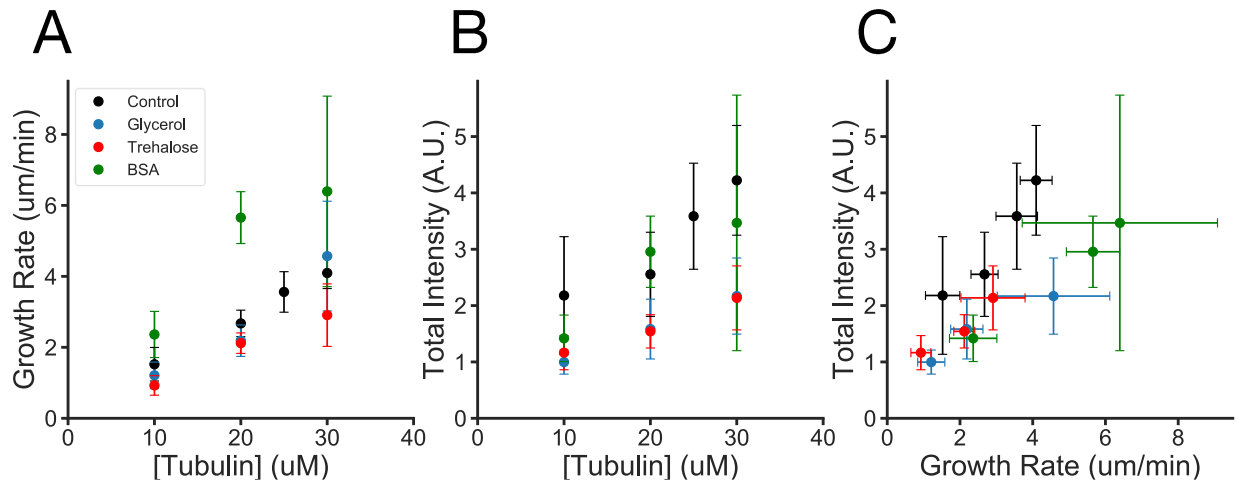


Figure 2.9 EB comet intensity increases with microtubule growth rate

A. Growth rates at increasing tubulin concentrations measured by TIRF microscopy of EB3-GFP signal on the growing ends. B. Total intensity of aligned and averaged EB3-GFP comets measured by TIRF microscopy at increasing tubulin concentrations. C. Total intensity of aligned and averaged EB3-GFP comets as a function of microtubule growth rate. At 1.5 cP, comet intensity is decreased compared to control (1.0 cP), even at comparable growth rates. Data represent means \pm standard deviation of at least 25 comets from 2-6 experiments for each condition. A linear regression was used to fit a line to the data from each condition and a one-way unpaired ANOVA test and Dunnett's multiple comparisons test confirmed that each viscosogen significantly lowered the slope of the line compared to control (glycerol $p \leq 0.001$, trehalose $p \leq 0.01$, and BSA $p \leq 0.001$).

In summary, these experiments show two things. First, that increasing viscosity lowers EB3 comet brightness. While one explanation is that viscosity increases GTP hydrolysis rates and makes GTP caps smaller, a more likely explanation is that increased viscosity slows EB binding to the GTP cap. Simulations of EB binding suggest that a decrease in EB on-rate would indeed result in lower EB comet brightness, as we observe in our experiments when we increase viscosity (Gonzalez et al., 2022). Thus, GTP cap size is not detectably affected by increased viscosity. Second, EB comet brightness is correlated with growth rates, not lifetimes, as demonstrated by glycerol and trehalose decreasing comet brightness and slowing growth rates while extending

lifetimes. Thus, glycerol likely stabilizes microtubules by slowing some post-hydrolysis conformational change. Since glycerol slows the transition more effectively than trehalose, the size scale of the conformational change in question is likely in the range of 3-4 Å.

2.2.5 Viscosity promotes templated nucleation

The experiments above have demonstrated that viscosity changes the relationship between tubulin concentration, growth rate, shrinkage rate, GTP hydrolysis, catastrophe, and rescue. One phase of dynamic instability that is particularly sensitive to each of these variables is microtubule nucleation. Indeed, microtubule nucleation is known to be a kinetically unfavorable process which can be facilitated by suppression of catastrophe (Roostalu & Surrey, 2017; Wieczorek et al., 2015). Since glycerol suppressed catastrophes and promoted rescues more than trehalose or BSA, we wondered whether these effects might explain glycerol's ability to promote nucleation (Keates, 1980; Voter & Erickson, 1984), as demonstrated by its use in tubulin purification protocols (Ashford & Hyman, 2006; Gell et al., 2011).

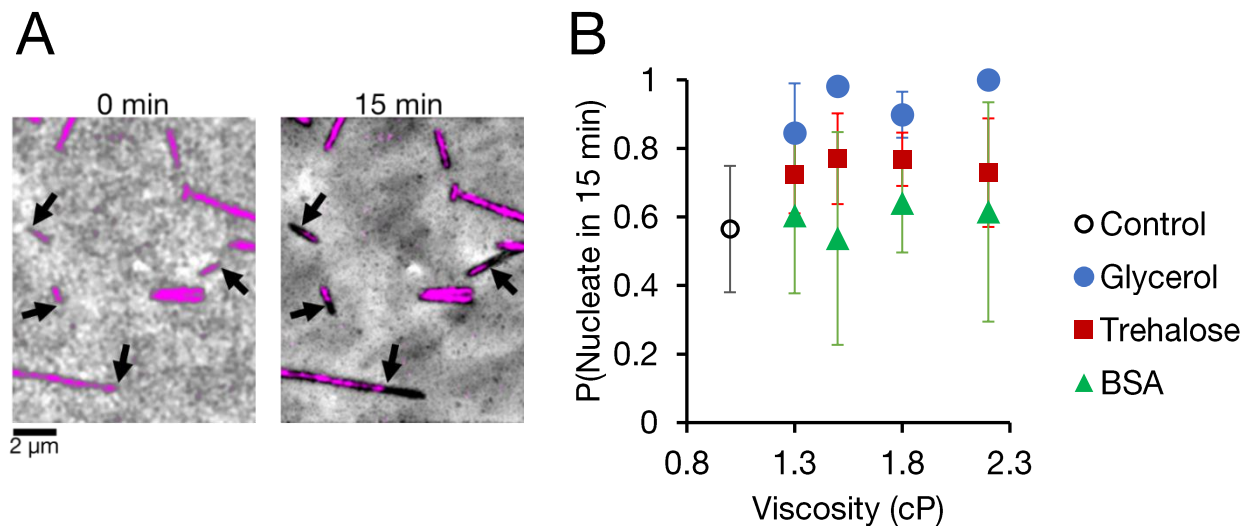


Figure 2.10 Small viscogens increase the probability of templated nucleation

A. Representative field of view of GMPCPP seeds (pseudocolored in magenta) before tubulin addition (left) and 5 minutes after tubulin addition (right). Dynamic microtubules in black. Arrows indicate seeds that nucleated. B. Probability to nucleate in 15 min for GMPCPP seeds in the presence of viscogens. The probability to nucleate is calculated as the ratio between the number of seeds that nucleated in 15 min and the total number of seeds in the field of view. An unpaired one-way ANOVA test confirmed that glycerol increased the probability to nucleate in 15 min, $p = 0.0013$, while trehalose and BSA did not, $p = 0.2402$ and $p = 0.9842$, respectively.

To determine how viscosity affects templated microtubule nucleation, we measured the probability for GMPCPP seeds to nucleate in the presence of our three viscogens, as well as the time lag between tubulin addition and microtubule nucleation. First, the probability to nucleate is calculated as the number of seeds that nucleated in a given time window over the total number of seeds in the field of view. While all three viscogens did increase the probability to nucleate in 15 min, glycerol had a stronger effect than trehalose and BSA. We also measured the time required for each seed to nucleate, i.e., the time between addition of soluble tubulin and the start of microtubule growth. Increasing viscosity from 1.0 cP to 2.2 cP with glycerol reduced the mean

nucleation lag time from 7.9 ± 4.9 min (mean \pm SD, $n = 64$) to 3.2 ± 1.7 min (mean \pm SD, $n = 59$, $p < 0.0001$, Kolmogorov-Smirnov test). The mean nucleation lag times is instead reduced to 5.0 ± 4.0 min (mean \pm SD, $n = 49$, $p = 0.0580$, Kolmogorov-Smirnov test) in the presence of trehalose and 7.243 ± 8.219 min (mean \pm SD, $n = 58$, $p = 0.5891$, Kolmogorov-Smirnov test) in the presence of BSA. In addition, the cumulative distributions of nucleation times show that glycerol significantly shifts the distributions to the left, towards shorter nucleation times, or faster nucleation. In comparison, trehalose and BSA also shift the distributions to the left, but to a lesser extent than glycerol does. The ability of glycerol and trehalose to suppress catastrophe and promote rescues is likely contributing to their ability to promote nucleation, likely by stabilizing early nucleation intermediates building on GMPCPP seeds. BSA, on the other hand, may be relying on its ability to slow shrinkage while accelerate growth to promote nucleation to a lesser extent than trehalose and glycerol.

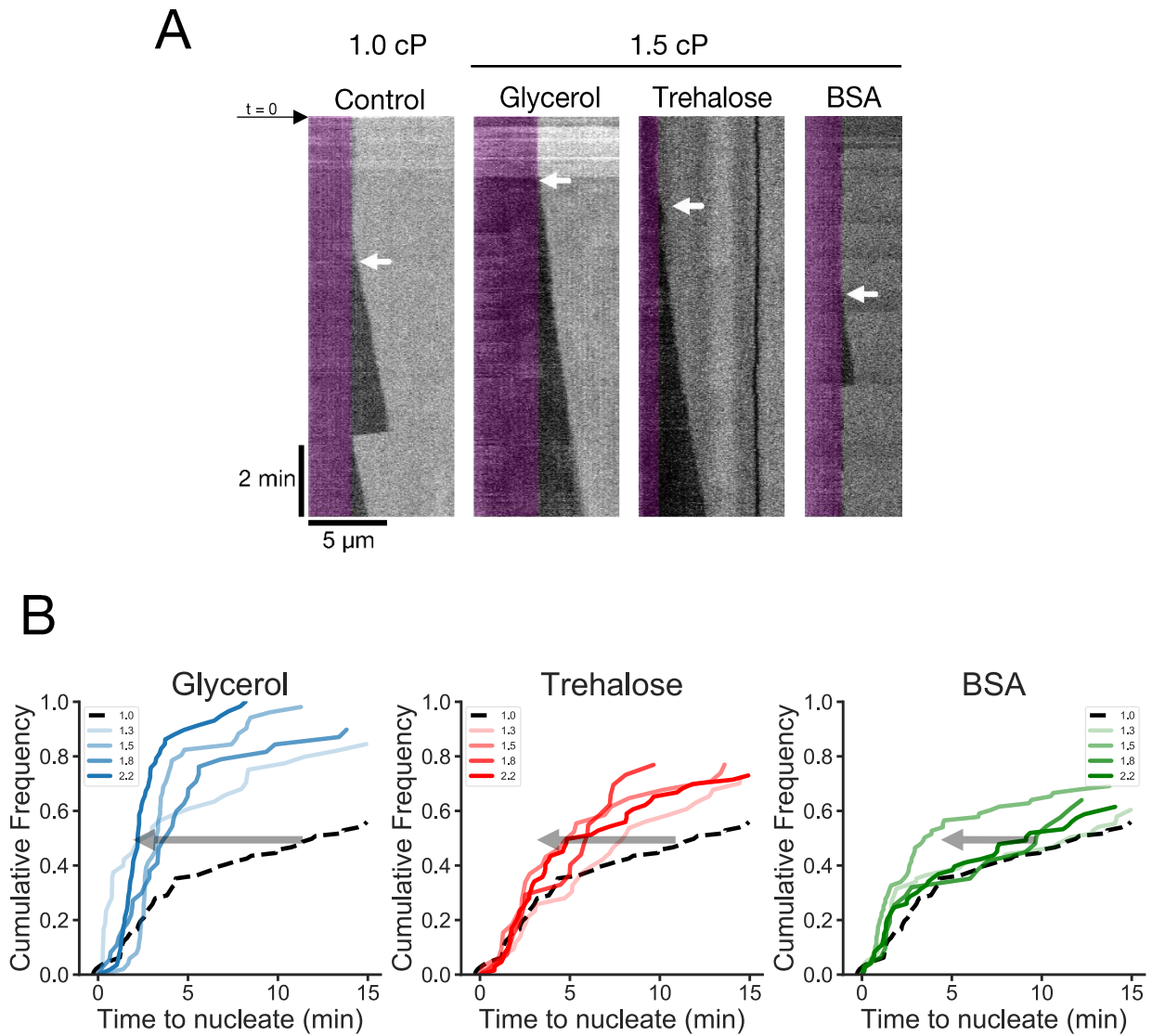


Figure 2.11 *The lag time to templated nucleation is sensitive to viscosity and viscogen size*
 A. Representative kymographs of microtubules growing from stable GMPCPP seeds (pseudocolored in magenta) at 5 μM tubulin. The lag time to nucleation is measured as the time between tubulin addition to the channel (t = 0) and the start of microtubule growth (white arrows). C. Cumulative distributions of nucleation lag times at increasing viscosities at 5 μM tubulin with three different viscogens. Glycerol shifted the distribution of nucleation times to the left, towards faster nucleation. Trehalose and BSA also shifted the distribution, but to a lesser extent. A Brown-Forsythe ANOVA test was used to confirm that glycerol significantly shifted the distribution of nucleation lag times ($p < 0.0001$) while trehalose and did not ($p = 0.0609$, and $p = 0.0888$, respectively).

2.2.6 Spontaneous nucleation is sensitive to viscosogen size

To measure the effects of viscosity on spontaneous nucleation, we used a microtubule pelleting assay (Figure 2.12). In this assay, tubulin is incubated at 37 °C with GTP and left to polymerize for 1 hour. After the incubation, the solution is centrifuged to separate any polymerized microtubules from the remaining soluble tubulin in the supernatant. We used SDS-PAGE and Coomassie staining to quantify the tubulin concentration in the supernatant and the pellet for each reaction. We refer to the minimal amount of tubulin required to spontaneously nucleate microtubules as the “critical concentration”. When tubulin is incubated at concentrations above the critical concentration, microtubules will be nucleated and recovered in the pellet. Modifications that promote microtubule nucleation will shift the critical concentration left, towards lower values, and modifications that impede nucleation will shift the critical concentration to the right, towards higher values (Figure 2.12 A).

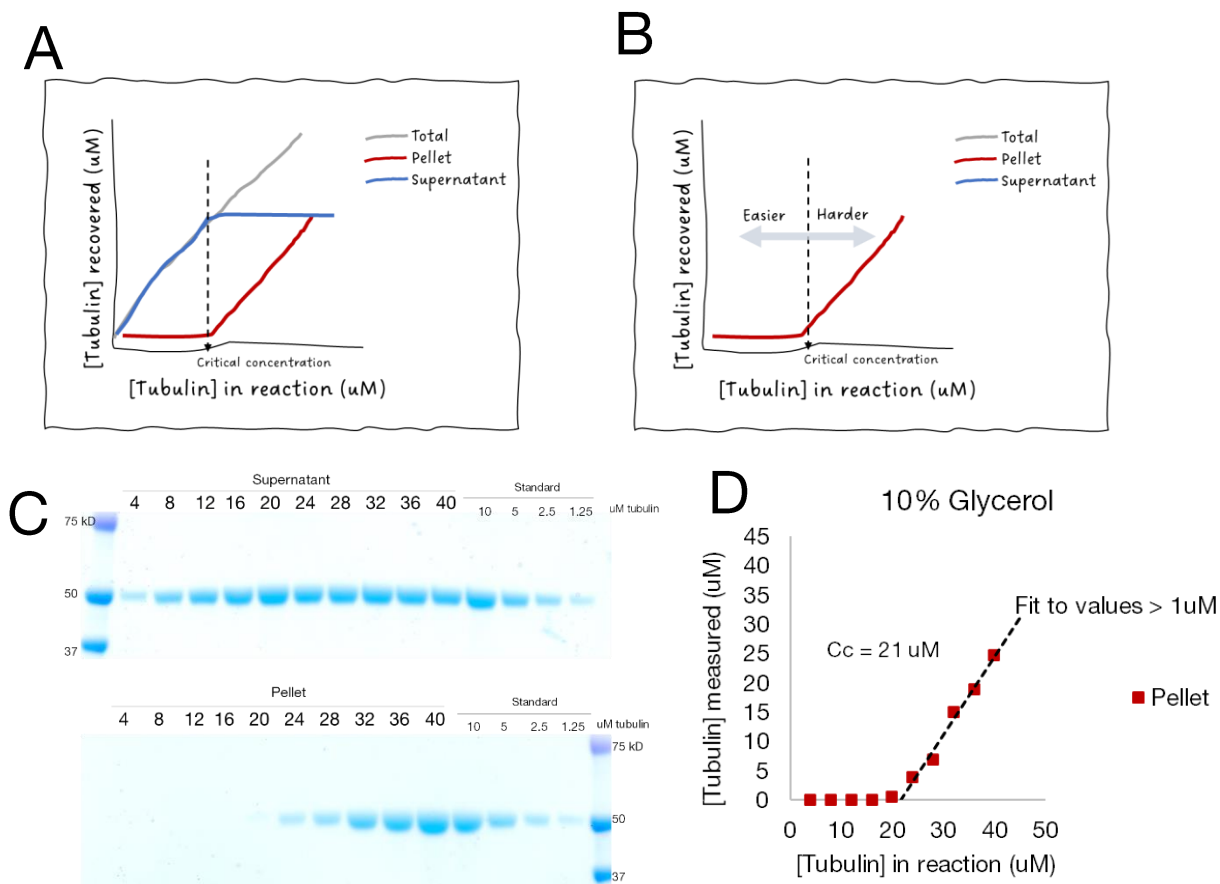


Figure 2.12 Pelleting assay for measuring spontaneous nucleation.

A. Conceptual schematic of the pelleting assay. When the concentration of tubulin in the reaction is higher than the critical concentration, the concentration of tubulin recovered in the pellet will increase, while the concentration of tubulin in the supernatant will plateau.

B. Conceptual schematic demonstrating that modifications that shift the critical concentration to the left, towards lower tubulin concentrations, make nucleation easier, while modifications that move the critical concentration to the right, towards higher tubulin concentrations, make nucleation harder.

C. Representative gel of supernatant samples and pellet samples stained with Coomassie. D. Quantification of the pellet bands on the gel in C. The critical concentration is calculated by fitting a line to the data points above a threshold. In this case $1\mu\text{M}$.

We determined the critical concentration by calculating the x-axis intercept of the tubulin concentration measured in the pellet versus the tubulin concentration in the reaction. Specifically, the x-axis intercept was calculated from a linear fit to data points above $> 1 \mu\text{M}$ (Figure 11C). We repeated this technique in control buffer (1.0 cP) and then at increasing concentrations of glycerol. Consistent with historical data, glycerol greatly lowered the critical concentration for spontaneous nucleation, especially at high viscosities. Tubulin purification or cycling protocols, for example, call for 33% glycerol (3.0 cP) to promote microtubule stability during these preparations (Ashford & Hyman, 2006). At 33% glycerol, the critical concentration for spontaneous nucleation is reduced from around $21 \mu\text{M}$ to as low as $4 \mu\text{M}$ (Figure 12), consistent with previous data (Voter & Erickson, 1984).

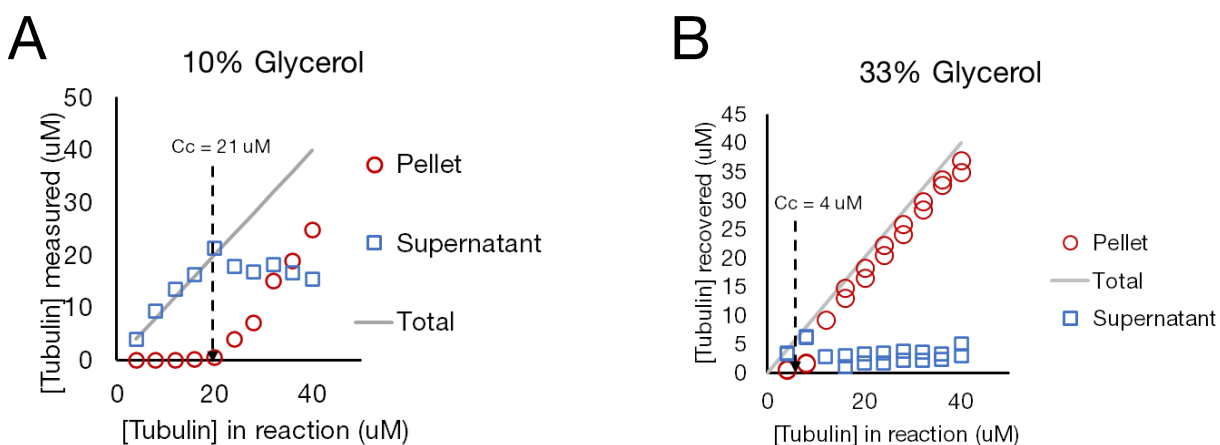


Figure 2.13 Glycerol lowers the critical concentration for spontaneous nucleation.

Representative datasets for a pelleting assay performed with 10% glycerol (1.5 cP) (left) or 33% glycerol (3.0 cP) (right). By increasing the viscosity with glycerol, the critical concentration for spontaneous nucleation goes down from $21 \mu\text{M}$ to $4 \mu\text{M}$.

We then compared glycerol to trehalose in their abilities to promote spontaneous nucleation. At 3 cP, a viscosity at which glycerol lowers the critical concentration by 5-fold, trehalose on the other hand has little to no effect on spontaneous nucleation. At the same viscosity, BSA may slightly promote spontaneous nucleation (see methods for caveats) but not nearly to the degree that glycerol does (Figure 13).

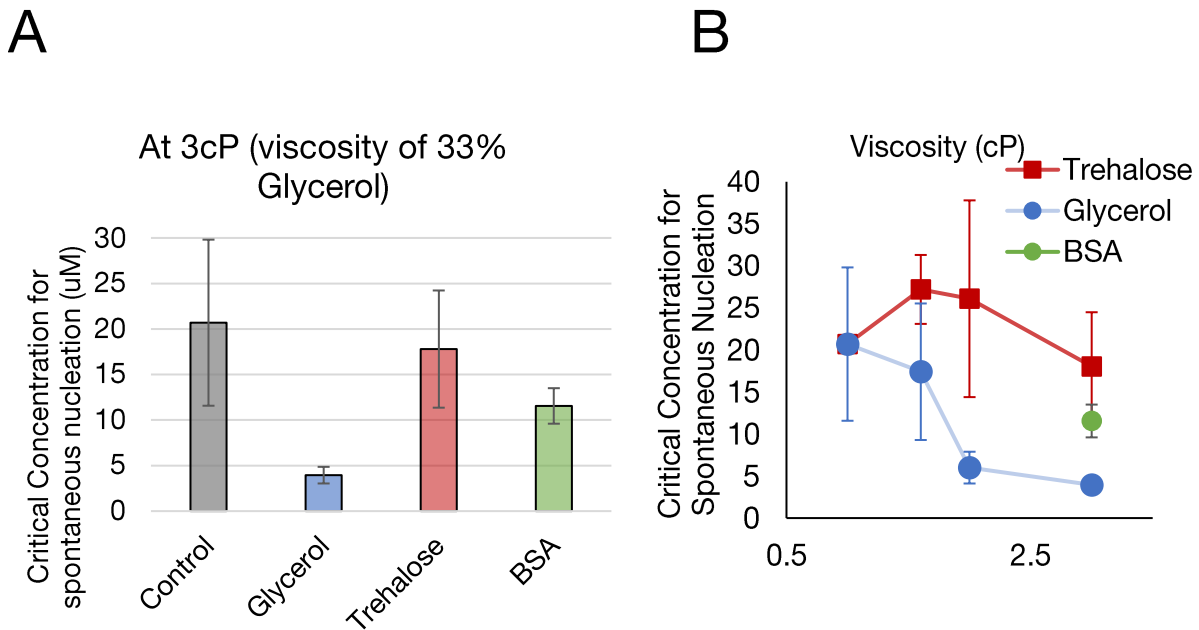


Figure 2.14 Glycerol significantly lowers the critical concentration for spontaneous nucleation.

A. Critical concentration for spontaneous nucleation in different viscogens at 3.0 cP, compared to the 1.0 cP control. Glycerol lowers the critical concentration 5-fold. B. Critical concentration as a function of viscosity in different viscogens. Glycerol lowers the critical concentration at lower viscosities and reduces it up to 5-fold.

Since glycerol far outperforms trehalose in its ability to promote spontaneous nucleation, it is likely that it does so because of its suppression of catastrophes and promotion of rescues. Early oligomers of tubulin that form during spontaneous nucleation are very unstable and can disassemble quickly (Kuchnir Fyngenson et al., 1995; Rice et al., 2021; Voter & Erickson, 1984). Glycerol could therefore be promoting nucleation by preventing the disassembly of these fragile intermediates by preventing catastrophes and promoting rescues in the event of a rare catastrophe. Since trehalose is far weaker at suppressing catastrophes and promoting rescues, it is little help when it comes to forming a microtubule from soluble tubulin. In the case of BSA, nucleation may be promoted because of the macromolecular crowding effects of this large crowder accelerating tubulin assembly.

2.2.7 Glycerol stabilizes microtubules in the absence of tubulin

Glycerol has a surprisingly strong stabilizing effect on microtubules. This is particularly evident by the increase in microtubule lifetime and frequency of rescues in the presence of glycerol. Since there are so few catastrophes at higher glycerol concentrations, it became virtually impossible to measure shrinkage rates at glycerol concentrations above 15 %. Measurements of microtubule dynamics were made even more difficult because, as demonstrated above, glycerol lowers the critical concentration for spontaneous nucleation. At high glycerol concentrations, the field of view quickly gets overtaken by spontaneously nucleated microtubules. Therefore, to measure the effect of glycerol on microtubules at higher viscosities, we used a solution exchange experiment. First, microtubules were grown at 10 μ M tubulin at a low glycerol concentration (10%). Then, the tubulin was washed out by exchanging the buffer for one containing a given

glycerol concentration and no tubulin. This way, we could measure shrinkage rates of microtubules at high glycerol concentrations (Figure 2.15).

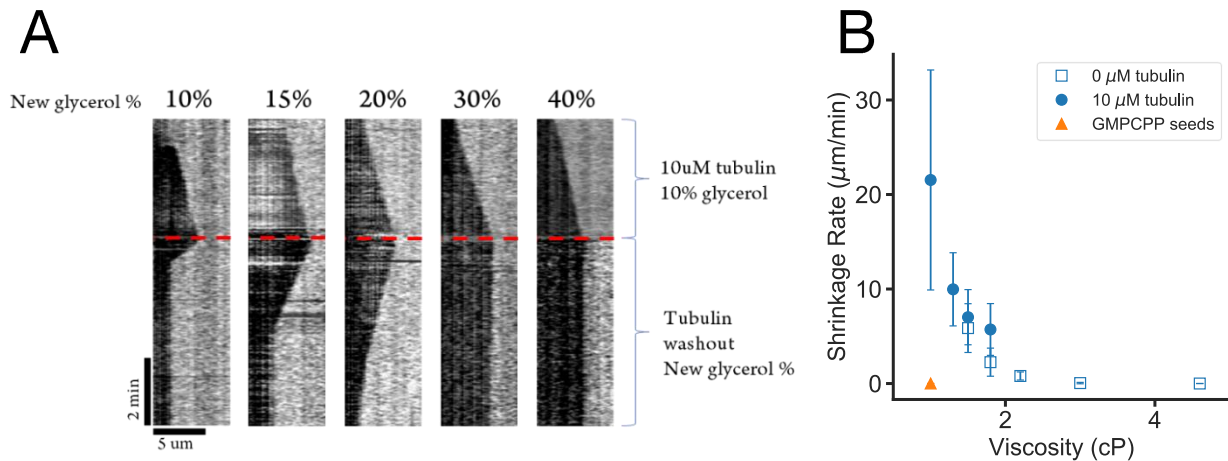


Figure 2.15 Glycerol slows shrinkage even in the absence of tubulin.

A. Representative kymographs of washout experiments. Upper half: microtubules growing at 10 μM tubulin and 10% glycerol (1.5 cP). Lower half: buffer is exchanged for one containing no tubulin and the indicated final concentration of glycerol. Dashed red line marks time of buffer exchange. B. Quantification of microtubule shrinkage rates before and after tubulin washout at the indicated glycerol concentration. At high enough viscosities, glycerol stops microtubule shrinkage altogether.

Strikingly, at concentrations above 30% glycerol (~3 cP), microtubules do not undergo any catastrophes. The shrinkage rate of these microtubules was $> 0.01 \mu\text{m}/\text{min}$, comparable to that of GMPCPP seeds. This observation further explains why glycerol is so effective at promoting microtubule polymerization during tubulin purifications. First, the critical concentration for nucleation is drastically lowered, meaning that small nucleation intermediates can bind more and more tubulin rather than disassembling. Second, once microtubules do form and start to grow, they rarely undergo catastrophe. Third, even if the GTP cap is lost, glycerol can slow shrinkage to the point where tubulin in solution has plenty of time to bind to the tip and induce a rescue.

2.3 Discussion

In this chapter, we have shown the dependence of reaction rates on viscogen size for each phase of dynamic instability. For the first time, we have measured the effects of viscosity on all phases of dynamic instability at the single-filament level. Consistent with previous reports, we showed that small viscogens slow growth rates while large crowders accelerate growth (Figure 2.3) (Molines et al., 2022; Wieczorek et al., 2013). To the best of our knowledge, we show for the first time the effect of viscosity on microtubule shrinkage, with viscogens of all sizes slowing shrinkage (Figure 2.4). Somewhat surprisingly, we show that the frequencies of transitions (catastrophes and rescues) are particularly sensitive to viscogen size. Indeed, the smallest viscogen used, glycerol (3 Å), is far more effective than a slightly larger viscogen, trehalose (4 Å), at suppressing catastrophes and promoting rescues (Figure 2.5 and 2.6), allowing it to strongly promote nucleation, both templated and spontaneous (Figure 2.10 and 2.14). The difference in the effects of glycerol and trehalose on microtubule lifetimes suggest that catastrophes are limited by a small conformational change in tubulin on the order of 3 Å. But what exactly is this conformational change in tubulin that limits the transition to catastrophe?

One hypothesis is that glycerol slows the post-hydrolysis compaction of tubulin more effectively than trehalose. Indeed, comparisons of cryo-EM structures of GDP and GMPCPP microtubules suggests that tubulin undergoes a longitudinal compaction from 84 to 82 Å following GTP hydrolysis (Alushin et al., 2014; R. Zhang et al., 2018; X. Zhang et al., 2015). Longitudinal compaction of tubulin is thought to create strain in the lattice because of the asymmetry in the movements in the dimer (Manka & Moores, 2018). Compaction is therefore proposed to weaken lateral bonds while strengthening longitudinal bonds. Thus, small viscogens like glycerol may slow catastrophe by slowing tubulin compaction.

An alternative hypothesis is that viscosity prevents catastrophe by slowing an intermediate state in the path from straight to curved tubulin. In order for tubulin dimers to curve outward during catastrophe, they first need to start breaking lateral bonds. Increased viscosity may be slowing catastrophe by preventing small conformational changes in tubulin that cause the breaking of lateral bonds and allow tubulin to start curving. Many computational models highlight the importance of modulating lateral bond strength as a function of GTP hydrolysis to describe dynamic instability (Alexandrova et al., 2022; Coombes et al., 2013). Specifically, some models describe the implications of “cracks” in the lattice, or regions where lateral bonds are broken between joining protofilaments (Li et al., 2014; Margolin et al., 2011). This suggests that there are intermediate conformations of tubulin between the fully straight and fully curved structures that can be seen by cryo-EM and crystallography.

Mutations in tubulin can produce similar effects as those we observed in the presence of small viscogens. In 2015, Geyer et al. showed that a point mutation in yeast tubulin, T238A, increased lifetimes without significantly changing growth rates. Like glycerol, this mutation also slowed shrinkage rates and increased the frequency of rescues. T238A was shown to dampen post-hydrolysis conformational changes, uncoupling tubulin’s GTPase cycle from its conformation cycle. Specifically, the authors proposed that T238A was slowing the compaction of tubulin following GTP hydrolysis. This was supported by the localization of the yeast homologue of EB1, Bim1. On wild type microtubules, Bim1 bound specifically to the ends of growing microtubules, at the GTP-cap. On T238A microtubules though, Bim1 bound all over the lattice. The T238A mutation therefore slowed the transition from an expanded “GTP-like” conformation to a compacted “GDP-like” conformation, despite no measured change in the GTPase activity compared to wild type.

These results are in contrast with our data on the effect of viscosogens on EB3 binding. In the presence of viscosogens, EB3 comets are not significantly larger, and in fact appear dimmer (Figure 2.9). EBs have been shown to bind preferentially to microtubules in the expanded state, and dissociate following tubulin compaction in the lattice after GTP hydrolysis (LaFrance et al., 2021; R. Zhang et al., 2018). Since we observed dimmer EB3 comets in the presence of viscosogens, we conclude that viscosity does not affect tubulin compaction enough to change EB3 comet dynamics. Thus, the ability of small viscosogens to increase lifetimes, rescue frequency, and nucleation times despite slowing growth rates is likely unrelated to the expansion-compaction dynamics of tubulin in the microtubule lattice. Therefore, tubulin compaction is likely not the rate-limiting conformational change leading to catastrophe.

We therefore favor a mechanism by which catastrophe occurs as a result of many small conformational changes in the tubulin in the lattice. Recent work with the protein CLASP suggest that some MAPs may promote rescue and suppress catastrophe by stabilizing a metastable intermediate curved conformation of tubulin at microtubule ends (Lawrence et al., 2022). We therefore propose that small viscosogens like glycerol slow the transition between straight and curved tubulin, stabilizing an intermediate state that may include the loss of lateral bonds.

In the future, it will be important to ensure that the differences observed between the effects of glycerol and trehalose are specifically due to differences in viscosogen size, and not from other properties of these different molecules used here as viscosogens. One possible way to address this question would be to use viscosogens of similar size ranges but with different chemical properties. Our preliminary observations using ethylene glycol instead of glycerol and sucrose instead of trehalose suggest that a similar difference in effect is observed with these two alternative viscosogens. Further characterization of alternative viscosogens will be needed to fully rule out the

hypothesis that factors other than size distinguish glycerol and trehalose in their ability to suppress microtubule catastrophe.

2.4 Methods

2.4.1 Tubulin purification

Tubulin was purified from juvenile bovine brains via cycles of polymerization and depolymerization, as described previously (Ashford & Hyman, 2006) except that the chromatography column used after the third cold centrifugation contained Fractogel EMD SO_3^- (M) resin, not Whatman P11 Phosphocellulose resin (this resin has been discontinued). Briefly, the brains were homogenized in a chilled blender and clarified by centrifugation, followed by filtration through cheese cloth. The purification cycles involve (1) microtubule polymerization at 35°C, (2) isolation of the polymer by centrifugation at 35°C, (3) depolymerization of the polymer at 4°C, and (4) removal of debris by centrifugation at 4°C. This cycle was repeated, and tubulin from the final cold centrifugation step was loaded onto a column. The pooled tubulin eluate was flash frozen in liquid nitrogen and stored at -80°C until aliquots of this eluate were subjected to an additional cycle of polymerization and depolymerization, and frozen as concentrated tubulin aliquots for use in experiments. Purity was determined by SDS-PAGE (data not shown) and concentration was determined by absorbance at 280 nm with a DS-11 FX spectrophotometer (DeNovix, Inc.).

2.4.2 Microtubule growth reconstitution assay

To visualize microtubule growth *in vitro*, we used a reconstitution assay to grow dynamic microtubules from surface-bound, stabilized microtubule seeds (Gell et al., 2010). Cover glass was

cleaned, as previously described (Helenius et al., 2006), with the exception that, after soaking in acetone and sonicating in 50% methanol then 0.5M KOH, cover glass was treated with plasma for 3 min in a plasma oven (Plasm Etch) instead of treatment with piranha solution. Cleaned cover glass was silanized by soaking in 0.1% Dichlorodimethylsilane (DDS) in n-Heptane and sonicated in n-heptane then ethanol before rinsing with water and drying with nitrogen gas before storage. Two silanized cover glasses (22 x 22 mm and 18 x 18 mm) were separated by multiple strips of double-sided tape on custom-machined mounts to create channels for solution exchange.

GMPCPP-stabilized MT seeds were prepared by polymerizing a 1:4 molar ratio of tetramethylrhodamine (TAMRA, ThermoFisher Scientific) labeled:unlabeled tubulin (Hyman, 1991) in the presence of GMPCPP (Jena Biosciences) in two cycles, as described previously (Gell et al., 2011). Channels were prepared for experiments by flowing in anti-TAMRA antibodies (ThermoFisher Scientific) and blocking with 1% Pluronic F-127 for 20 min. Channels were rinsed three times with BRB80 before flowing in seeds and placing the chamber on the microscope stage, where the objective was heated to 34 °C with a CU-501 ChamSlide lens warmer (Live Cell Instrument).

For consistency, an aliquot of tubulin was thawed on the day of each experiment, sub-aliquoted, and stored in liquid nitrogen. A separate sub-aliquot was thawed right before each individual experiment. Dynamic microtubules were grown from GMPCPP seeds by filling the channel with reaction buffer: BRB80 (80 mM PIPES-KOH pH 6.9, 1 mM EGTA, 1 mM MgCl₂), 1 mM GTP, 0.1 mg/mL BSA, 10 mM dithiothreitol, 250 nM glucose oxidase, 64 nM catalase, 40 mM D-glucose, and the indicated concentration of tubulin and viscogen. Viscogens were stored in concentrated stock solutions in BRB80 and added to the indicated final concentrations.

2.4.3 Viscosity measurements

Viscosity of glycerol, trehalose, and BSA solutions was measured using an mVROC Viscometer (Rheosense) at room temperature (23°C as measured by the viscometer). Measurements were made at a flow rate of 1000 $\mu\text{l}/\text{min}$ for 5 sec for three replicates of each solution. Concentrated stock solutions of each viscogen were used to achieve the desired viscosity.

2.4.4 Interference reflection microscopy

For IRM imaging (Mahamdeh & Howard, 2019), a 50/50 mirror (Chroma) was installed inside a filter cube of a Zeiss Axiovert Z1 microscope chassis with a 100X 1.45 NA Plan-apochromat objective lens. A 440 nm LED from a pE-100 illumination system (CoolLED) was used to illuminate the sample, and images were captured on an Andor Neo sCMOS camera with a pixel size of 63 nm. The aperture iris and field diaphragm were adjusted manually to optimize contrast. Time-lapse image sequences were acquired at 1 sec intervals for 30 minutes. The contrast was optimized such that averaging of images between time points was not necessary. Image acquisition was controlled using MetaMorph (Molecular Devices). After each experiment, a background image was generated from the median of 200 images acquired while moving the sample stage. This background image was subtracted from image sequences to increase contrast before analysis.

2.4.5 Analysis of microtubule dynamics

Microtubule dynamics were analyzed by manually fitting “multi-segmented lines” to kymographs of growing microtubules using FIJI. Each segment measured either a growth event, a shrinking event, or a pause in between. Sorting of these segments and conversion to lengths, times and rates was done with a custom-built Python script. All statistical testing was carried out in GraphPad Prism.

2.4.6 Microtubule pelleting assay

To determine the effect of viscoogens on spontaneous nucleation of microtubules, we used a pelleting assay (adapted from Mitchison & Kirschner, 1984 and Wieczorek et al., 2015). First, tubulin, at a concentration ranging from 4 μM to 40 μM , was incubated with 1mM GTP in 1X BRB80 on ice for 5 minutes. Then, the tubes were transferred to a heating block and incubated at 35°C for 1 hour. The solution was then transferred to tubes for centrifugation in an airfuge air-driven centrifuge (Beckman) at 30psi at room temperature for 5 minutes. The supernatant was promptly removed, and the pellets were resuspended in 1X BRB80 and incubated on ice at least 10 minutes. Samples were diluted 1:1 with BRB80 and mixed with 2X SDS-PAGE loading buffer. Samples were boiled for 10 minutes and loaded onto a 4-12% SDS-PAGE gel (GenScript). The gel was run at 140 V for 1 hour, then rinsed with water and stained with Coomassie for 1 hour. Gels destained in a 10% acetic acid solution overnight. The intensity of the bands was analyzed with the “Gels” analysis tool in FIJI (Schindelin et al., 2012). To determine the critical concentration for spontaneous nucleation, the x-axis intercept was calculated from a line of fit to all points $> 1 \mu\text{M}$.

2.4.7 Buffer exchange

Before exchanging the buffer in the channel, microtubules were grown from 10 μM tubulin in BRB80 buffer with 10% glycerol at 32 °C for at a few minutes. Then, the buffer was manually exchanged using a pipette and a piece of filter paper. The buffer exchange happened quickly < 1 minute. The final buffer contained 0 μM tubulin and the indicated concentrations of glycerol.

2.4.8 EB3-GFP purification

The coding sequence for EB3 was inserted into a modified pHAT vector containing an N-terminal 6xHis-tag followed by a PreScission site and a carboxy-terminal EGFP followed by a

Strep-tag II (Bechstedt & Brouhard, 2012). Recombinant EB3 was expressed and purified as described with a few minor modifications (Chaaban et al., 2018; Wieczorek et al., 2013). Briefly, EB3 was expressed overnight in BL21(DE3) cells at 18 °C, then harvested by centrifugation and cell lysis using an EmulsiFlex-C5 (Avestin). Then, EB3 was purified through His60 Ni Superflow resin (Takara Bio Inc.) and eluted from the column by cleavage of the His-tag at the PreScission site. His-tag cleavage was achieved by incubating the resin overnight with PreScission protease at 4 °C. The cleaved EB3 was then applied to a StrepTactin Sepharose column from which it was eluted with wash buffer (100 mM Tris-HCl, 150 mM NaCl, 1 mM EDTA, pH 8.0) containing 2.5 mM desthiobiotin and 10% glycerol. Protein purity and concentration were assessed by SDS-PAGE, and by absorbance at 488 nm with a DS-11 FX spectrophotometer (DeNovix, Inc.).

2.4.9 EB comet imaging and analysis

To image EB comets, dynamic microtubules were prepared using the standard reaction mix (80 mM PIPES-KOH pH 6.9, 1 mM EGTA, 1 mM MgCl₂), 1 mM GTP, 0.1 mg/mL BSA, 10 mM dithiothreitol, 250 nM glucose oxidase, 64 nM catalase, 40 mM D-glucose). EB3-GFP was added to this mix at 30 nM along with 50 mM KCl to promote preferential binding to the GTP cap, and as well as 0.1 % methylcellulose to minimize fluctuations of growing microtubule ends. To promote protein stability, EB3-GFP aliquots were thawed and kept on ice rather than freezing sub-aliquots and thawing one out for each experiment, as is the case with tubulin.

Time lapse images of EB comets were acquired at 1 second intervals by TIRF microscopy. Total internal reflection fluorescence (TIRF) was achieved by coupling a 488 nm laser to an iLas2 targeted laser illumination system (BioVision, Inc.) equipped with 360° TIRF. The objective was heated to 34°C with with a CU-501 Chamlide lens warmer (Live Cell Instrument). Images were recorded on an Andor iXon + DV-897 EMCCD camera with a pixel size of 160 nm.

2.4.10 Analysis of EB comets

EB comets were selected manually by clicking on the position of the comet near shortly after it appears and shortly before it disappears (or before the end of the time lapse). After this manual selection, a Python script was used to generate average intensity profiles for each condition.

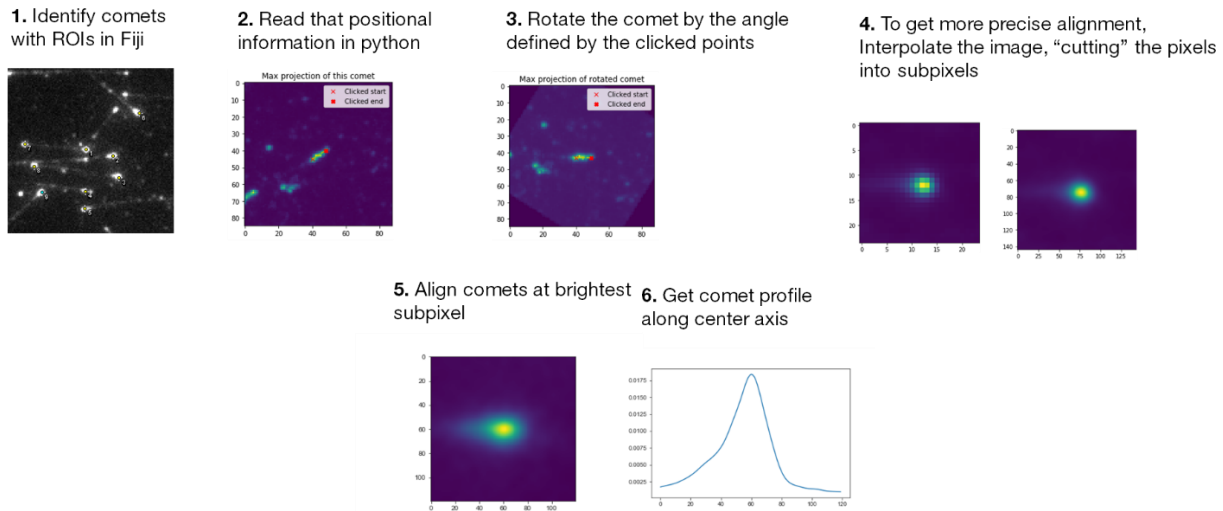


Figure 2.16 Workflow for EB comet analysis

Briefly, for each comet, the manually selected points were used to crop the timelapse around the individual comets. Then, the cropped movies were rotated to align the axis of movement of all comets. Each frame of the cropped movies was interpolated by a factor of 6, to allow for sub-pixel alignment of each frame in the movie at the peak sub-pixel. After background subtraction, these aligned comet timepoints were averaged to each other and combined with the averages of all other comets in that movie to generate average profiles for each condition. The total intensity of each averaged comet was calculated from a line profile 3-pixels wide across the center longitudinal axis of the comet. In these experiments, microtubule growth rate was calculated from the distance in time and space between the manually selected comet positions.

3 The combined effects of DCX and EB3 on dynamic instability

3.1 Introduction

Since the discovery of tubulin, many technological advances have allowed a more and more detailed picture of dynamic instability to form. The identification, purification, and characterization of many MAPs have also provided additional insight into the mechanisms of dynamic instability. A wide array of MAPs regulates and controls microtubule dynamics throughout the cell cycle. Studying the mechanisms of action of these microtubule regulators has taught the field not only about the MAPs themselves, but also about important aspects of dynamic instability intrinsic to microtubules. Here I will discuss a few MAPs that have been instrumental in developing our current understanding of dynamic instability.

3.1.1 XMAP215 and the two-step model for microtubule growth

Originally, microtubule growth was thought of as a single-step reaction where tubulin is bound to a microtubule upon collision with the growing end, with a net growth rate equal to the on-rate constant times the concentration of soluble tubulin (discussed in Chapter 1). However, this model needed to be expanded to explain how microtubule growth could be accelerated by the polymerase XMAP215 (Gard & Kirschner, 1987).

In vitro, XMAP215 accelerated microtubule growth rates by 5-fold, making it the fastest known polymerase at the time (Brouhard et al., 2008). According to a simple one-step model for microtubule growth, a polymerase could act by increasing the rate of tubulin arrival at the tip. Some proposed a mechanism of action where XMAP215 could bind multiple tubulin dimers with

its multiple tubulin-binding TOG domains, effectively increasing the local tubulin concentration at the microtubule end (Gard & Kirschner, 1987; Kerssemakers et al., 2006; Slep & Vale, 2007; Vasquez et al., 1994). However, further work demonstrated that XMAP215 and its homologues bound only a single tubulin dimer (Al-Bassam et al., 2006; Brouhard et al., 2008), and that a single tubulin dimer could bind only a single TOG domain at any given time (Ayaz et al., 2012). The “shuttle” model, by which XMAP215 brings multiple tubulin dimers to the end to accelerate growth, was therefore rejected based on the stoichiometry of XMAP215 and tubulin and the long residence time of XMAP215 at the end of the growing microtubule (Brouhard et al., 2008).

The one-step model for microtubule growth thus does not leave any room for XMAP215 to accelerate growth by “shuttling” tubulin to the growing end. Failure of the one-step model to explain the effects of XMAP215 therefore motivated the expansion to a two-step model. The proposed model involved two steps: first, tubulin is bound loosely to the growing end through a diffusion-limited reaction, forming a collision complex. Then, tubulin undergoes an isomerization, or conformational change, to become tightly incorporated into the lattice. The two-step model was supported by the observation that XMAP215 accelerated not only the growth of microtubules, but also their shrinkage in the absence of soluble tubulin (Brouhard et al., 2008). Structural studies followed a few years later, showing that TOG domains preferentially bind to curved tubulin dimers, suggesting that XMAP215 stabilizes a curved intermediate in the growth reaction (Ayaz et al., 2012, 2014; Brouhard & Rice, 2014).

Though the exact nature of tubulin isomerization during growth is still debated, the idea that microtubule growth is limited by conformational changes independent of tubulin diffusion rates remains. Studies of the polymerase XMAP215 have therefore shaped the way we think about microtubule growth to this day. These studies showed us that there exists an intermediate

conformational state, and thus that microtubule growth is more complex than other biological polymers like actin for example.

3.1.2 EBs and the GTP-cap

End-binding proteins (EBs) have been an important tool in developing our modern understanding of the GTP-cap (see section 1.6.1). The GTP-cap model was originally proposed in the early 1980s (Carlier & Pantaloni, 1981; Mitchison & Kirschner, 1984). At the time, microtubules could only be studied in bulk biochemical assays and electron microscopy snapshots. Later, thanks to video light microscopy, researchers could measure the dynamics of individual microtubules *in vitro* for the first time (Horio & Hotani, 1986; Walker et al., 1988). The ability to observe individual filaments allowed for testing of the GTP-cap model. For example, if the rate of GTP hydrolysis is constant, then increasing microtubule growth rates by increasing tubulin concentration would result in longer microtubule lifetimes, which is indeed what is observed (Walker et al., 1988). Dilution experiments suggested the GTP-cap is small (Voter et al., 1991; Walker et al., 1991), and use of GTP analogues suggested only a few rows of GTP tubulin could be sufficient to stabilize the microtubule (Caplow & Shanks, 1996; Drechsel & Kirschner, 1994). However, without a way of visualizing the GTP-cap, the shape and size of the stabilizing structure could not be measured.

The solution came in the form of end binding proteins (EBs). In cells and *in vitro*, fluorescently tagged EB proteins bind to microtubule ends and produce a characteristic “comet” shaped signal. *In vitro*, EBs were shown to bind differentially to microtubules made from different nucleotide analogues (Maurer et al., 2011; Zanic et al., 2009). EBs had a high affinity for GTP-analogue microtubules, and a low affinity for GDP-microtubules, suggesting that EBs tracked the ends of growing microtubules by recognizing the nucleotide state of the tubulin, i.e. recognizing

the GTP-cap. With this new knowledge about binding preferences of EBs, the field now had a tool to visualize the size of the GTP-cap throughout dynamic instability.

Detailed characterization of EB binding profiles showed that EB comets become longer with increasing growth rates (Bieling et al., 2007; Duellberg, Cade, Holmes, et al., 2016; Maurer et al., 2014). This observation confirmed the hypothesis mentioned above that the GTP-cap is larger when microtubules grow faster. The protective nature of the GTP-cap was also supported by experiments showing that microtubules with larger GTP-caps survived longer than microtubules with shorter GTP-caps when tubulin is removed from solution (Duellberg, Cade, Holmes, et al., 2016; Duellberg, Cade, & Surrey, 2016).

Since fluorescently tagged EBs allowed for visualization of GTP cap size, they provided a tool for better understanding catastrophes and GTP cap loss. If the EB-comet size is a predictor of microtubule stability (Duellberg, Cade, Holmes, et al., 2016), then detailed characterization of EB-comets could uncover underlying GTP-cap dynamics leading up to catastrophe. Indeed, careful study of EB-comet profiles showed that the peak of EB binding is a few nm before the tip of the microtubule (Maurer et al., 2014). This observation revealed three distinct regions on the microtubule, 1) a low-affinity “mature” microtubule body made up of mostly GDP-tubulin 2) a high-affinity end region made up of mostly GTP-tubulin 3) a low-affinity “fresh” region at the distal tip of the microtubule. Thus, tubulin has three distinct conformations in the microtubule with different affinities for EBs.

Interestingly, EBs are well-known catastrophe factors, making them a useful tool for understanding the relationship between the GTP-cap and catastrophe (Vitre et al., 2008; Zanic et al., 2013). When EB concentration is increased, the size of EB-comets decreases, indicating that the size of the high-affinity region at the tip decreases. EB therefore accelerates the transition of

tubulin from a high to a low affinity conformation, catalyzing the destruction of its own binding site (Maurer et al., 2014). Cryo-EM reconstitutions suggest that EBs induce a compaction and a twist of tubulin in the microtubule lattice (LaFrance et al., 2022; Zhang et al., 2015, 2018). Lattice compaction and twisting may therefore be two critical transitions leading to catastrophe. Accelerating these transitions by increasing EB concentration would therefore increase the likelihood of catastrophes, resulting in shorter lifetimes.

Studying their mechanism of action has provided evidence for a nucleotide-dependent stabilizing structure at the ends of growing microtubules that prevents catastrophes until it is lost. EBs have also provided clues as to the structural changes occurring in tubulin leading to catastrophe, such as compaction and twisting. Together, experiments using EBs helped develop our understanding of the relationship between microtubule growth rate, GTP-cap size, and microtubule lifetime. That EBs bind to a region that is hundreds of dimers long suggests the GTP-cap is large (Bieling et al., 2007), in contrast with some earlier models (Voter et al., 1991; Walker et al., 1991). This large GTP-cap disappears moments before catastrophe (Maurer et al., 2014), confirming the importance of the GTP-cap in stabilizing microtubules. Finally, the exponential decay of the comet shaped EB signal at the ends of growing microtubules is consistent with a first order GTP-hydrolysis rate constant (Bieling et al., 2007; Carlier & Pantaloni, 1981).

3.1.3 Combining XMAP215 and EB revealed allostery in the lattice

The *in vitro* study of individual MAPs can provide valuable information about the mechanisms underlying dynamic instability. In cells, however, MAPs do not work alone. They interact with and compete with other MAPs and cytoplasmic components, and they are influenced by the physical properties of their cytoplasmic environment (see Chapter 2). Using multiple MAPs *in vitro* to study their combined effect can yield surprising results and further our understanding

of dynamic instability. For example, the combination of XMAP215 and EB1 yielded surprising synergistic effects, suggesting that MAPs can interact indirectly through allosteric changes in the microtubule itself (Zanic et al., 2013).

On its own, XMAP215 can increase growth rates up to 5-fold (Brouhard et al., 2008; Zanic et al., 2013). EB1 on the other hand has only a modest effect on growth rates, increasing them by up to 50% at comparable concentrations (Molines et al., 2020; Vitre et al., 2008; Zanic et al., 2013). When XMAP215 and EB1 are used together *in vitro*, microtubule growth rates are increased over 30-fold, much higher than the sum of their individual effects (Zanic et al., 2013). Since no direct interaction was found between EB1 and XMAP215 the synergy must occur through allostery in the microtubule itself, i.e. long-range propagation of conformational changes. As discussed above, XMAP215 catalyzes microtubule growth by stabilizing an intermediate complex in the reaction (i.e. the loosely bound tubulin dimer on the end of a growing microtubule). What remains in the growth reaction is for tubulin to isomerize and incorporate into the lattice. Based on the synergy between XMAP215 and EB1, it is likely that EB1 further promotes microtubule growth by facilitating the isomerization step. EB1 could therefore facilitate isomerization by straightening protofilaments and enhancing lateral tubulin bonds (Vitre et al., 2008). The synergistic behavior of XMAP215 and EB1 not only provides additional support for the two-step model for microtubule growth, but also demonstrates that MAPs can interact indirectly by allosterically changing the conformation of the microtubule. This data demonstrates that the microtubule lattice is malleable and that MAPs can modulate each other's activity by producing long-range changes in tubulin conformation along the lattice.

3.1.4 DCX and the nucleotide-independent end structure

EBs are sensitive to the nucleotide state of tubulin, and so have been useful in characterizing the organization of nucleotide-dependent conformations of tubulin at the ends of growing microtubules. However, there are features of the growing microtubule end that are independent of the nucleotide state of tubulin. This became apparent thanks to the protein doublecortin (DCX), shown to recognize curvature in the microtubule lattice.

DCX is a neuronal MAP important for regulating microtubules during neuronal migration and brain development (des Portes et al., 1998; Gleeson et al., 1998). Though the exact mechanism of action of DCX in the brain is still under investigation, work *in vitro* has revealed some of its effects on microtubules. One of the best-known characteristics of DCX is that it strongly promotes microtubule nucleation *in vitro* (Bechstedt & Brouhard, 2012; Moores et al., 2004). In addition, DCX has been shown to specify a 13-protofilament architecture (Moores et al., 2004, 2006), though this specification is not required for nucleation activity, and vice versa. Otherwise, microtubules spontaneously nucleated *in vitro* (i.e. in the absence of any templates) have a range of protofilament numbers, most having 14 (Pierson et al., 1978). This is in contrast to most microtubules found *in vivo* which contain 13 protofilaments, specified by templates such as the γ -TuRC (Chaaban & Brouhard, 2017).

Interestingly, DCX shares a lot of similarities with EBs (Table 1). For example, they both share a binding site at the vertex of four tubulin dimers (Fourniol et al., 2010; Maurer et al., 2012), and compact the lattice (Manka & Moores, 2018; R. Zhang et al., 2015, 2018). In addition, like EBs, DCX also tracks growing microtubule ends *in vitro* (Bechstedt et al., 2014; Bechstedt & Brouhard, 2012). However, unlike EBs, DCX follows growing ends in a manner independent of nucleotide state. Indeed, DCX does not preferentially bind to microtubules made with GTP

analogues, unlike EB (Bechstedt et al., 2014). This difference in ability to recognize or prefer nucleotide states is likely due to the differences between the contacts made with DCX or EB with the microtubule. Though DCX and EB share a binding site, EB makes additional connections with the nucleotide binding pocket that DCX lacks (specifically, through the H3 helix of β -tubulin) (Fourniol et al., 2010; Maurer et al., 2012).

In contrast to EB comets, the size of DCX comets is independent of microtubule growth rates, and increases with DCX concentration (Bechstedt et al., 2014). Therefore, DCX must recognize a feature of the growing end that is distinct from lattice and independent of tubulin nucleotide state. Though the exact structure of the growing microtubule end is still up to debate, the presence of curved tubulin structures (either sheets or individual/double protofilaments) at the ends is generally accepted (Brouhard & Rice, 2018; Chretien et al., 1995; Cleary & Hancock, 2021; V. J. Farmer & Zanic, 2022; Mandelkow et al., 1991; McIntosh et al., 2018) (see section 1.5). Interestingly, DCX preferentially binds to curved regions of stabilized microtubules *in vitro*. In addition, straightening protofilaments at the growing end using the drug taxol abolished DCX's tip tracking behavior (Bechstedt et al., 2014). Together, these observations support a mechanism where DCX recognizes the growing end by preferentially binding to curved tubulin structures. Work on DCX has therefore demonstrated that there are structural features of the growing microtubule end that are independent of nucleotide state.

3.1.5 Combining EB and DCX to untangle nucleation and catastrophe

EB and DCX share many similarities (see Table 1). They both bind at the vertex between four tubulin dimers (Fourniol et al., 2010; Maurer et al., 2012), specify a 13-protofilament architecture (Moores et al., 2004; Vitre et al., 2008), and compact the microtubule lattice (Manka & Moores, 2018; R. Zhang et al., 2015, 2018). They both recognize and track the ends of growing

microtubules, albeit through distinct mechanisms (Bechstedt & Brouhard, 2012; Bieling et al., 2007).

Despite these many similarities, EB and DCX have opposing effects on two phases of dynamic instability: catastrophe and nucleation (see Table 1). As mentioned above, EB is a known catastrophe factor. EB catalyzes GTP hydrolysis, making the GTP-cap smaller and promoting catastrophes (Maurer et al., 2014). Since EB accelerates catastrophes, it also slows microtubule nucleation (Wieczorek et al., 2015). In contrast, DCX is a potent microtubule nucleator (Bechstedt & Brouhard, 2012; Moores et al., 2004, 2006). Since DCX was shown to preferentially bind to curved regions either in a bent lattice or at the end of a growing microtubule (Bechstedt et al., 2014), it is thought that DCX promotes nucleation by stabilizing small curved tubulin nucleation intermediates. Conversely, DCX also stabilizes more mature growing microtubules, reducing the catastrophe frequency (Manka & Moores, 2020; Moores et al., 2006).

Since EB and DCX have opposite effects on catastrophe and nucleation, we wondered what their combined effects would be on microtubule dynamics. We hypothesized that, since the two proteins compete for the same binding site, mixing the two together would result in microtubules with intermediate lifetimes and intermediate nucleation times. However, we do not see an intermediate phenotype. Instead, we measured microtubules with “EB-like” lifetimes and “DCX-like” nucleation times when both MAPs were present, suggesting that EB and DCX do not interact allosterically through the lattice.

Table 2 Comparison of the properties of DCX and EB

DCX	EB
Similarities	
Binds between 4 tubulin dimers (Fourniol et al., 2010)	Binds between 4 tubulin dimers (Maurer et al., 2012)
Compacts the lattice (Manka & Moores, 2018)	Compacts the lattice (Zhang et al., 2015, 2018).
Specifies 13-protofilaments (Moores et al., 2004, 2006)	Specifies 13-protofilaments (Vitre et al., 2008)
Tip tracks independently (Bechstedt et al., 2014)	Tip tracks independently (Bieling et al., 2007)
Increases growth rates (Manka & Moores, 2020)	Increases growth rates (Molines et al., 2020; Roth et al., 2018; Vitre et al., 2008; Zanic et al., 2013)
Slows shrinkage (Moores et al., 2006)	Slows shrinkage (Molines et al., 2020; Vitre et al., 2008; Zanic et al., 2009)
Differences	
Prevents catastrophe (Moores et al., 2006)	Promotes catastrophes (Molines et al., 2020; Vitre et al., 2008; Zanic et al., 2013)
Promotes nucleation (Bechstedt & Brouhard, 2012; Moores et al., 2006)	Prevents nucleation (Wieczorek et al., 2015)
Binds to curved regions (Bechstedt et al., 2014)	No preference for curved regions (Bechstedt et al., 2014)
Comet size insensitive to growth rate (Bechstedt et al., 2014)	Comet size correlated with growth rate (Bieling et al., 2007)
Insensitive to nucleotide state of microtubule (Bechstedt et al., 2014)	Sensitive to nucleotide state of tubulin (Zanic et al., 2009)

3.2 Results

In order to measure the combined effects of DCX and EB3 on microtubule dynamics, we expressed and purified human DCX and EB3 from bacteria. We reconstituted microtubule dynamic instability *in vitro* using the assay described in Chapter 2 (Gell et al., 2010). As described in Chapter 2, we used IRM to visualize unlabeled dynamic microtubules growing from stabilized GMPCPP seeds (Mahamdeh et al., 2018; Mahamdeh & Howard, 2019). By adding either DCX, EB3, or both proteins at once to our *in vitro* assay, we measured the effects on all parameters of dynamic instability.

3.2.1 EB promotes catastrophes and suppresses nucleation

First, we measured the effects of EB3 alone on microtubule dynamics (Figure 3.1 A). We grew microtubules from GMPCPP seed attached to a coverslip with 6 μM soluble unlabeled tubulin and measured the effects of the addition of 10-40 nM EB3. Increasing the concentration of EB3 reduced microtubule lifetimes (Figure 3.1 B-C), in agreement with previous characterizations of EB1 (Molines et al., 2020; Vitre et al., 2008; Zanic et al., 2013). For example, adding 20 nM EB3 reduced lifetimes from 4.9 ± 3.7 min (mean \pm SD, $n = 932$) to 1.5 ± 1.0 min (mean \pm SD, $n = 230$, $p < 0.0001$, Brown-Forsythe ANOVA and Dunnett's multiple comparison test).

If catastrophes of early tubulin oligomers prevent microtubule nucleation, as suggested previously, then a catastrophe factor like EB3 should also suppress nucleation. To test this, we measured the lag time between addition of soluble tubulin and microtubule nucleation from templates (in this case GMPCPP seeds). Indeed, the lag time for templated nucleation increased with increasing concentrations of EB3 (Figure 3.1D-E). Adding 20 nM EB3, for example, increased the mean lag time for templated nucleation from 4.7 ± 5.9 min (mean \pm SD, $n = 263$) to 8.2 ± 7.3 min (mean \pm SD, $n = 39$, $p = 0.0414$, Brown-Forsythe ANOVA and Dunnett's multiple

comparison test). This observation is consistent with a previous characterization of EB1's effects on microtubule dynamics, showing a correlation between short lifetimes and long lag times for templated nucleation (Wieczorek et al., 2015). We conclude therefore that EB3 and EB1 similarly promote catastrophe and inhibit nucleation, and that our purified EB3 is behaving as expected.

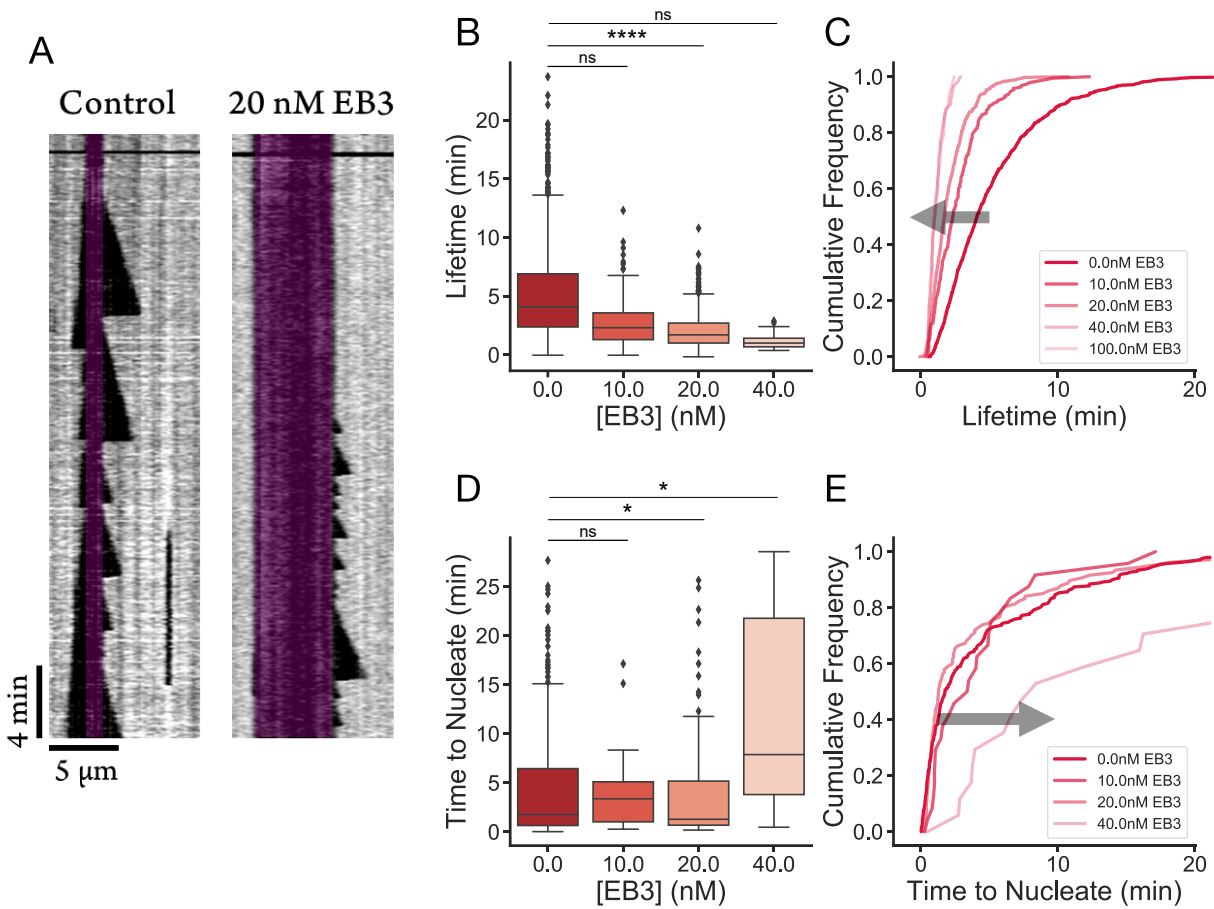


Figure 3.1 EB3 shortens lifetimes and suppresses templated nucleation

A. Representative kymographs of dynamic microtubules growing from stable GMPCPP seeds (pseudocolored in magenta) at 6 μ M tubulin in the absence or presence of EB3. B. Microtubule lifetime as a function of EB3 concentration. Boxplots represent 62-1132 growth events per condition. C. Cumulative distribution of lifetimes for increasing concentrations of EB3 (same data as plotted in B). Adding EB3 shifts the distribution to the left, towards shorter lifetimes. D. Nucleation lag time for microtubules as a function of EB3 concentration. Boxplots represent 18-283 nucleation events per condition. E. Cumulative distribution of nucleation times as a function of EB3 concentration (same data as plotted in D). Adding EB3 shifts the distribution to the right, towards longer nucleation times. For B and D, boxplots show the median and interquartile range, with whiskers indicating the maximum and minimum values based on the interquartile range, and outlier values are indicated by diamond data points. For B and D, a one-way unpaired Brown-Forsythe ANOVA test followed by a Dunnett's post-hoc multiple comparisons test was used to compare the means of each group to control (**** $p \leq 0.0001$, *** $p \leq 0.001$, ** $p \leq 0.01$, * $p \leq 0.05$, ns $p > 0.05$).

3.2.2 DCX suppresses catastrophes and promotes nucleation

We next measured the effects of DCX on microtubule dynamics using the same assay (Figure 3.2A). First, we measured the mean lifetimes of microtubules grown in the presence of 10-100 nM DCX and saw that increasing DCX concentrations resulted in longer lifetimes. For example, adding 100 nM DCX increased lifetimes from 4.9 ± 3.7 min (mean \pm SD, $n = 932$) to 7.5 ± 5.1 min (mean \pm SD, $n = 135$, $p < 0.0001$, Brown-Forsythe ANOVA and Dunnett's multiple comparison test). This observation is consistent with previous data showing DCX suppressing catastrophe *in vitro* (Manka & Moores, 2020; Moores et al., 2006).

In addition to suppressing catastrophes, DCX is known to promote spontaneous nucleation of microtubules. This effect had been previously measured in turbidity experiments which measure the bulk concentration of polymer in a solution (Bechstedt & Brouhard, 2012; Manka & Moores, 2020; Moores et al., 2006). However, to our knowledge, the effect of DCX on templated nucleation has not been published. Therefore, in order to confirm that DCX promoted both spontaneous and templated nucleation, we measured the lag time for microtubule nucleation from GMPCPP with increasing concentrations of DCX. Adding 80 nM DCX for example reduced nucleation lag times from 4.7 ± 5.9 min (mean \pm SD, $n = 263$) to 2.9 ± 0.4 min (mean \pm SD, $n = 66$, $p = 0.0267$).

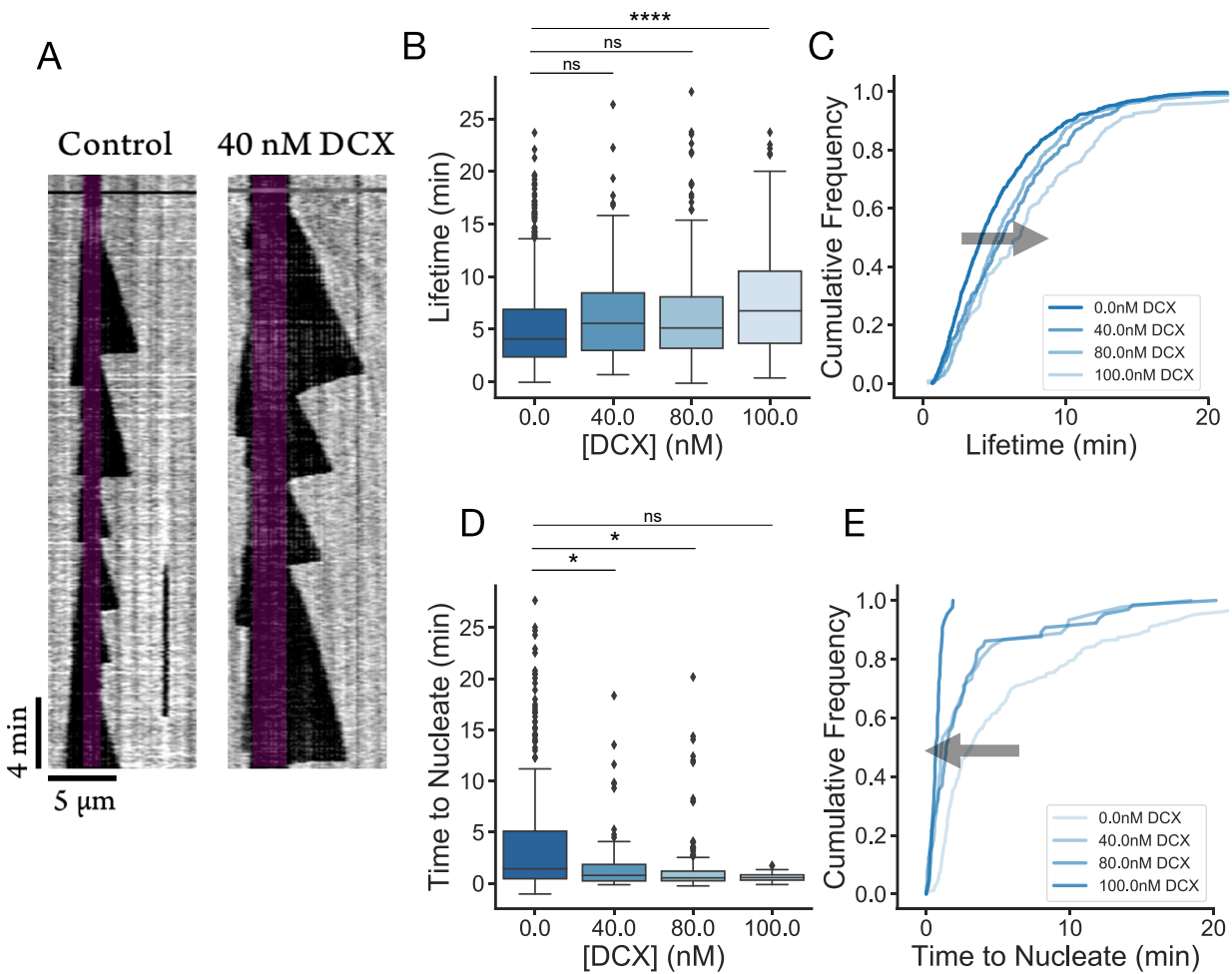


Figure 3.2 DCX extends lifetimes and reduces nucleation times

A. Representative kymographs of dynamic microtubules growing from stable GMPCPP seeds (pseudocolored in magenta) at 6 μM tubulin in the absence or presence of DCX (control kymograph is the same as in Figure 3.1). B. Microtubule lifetime as a function of DCX concentration. Data represent 135-1132 growth events for each condition. C. Cumulative distribution of lifetimes for increasing concentrations of DCX (same data as plotted in B). Adding DCX shifts the distribution to the right, towards longer lifetimes. D. Nucleation time for microtubules as a function of DCX concentration. Data represent 44-283 nucleation events for each condition. E. Cumulative distribution of nucleation times as a function of DCX concentration (same data as plotted in D). Adding DCX shifts the distribution to the left, towards shorter nucleation times. For B and D, boxplots show the median and interquartile range, with whiskers indicating the maximum and minimum values based on the interquartile range, and outlier values are indicated by diamond data points. For B and D, a one-way unpaired unpaired Brown-Forsythe ANOVA test followed by a Dunnett's post-hoc multiple comparisons test was used to compare the means of each group to control (**** $p \leq 0.0001$, *** $p \leq 0.001$, ** $p \leq 0.01$, * $p \leq 0.05$, ns $p > 0.05$).

3.2.3 EB3 reduces microtubule lifetimes even in the presence of DCX

Having confirmed that EB3 and DCX have the expected opposing effects on templated nucleation and lifetimes, we wondered how the combination of both proteins would affect microtubule dynamics. Since DCX and EB3 share a binding site between four tubulin dimers, we expect them to compete for microtubule binding. Therefore, one might expect the resulting lifetimes and nucleation lags to be at some intermediate between dynamics in the presence of EB3 alone (short lifetimes and long nucleation lags) and DCX alone (long lifetimes and short nucleation lags). To test this, we compared the dynamics of microtubules grown with DCX only, EB3 only, or both MAPs together (Figure 3.3). We chose sub-saturating concentrations of each protein which would allow us to measure potential upward or downward shifts in each parameter of dynamic instability.

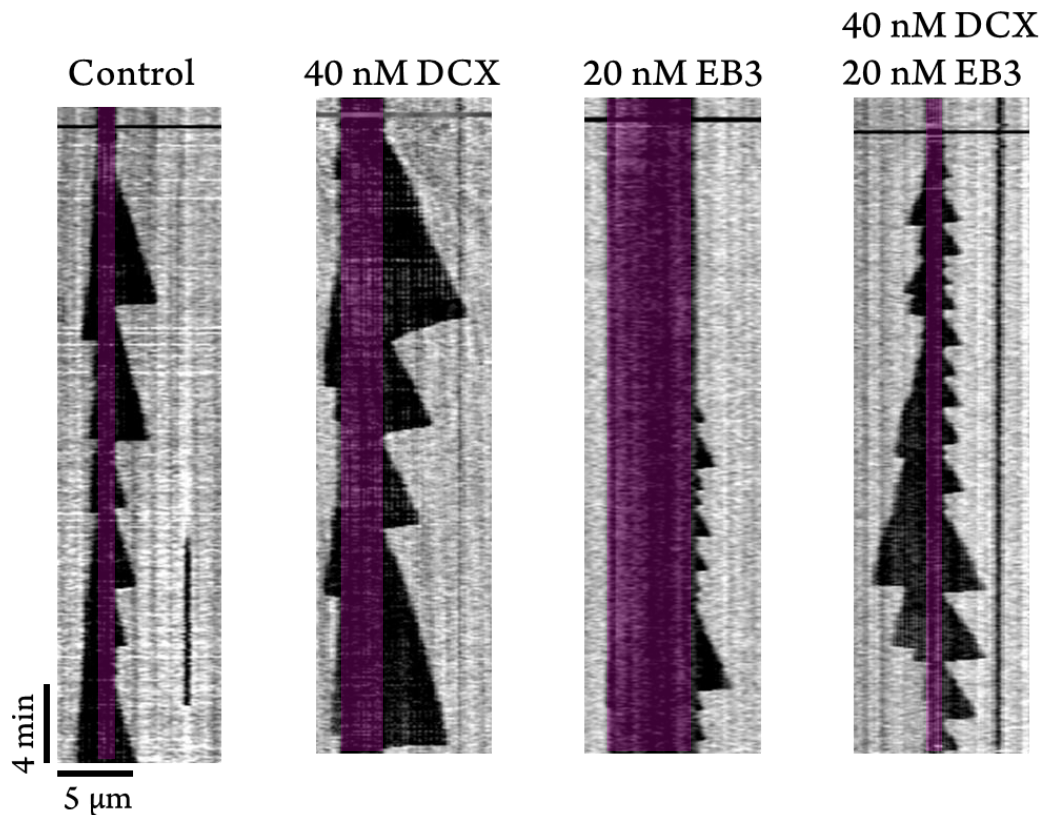


Figure 3.3 Combining DCX and EB3 changes microtubule dynamics

Representative kymographs of dynamic microtubules growing from stable GMPCPP seeds (pseudocolored in magenta) in the absence or presence of EB3, DCX, or both MAPs together (control, DCX only and EB3 only kymographs are reused from figures 3.1 and 3.2). Microtubules were visualized by IRM.

First, we measured mean microtubule lifetime in the presence of 40 nM DCX and 20 nM EB3. Surprisingly, combining both proteins did not result in intermediate lifetimes. Rather, microtubules grown with both DCX and EB3 had lifetimes of 1.5 ± 1.0 min (mean \pm SD, $n = 230$), no different from lifetimes with EB3 alone 1.5 ± 1.0 min (mean \pm SD, $n = 233$, $p > 0.9$, Brown-Forsythe ANOVA and unpaired Welch's t-test) (Figure 3.4). One explanation for this effect could be that EB3 has a higher affinity than DCX for their common binding site, leaving no room for

DCX to bind to and stabilize microtubules. If that were the case, then we would expect the same trend in nucleation lag times, with the effects of EB3 dominating.

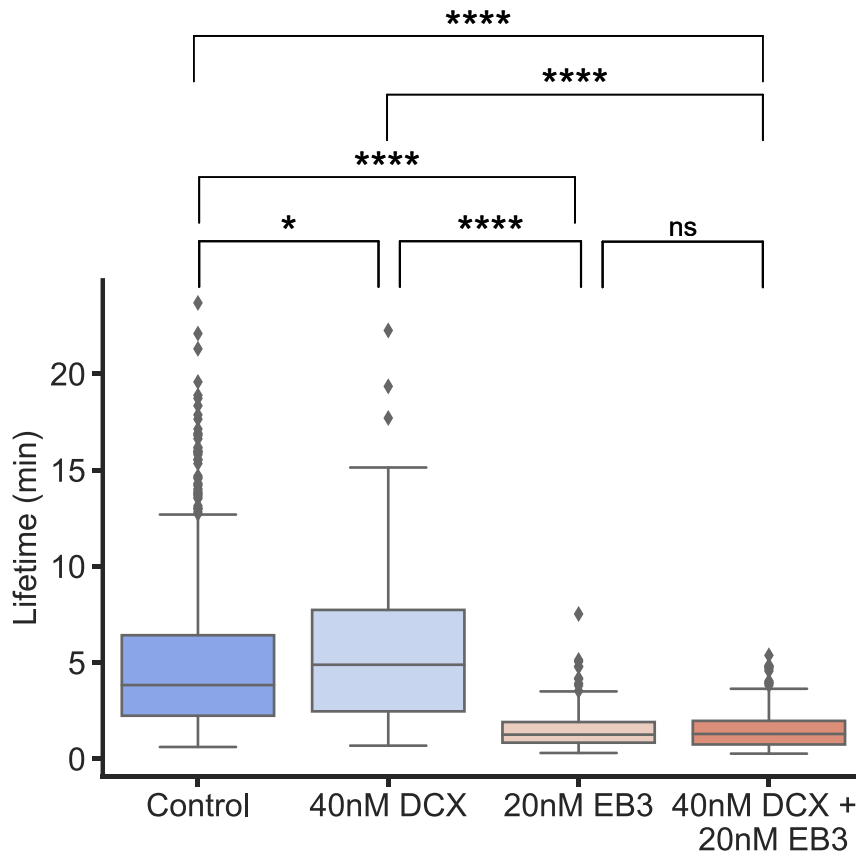


Figure 3.4 EB3 concentration determines lifetimes

Comparison of the lifetimes of microtubules growth from GMPCPP seeds at $6\mu\text{M}$ tubulin (control), with DCX only, EB3 only, or both DCX and EB3 together. Boxplots represent data from 157-1027 growth events analyzed for each condition, and show the median and interquartile range, with whiskers indicating the maximum and minimum values based on the interquartile range, and outlier values indicated by diamond data points. A one-way unpaired Brown-Forsythe ANOVA test followed by an unpaired Welch's t-test was used to compare the means of each group (**** $p \leq 0.0001$, *** $p \leq 0.001$, ** $p \leq 0.01$, * $p \leq 0.05$, ns $p > 0.05$).

3.2.4 DCX accelerates microtubule nucleation, even in the presence of EB3

We next compared the lag time for templated nucleation from GMPCPP seeds in the presence of 40 nM DCX, 20 nM EB3, or both. If EB3 were effectively outcompeting DCX, preventing it from binding, we would expect nucleation to be affected similarly to lifetimes. However, we observe the opposite. Microtubules grown in the presence of DCX alone nucleated in 2.8 ± 4.0 min (mean \pm SD, $n = 46$) and adding EB3 did not cause a statistically significant change in nucleation lag times compared to DCX alone (4.3 ± 6.1 min, $p = 0.3296$, Brown-Forsythe ANOVA and unpaired Welch's t-test) (Figure 3.5).

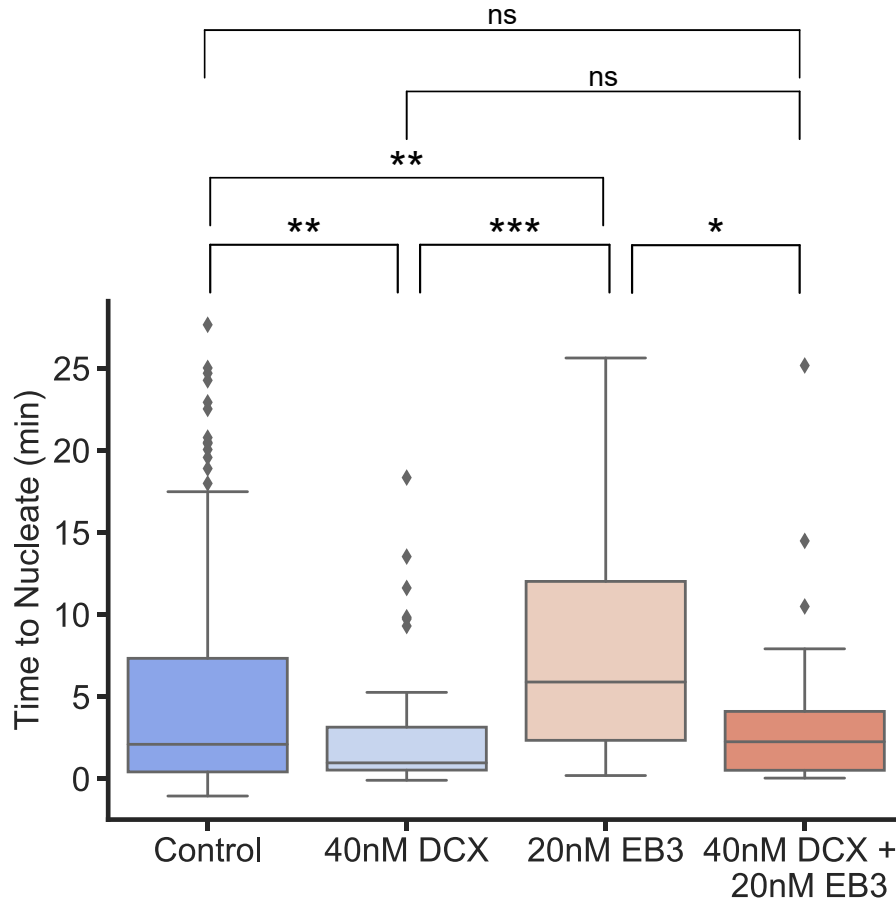


Figure 3.5 Nucleation time is determined by the concentration of DCX
 Comparison of lag times between tubulin addition and microtubule nucleation from GMPCPP seeds from 6 μ M tubulin alone (control), with DCX only, EB3 only, or both DCX and EB3 together. Boxplots represent data from 21-283 nucleation events for each condition, and show the median and interquartile range, with whiskers indicating the maximum and minimum values based on the interquartile range, and outlier values indicated by diamond data points. A one-way unpaired Brown-Forsythe ANOVA test followed by an unpaired Welch's t-test was used to compare the means of each group (**** $p \leq 0.0001$, *** $p \leq 0.001$, ** $p \leq 0.01$, * $p \leq 0.05$, ns $p > 0.05$).

3.2.5 DCX and EB3 promote rescues together

Since the combination of DCX and EB3 produced unexpected effects on lifetimes and nucleation times, we expanded our analysis to include other parameters of dynamic instability as well. We were particularly curious about the effects of these two proteins on rescues because of

the similarities with nucleation and catastrophe. During both rescue and nucleation, curved tubulins must bind to either a blunt seed or a curled shrinking end to form a growing end. This is the conceptual opposite of a catastrophe, where straight tubulin curves outward to separate from its neighbors.

In order to observe enough rescues for analysis, we increased the concentration of tubulin in our assays to 12 μM and increased the concentration of DCX to 80 nM. With tubulin alone, we observed only a single rescue, making the frequency negligible (Figure 3.6). Adding 80 nM DCX slightly increased the rescue frequency to 0.01 ± 0.004 rescues per μm (mean \pm SD, $n = 3$, $p = 0.5964$, one-way ANOVA and Fisher's LSD), in agreement with previous work (Manka & Moores, 2020). Similarly, adding 20 nM EB3 also increased the rescue frequency to 0.01 rescues per μm ($p = 0.6502$ one-way ANOVA and Fisher's LSD). This is consistent with previous work on EB1 and EB3 showing little to no effect of EBs on the frequency of rescues (Lawrence et al., 2018; Mohan et al., 2013; Molines et al., 2020; Rai et al., 2019; Zanic et al., 2013).

If DCX promotes rescues and EB3 has no effect on them, we might expect an intermediate rescue frequency in the presence of both proteins. However, since lifetimes and nucleation lag times reflected the effects of one protein over the other, the same could be true for rescues. However, just as before, combining the two MAPs produced a somewhat unexpected result. With 80 nM DCX and 20 nM EB3, we observed a rescue frequency of 0.05 ± 0.02 rescues per μm ($n = 2$, $p = 0.0486$, one-way ANOVA and Fisher's LSD), higher than with DCX or EB3 alone.

That a catastrophe factor could promote rescues is a somewhat unexpected result, as catastrophes and rescues are conceptual opposites. There is some evidence though that EB1 can increase the frequency of rescues at higher concentrations ($> 1\mu\text{M}$) than what we used here (Vitre et al., 2008). In addition, EB1 and EB3 were shown to increase rescue frequency in the presence

of microtubule destabilizing drugs (Mohan et al., 2013). It is possible then that EBs alone do not have a significant effect on rescues, but that their binding between four dimers is enough to promote lateral bond formation in the presence of an additional rescue factor like a microtubule destabilizing drug or DCX.

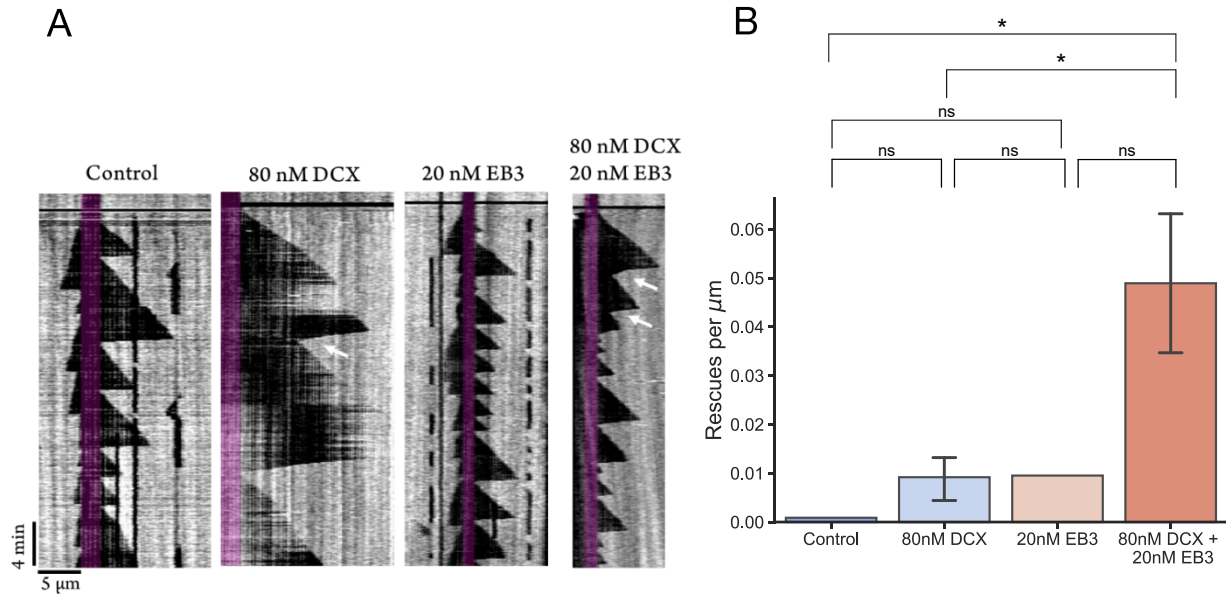


Figure 3.6 DCX and EB3 promote rescue together

A. Representative kymographs of dynamic microtubules growing from stable GMPCPP seeds (pseudocolored in magenta) in the absence or presence of EB3, DCX, or both MAPs together, at 12 μM tubulin. White arrows indicate rescue events. B. Mean frequency of rescues observed in dynamic microtubules growth from stable GMPCPP seeds at 12 μM tubulin (control), with 80 nM DCX alone, 20 nM EB3 alone, or DCX and EB3 together. Error bars show standard deviation. Rescue frequency was determined as the number of rescues observed per μm length shrunk. Rescues were counted from 484-1365 shrinkage events. A one-way unpaired ANOVA test followed by an uncorrected Fisher's LSD was used to compare the means of each group (**** $p \leq 0.0001$, *** $p \leq 0.001$, ** $p \leq 0.01$, * p

3.2.6 DCX and EB3 slow shrinkage rates

To understand the effects of DCX and EB3 on lifetimes, nucleation lag times, and rescues, it is important to consider the conformation of tubulin throughout dynamic instability. During

catastrophe, nucleation, and rescue, tubulin changes between curved and straight conformations. We therefore measured shrinkage rates in the presence of 40 nM DCX and 20 nM EB3 to see whether these MAPs were changing the speed at which protofilaments are separated after catastrophe. This would help us to understand why DCX and EB3 can increase rescue frequency together while seemingly not even competing over nucleation times and lifetimes.

DCX and EB3 could be working together to promote rescues by slowing shrinkage, providing more time for incoming tubulin to bind to an otherwise disappearing structure. We found that 40 nM DCX alone slowed shrinkage rates from $17.7 \pm 10 \mu\text{m}/\text{min}$ (mean \pm SD, $n = 829$) to $13.8 \pm 10 \mu\text{m}/\text{min}$ (mean \pm SD, $n = 131$, $p < 0.0001$, one-way unpaired ANOVA test and uncorrected Fisher's LSD) (Figure 3.7), in agreement with previous measurements of microtubule shrinkage at higher DCX concentrations (Moore et al., 2006). Similarly, we found that 20 nM EB3 also slowed shrinkage to $13.7 \pm 9.6 \mu\text{m}/\text{min}$ (mean \pm SD, $n = 216$, $p < 0.0001$ one-way unpaired ANOVA test and uncorrected Fisher's LSD), similar to measurements of shrinkage in the presence of EB1 (Molines et al., 2020; Vitre et al., 2008; Zanic et al., 2013). When we combined DCX and EB3, shrinkage rates were $12.1 \pm 7.7 \mu\text{m}/\text{min}$ (mean \pm SD, $n = 225$, $p < 0.0001$, one-way unpaired ANOVA test and uncorrected Fisher's LSD). Based on this data, it seems that, though EB3 and DCX work together to increase the frequency of rescues, this cooperation does not apply to slowing shrinkage beyond the sum of the individual effects. Still, slower shrinkage rates suggest slower tubulin curving and slower tubulin dissociation from the microtubule end, both of which could contribute to more frequent rescues as well as fast nucleation.

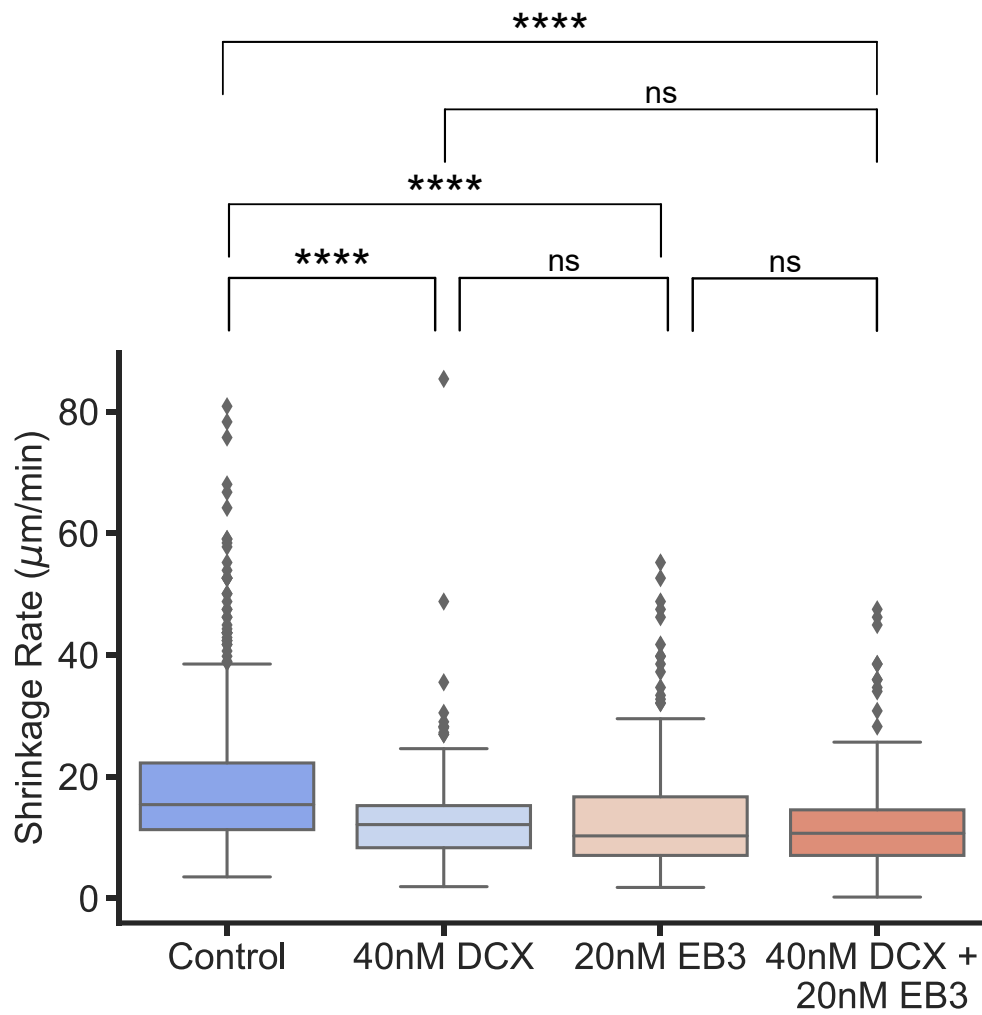


Figure 3.7 Shrinkage rates are slowed by DCX and EB3

Comparison of shrinkage rates of dynamic microtubules growth from GMPCPP seeds from 6μM tubulin alone (control), with DCX only, EB3 only, or both DCX and EB3 together. Boxplots represent data 131-914 shrinkage events for each condition, and show the median and interquartile range, with whiskers indicating the maximum and minimum values based on the interquartile range, and outlier values indicated by diamond data points. A one-way unpaired ANOVA test followed by an uncorrected Fisher's LSD was used to compare the means of each group (**** $p \leq 0.0001$, *** $p \leq 0.001$, ** $p \leq 0.01$, * $p \leq 0.05$, ns $p > 0.05$).

3.2.7 DCX and EB3 increase growth rates

EB3 and DCX together do not significantly slow shrinkage more than each individual MAP. Therefore, EB3 and DCX together must be promoting rescues through a mechanism unrelated to shrinkage rate. One possibility is that together, EB3 and DCX facilitate tubulin addition to a shrinking end, making a rescue more likely. We therefore measured the growth rates of microtubules in the presence of EB3, DCX, or both MAPs (Figure 3.8). We measured a slight increase in growth rates in the presence of DCX or EB3 alone, from $0.4 \pm 0.1 \mu\text{m}/\text{min}$ (mean \pm SD, $n = 930$) to $0.6 \pm 0.1 \mu\text{m}/\text{min}$ ($n = 157$, $p < 0.0001$, Brown-Forsythe ANOVA and unpaired Welch's t-test) and $0.7 \pm 0.2 \mu\text{m}/\text{min}$ ($n = 228$, $p < 0.0001$), respectively. Some previous work has shown DCX has no effect on growth rates (Bechstedt & Brouhard, 2012; Moores et al., 2006) though others do report an increase in growth rates in the presence of DCX (Manka & Moores, 2020). Our data is in agreement with the idea that DCX may increase growth rates slightly, though not to the extent of any *bona fide* polymerase like XMAP215 (Brouhard et al., 2008). Similarly, the observation that EB3 increases growth rates is in agreement with work on EB1 showing that EBs can accelerate growth, but like DCX, not to the extent that polymerases do (Molines et al., 2020; Vitre et al., 2008; Zanic et al., 2013).

When DCX and EB3 are combined, growth rates are even higher than in the presence of either individual protein ($0.9 \pm 0.1 \mu\text{m}/\text{min}$, $n = 233$, $p < 0.0001$, Brown-Forsythe ANOVA and unpaired Welch's t-test) (Figure 3.8). Therefore, the observed increase in rescue frequency in the presence of both DCX and EB3 may be a result of the combination of slower shrinkage rates together with faster growth rates (discussed below).

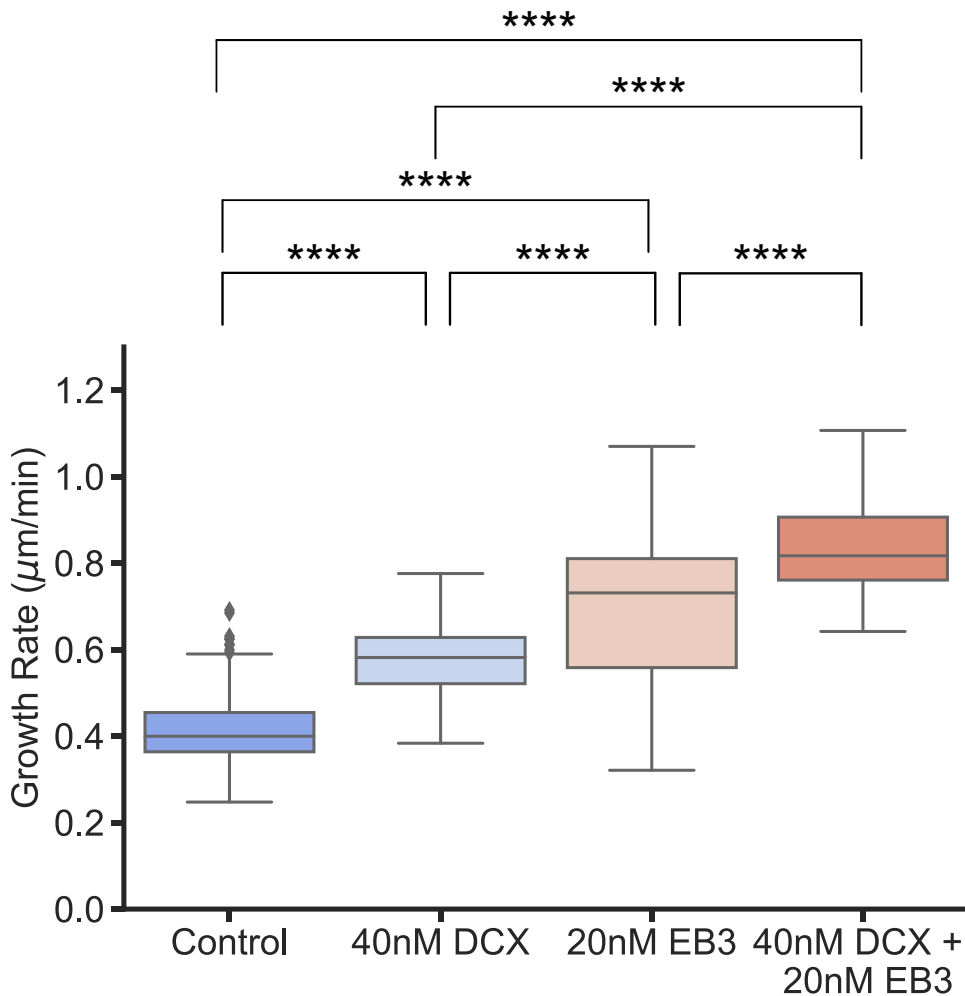


Figure 3.8 DCX and EB3 increase microtubule growth rates

Comparison of growth rates of dynamic microtubules grown from GMPCPP seeds from 6μM tubulin alone (control), with DCX only, EB3 only, or both DCX and EB3 together. Boxplots represent data 157-1027 growth events for each condition, and show the median and interquartile range, with whiskers indicating the maximum and minimum values based on the interquartile range, and outlier values indicated by diamond data points. A one-way unpaired Brown-Forsythe ANOVA test followed by a Dunnett's post-hoc test without correction for multiple comparisons was used to compare the means of each group (**** $p \leq 0.0001$, *** $p \leq 0.001$, ** $p \leq 0.01$, * $p \leq 0.05$, ns $p > 0.05$).

3.3 Discussion

The study of MAPs has always come hand in hand with the study of microtubules. Many hallmark MAPs have provided key insights into the intrinsic properties of microtubules in addition to their own properties. As discussed above, studies of XMAP215 prompted the development of the two-step model for microtubule growth (Brouhard et al., 2008), while studies of EB1 have revealed key details in the GTP-cap model (Bieling et al., 2007; Maurer et al., 2012; Roostalu et al., 2020). The symmetry between XMAP215 and EB1 provided additional evidence for the two-step model, showing that MAPs could interact indirectly, or allosterically, through the microtubule itself (Zanic et al., 2013). Together, XMAP215 and EB1 modulate the conformation of tubulin dimers at the end of a growing microtubule. While the precise structure of the microtubule end remains up to debate (Brouhard & Rice, 2018; Cleary & Hancock, 2021), the field generally agrees on the curved conformation of tubulins at the very end of a growing microtubule. Importantly, this curved conformation allows MAPs like XMAP215, CLASP, and DCX to track the growing end through a distinct mechanism than EBs (Ayaz et al., 2014; Bechstedt et al., 2014; Brouhard & Rice, 2014; Lawrence et al., 2020; Leano et al., 2013; Maurer et al., 2012).

Though EBs and DCX both track growing ends, they have opposing effects on microtubule dynamics (Table 1 – Differences). It is all the more surprising then, that they both similarly compact tubulin in the lattice and specify a 13-protofilament architecture (LaFrance et al., 2022; Manka & Moores, 2018; Vitre et al., 2008; R. Zhang et al., 2015, 2018). We therefore wondered if EBs and DCX could act synergistically like XMAP215 and EB1, or if their shared binding site would result in a competitive relationship between the two and intermediate microtubule dynamics.

First, we confirmed at the single-microtubule level that DCX suppresses catastrophes and accelerates nucleation (Bechstedt & Brouhard, 2012; Manka & Moores, 2020; Moores et al., 2006) (Figure 3.2). Specifically, we showed that DCX accelerates templated nucleation. We also confirmed that EB3 promotes catastrophe and slows templated nucleation (Molines et al., 2020; Vitre et al., 2008; Wieczorek et al., 2015; Zanic et al., 2009) (Figure 3.1). For the first time, we measured the combined effects of DCX and EB3 on microtubule lifetimes, nucleation lag times, rescue frequency, shrinkage rate, and growth rate.

Our results showed that while DCX extends lifetimes and EB3 promotes catastrophe, when the two are together, microtubule lifetimes match those with EB3 alone (Figure 3.3 and 3.4). Conversely, while DCX accelerates nucleation and EB3 slows it down, when the two are together, microtubules nucleate fast, like with DCX alone (Figure 3.5). In a competition for the same binding site, the protein with the higher affinity for that binding site should win out. Since DCX seems to be having a stronger effect on nucleating microtubules while EB3 seems to be having a stronger effect on growing, pre-catastrophe microtubules, it may be the case that DCX and EB3 are recognizing different conformations in the tubulin at these different stages of dynamic instability. This suggests that EB3 and DCX are indeed competing for binding sites which vary in affinity as the microtubule nucleates, grows, and undergoes catastrophe.

We next showed that DCX and EB3 together increase the frequency of rescues more than the sum of their individual effects (Figure 3.6), suggesting a synergistic interaction between the two proteins. It is possible that the increase in rescue frequency may be related to the combination of slower shrinkage rates (Figure 3.7) and faster growth rates (Figure 3.8) in the presence of both MAPs. However, there is no strong correlation between growth rates or shrinkage rates and rescue frequency. Accelerating growth rates by increasing the concentration of tubulin, for example, does

not significantly increase rescue frequency rate (Fees & Moore, 2019; Gardner et al., 2013; Walker et al., 1988). Even XMAP215 and EB1 together, which increase growth rates up to 30-fold, do not increase the number of rescues observed (Zanic et al., 2013). Conversely, increasing shrinkage rates using calcium ions does not significantly reduce the frequency of rescues observed in a variety of conditions (Fees & Moore, 2019). Indeed, the rescue factor CLASP promotes rescues without changing shrinkage or growth rates (Lawrence et al., 2018; Majumdar et al., 2018).

If the effects of DCX and EB3 on lifetime and nucleation lag times depend on the curvature state of tubulin at different moments of dynamic instability, the same may be true for rescues. One hypothesis to explain the increased rescue frequency in the presence of both proteins could be the combination of DCX's curvature recognition, combined with EB3s binding between 4 tubulin dimers, promoting lateral interactions. Overall, combining DCX and EB3 supports the idea of an evolving tip structure (Cleary & Hancock, 2021; Coombes et al., 2013; Duellberg, Cade, & Surrey, 2016; V. J. Farmer & Zanic, 2022). Though catastrophe factors can inhibit nucleation and nucleators can prevent catastrophe (Wieczorek et al., 2015), our data challenges the idea that small nucleation intermediates have the same structure as growing microtubules.

3.4 Methods

3.4.1 Protein purification

Tubulin was purified from juvenile bovine brains as described in Chapter 2 by cycles of polymerization, centrifugation, depolymerization, and centrifugation (Ashford & Hyman, 2006). EB3-GFP was expressed and purified as described in Chapter 2, and the His-tag was cleaved off with PreScission protease overnight at 4 °C.

DCX was purified as described previously (Bechstedt & Brouhard, 2012). Briefly, the coding sequence for DCX was inserted into a modified pHAT vector containing an N-terminal 6xHis-tag followed by a PreScission site and a carboxy-terminal EGFP followed by a Strep-tag II. DCX was eluted from the StrepTactin Sepharose column with Buffer E (100 mM Tris-HCl, 150 mM NaCl, 1 mM EDTA, 10% glycerol, 2.5 mM desthiobiotin, pH 8.0) aliquoted, flash frozen in liquid nitrogen, and stored at -80°C.

3.4.2 Reconstitution of microtubule dynamics *in vitro*

Microtubule dynamics were reconstituted *in vitro* as previously described (Gell et al., 2010) (see also methods in Chapter 2) with a few modifications. To promote preferential binding of EB to microtubule ends, 50 mM KCl was included in the reaction buffer. We also included 0.1 % methylcellulose in the reaction buffer to prevent large fluctuations of the dynamic microtubules. The final reaction buffer therefore contained BRB80 (80 mM PIPES-KOH pH 6.9, 1 mM EGTA, 1 mM MgCl₂), 1 mM GTP, 0.1 mg/mL BSA, 10 mM dithiothreitol, 250 nM glucose oxidase, 64 nM catalase, 40 mM D-glucose, 50 mM KCl, 0.1 % methylcellulose., and the indicated concentration of tubulin, DCX, and EB3. Sub-aliquots of DCX and EB3 were kept on ice between experiments while sub-aliquots of tubulin were kept in liquid nitrogen.

3.4.3 IRM imaging of dynamic microtubules

As in Chapter 2, dynamic microtubules were visualized by IRM imaging, but this time using a Prime 95B CMOS camera (Photometrics). Images were acquired at 5 second intervals. Each image represents an average of 10 frames for each time point. As in Chapter 2, microtubule dynamics were analyzed from kymographs manually generated in FIJI (Schindelin et al., 2012). All statistical testing was performed in GraphPad Prism.

4 Discussion

4.1 Introduction

Over thirty years after the discovery of dynamic instability, we are still searching for the underlying mechanisms. Structurally speaking, we don't yet understand how the different conformational states of tubulin contribute to creating an end structure that can store accumulated strain energy, and later release it. In the previous three chapters, I have given an overview of our current understanding of dynamic instability and described some my own contributions to the field. I have taken an *in vitro* approach to studying microtubules, characterizing changes to their dynamics in response to increased viscosity and in the presence of opposing MAPs.

In Chapter 2, I discussed the use of viscosity as a biophysical tool to understand the relevant spatial scales in the different phases of dynamic instability. We used three viscosogens of different sizes, glycerol, trehalose, and BSA, and measured their effects on growth, shrinkage, lifetime, GTP cap size, rescue, and nucleation. Viscosity affected dynamic instability, and for certain phases, the effect depended strongly on viscogen size. Increasing viscosity with the small viscosogens glycerol or trehalose slowed microtubule growth rates, while increasing viscosity with the larger of the three viscosogens, BSA, increased growth rates, consistent with previous reports (Molines et al., 2022; Wiczorek et al., 2013). For the first time, we showed that viscosity slows microtubule shrinkage rates. Notably, microtubule lifetimes, rescue frequency, and nucleation times were particularly sensitive to viscogen size. Increasing viscosity with the smallest viscogen, glycerol, significantly extended lifetimes, increased rescue frequency, and facilitated nucleation. In comparison, trehalose, only slightly larger than glycerol, only modestly increased lifetimes, while BSA actually slightly decreased them. Both trehalose and BSA slightly increased the frequency of

rescues, but their effects were negligible compared to that of glycerol. The time required for templated nucleation was not significantly affected by trehalose and BSA. While glycerol significantly decreased the minimal concentration required for spontaneous nucleation, trehalose and BSA had comparatively little effects. Interestingly, though lifetimes were very sensitive to viscogen size, the size of the GTP cap did not correlate with lifetimes. Increasing viscosity with any of the three viscogens reduced the intensity of EB3-GFP comets. In fact, comet intensity correlated with growth rates, not with lifetimes.

In Chapter 3, I discussed how the study of MAPs can provide insight into the intrinsic properties of microtubules. Specifically, we used a combination of two MAPs with opposing effects to study the relationship between nucleation and catastrophe. We confirmed that EB3 reduced microtubule lifetimes and increased the time required for templated nucleation (Molines et al., 2020; Roth et al., 2018; Vitre et al., 2008; Wieczorek et al., 2015; Zanic et al., 2013). In addition, we confirmed that DCX increased microtubule lifetimes and facilitated nucleation (Bechstedt & Brouhard, 2012; Manka & Moores, 2020; Moores et al., 2004, 2006), showing for the first time that DCX reduced the time required for templated nucleation, in addition to its known effect on spontaneous nucleation (Bechstedt & Brouhard, 2012; Moores et al., 2004, 2006). Since these two MAPs share a binding site on microtubules and yet have opposing effects on dynamics, we sought to characterize their combined effects. Surprisingly, rather than directly competing for binding sites and producing intermediate effects, EB3 and DCX seemed to affect different phases of dynamic instability. When both EB3 and DCX are present, microtubules lifetimes are the same as lifetimes with EB3 alone while the nucleation lag times are the same as with DCX alone.

In this final Chapter, I will review some of the key findings presented above and discuss them in the context of published literature in the field. I will be highlighting a few relationships

between parameters of dynamic instability that are often thought of as tightly linked, but can be uncoupled in different conditions. This suggests that the phases of dynamic instability each involve specific conformations of tubulin that cells can regulate to control their microtubule cytoskeleton.

4.2 Catastrophes are preceded by small conformational changes in tubulin

In Chapter 2, we used three viscosins of different sizes to probe the relevant spatial scale of the conformational changes in tubulin involved in each phase of dynamic instability. As mentioned, microtubule lifetimes were much longer in the presence of the smallest viscosin, glycerol (3 Å), than in the presence of a slightly larger viscosin, trehalose (4 Å) (Figure 2.4). This difference in effect depending on viscosin size suggests therefore that catastrophes are preceded by small conformational changes in tubulin rather large-scale rearrangements at the level of dimers or protofilaments.

Structural reconstructions of tubulin in different nucleotide states show that tubulin undergoes a 2 Å compaction upon GTP-hydrolysis (Alushin et al., 2014; Manka & Moores, 2020; R. Zhang et al., 2015, 2018). Compaction is thought to be responsible for the accumulation of strain in the lattice, released during catastrophe. In environments of increasing viscosity, a conformational change of this scale could be sensitive to small differences in viscosin size. It is therefore possible that glycerol, more than trehalose or BSA, slows catastrophe by slowing post-hydrolysis tubulin compaction.

There is indeed precedent for the “dampening” of post-hydrolysis conformational changes slowing catastrophes. The mutation T238A in yeast β -tubulin does just that (Geyer et al., 2015).

T238 is located on the H7 helix which is buried in the core of tubulin. This helix is of particular interest because its position depends on whether tubulin is in a straight or a curved conformation (Nogales et al., 1998; Ravelli et al., 2004), and on the nucleotide state of tubulin (Alushin et al., 2014). Because of its position at the core of tubulin, T238A was shown to dampen the conformational changes in tubulin following GTP hydrolysis (Geyer et al., 2015). As a result, T238A microtubules had longer lifetimes than wild type, despite having equivalent growth rates. In addition, these mutant microtubules were shown to have unimpaired GTPase activity, suggesting that the mutation prevented catastrophe through a mechanism unrelated to GTP hydrolysis.

To determine whether the T238A mutation in β -tubulin increased lifetimes by slowing tubulin compaction, Geyer et al. used the yeast homologue of EB1, Bim1. Like EBs, Bim1 binds between four tubulin dimers, preferentially binding to GTP-tubulin, thus tracking the growing end of the microtubule (Maurer et al., 2011; Zanic et al., 2009). On wild-type microtubules, Bim1-GFP bound preferentially to the growing end of the microtubules, as expected. On T238A microtubules, Bim1-GFP bound all along the lattice, suggesting that the mutation caused tubulin in these microtubules to remain in a “GTP-like” conformation, likely expanded (LaFrance et al., 2022; Roostalu et al., 2020). Thus, the T238A mutation in yeast β -tubulin uncoupled compaction from GTP hydrolysis.

In contrast, the extended lifetimes we observed in the presence of small viscoagents do not seem to be a result of slowed tubulin compaction. If that were the case, we would expect increased EB binding on microtubule ends, as measured by larger EB comets or EB binding along the whole lattice. However, that is not what we observed. EB3-GFP comet intensity was not increased in the

presence of any of the viscogens tested (Figure 2.8). We therefore conclude that small viscogens like glycerol likely do not slow tubulin compaction.

Though compaction may contribute to the accumulation of strain within the lattice (Alushin et al., 2014; R. Zhang et al., 2015, 2018), additional conformational changes must occur for that strain to be released during catastrophe. Our data suggests that these conformational changes are on the order of 3 Å, which could be involved in the rearrangement of the residues involved in lateral contacts, for example. Lateral contacts are formed by the interactions between residues on loops of the lateral surfaces of tubulin: the M loop on one side of the contact interacts with the H2-S3 and the H1-S3 loops on the other side (R. Zhang et al., 2015). Interestingly, the specific secondary structure of these loops has been shown influence microtubule growth rates in different species (Chaaban et al., 2018; Geyer et al., 2015; Vemu et al., 2017; R. Zhang et al., 2015).

When microtubules undergo catastrophe, these lateral contacts are broken so that tubulin can curl outwards and protofilaments can peel apart (Mandelkow et al., 1991). Therefore, small scale rearrangements of the residues in these loops likely precede any tubulin curving during catastrophe (Manka & Moores, 2018). Some have proposed a model in which catastrophes occur when a threshold number of lateral interactions between protofilaments is broken (Li et al., 2014; Margolin et al., 2011, 2012). In this model, a broken lateral bond may grow into a “crack” between protofilaments. The accumulation of cracks between joining protofilaments eventually destabilizes the growing end, and strain is released in catastrophe. Therefore, we propose that small viscogens like glycerol slow the rearrangement of loops involved in lateral contacts, thus increasing lifetimes without increasing growth rates or GTP-cap size.

4.3 Nucleation intermediates are different from growing ends

The mechanochemical changes that occur in tubulin during catastrophe are also at play during microtubule nucleation (Wieczorek et al., 2015). As such, inhibiting catastrophes by inhibiting the GTPase activity of tubulin greatly facilitates nucleation. This has been shown with non-hydrolysable GTP-analogues like GMPCPP (Hyman et al., 1992; Wieczorek et al., 2015) or with GTPase deficient recombinant mutant tubulin (Roostalu et al., 2020). The correlation between nucleation rates and lifetimes has also been demonstrated by the inhibition of nucleation by catastrophe factors like MCAK or EB1, or conversely, the acceleration of nucleation and suppression of catastrophes by nucleators like TPX2 (Wieczorek et al., 2015). Similarly, in Chapter 3, I discussed our own results using the catastrophe factor EB3, which slowed nucleation and shortened lifetimes, and the nucleator, DCX, which accelerated nucleation and prolonged lifetimes.

Based on the tight relationship between catastrophe and nucleation in the above-mentioned studies, when we mixed EB3 and DCX in our own experiments, we expected the basic trend to stay the same, that nucleation and lifetimes would remain correlated. However, mixing EB3 and DCX together uncoupled lifetimes from nucleation. This combination of MAPs produced microtubules that nucleated fast but had short lifetimes (Figure 3.4 and 3.5). These results suggest that there is a structural difference between nascent microtubules and more mature ones, since EB3 and DCX seem to be winning out over each other at different moments in the microtubule lifecycle. This supports the idea that the energetic barrier to nucleation involves not only the GTPase activity of tubulin, but also conformational changes that allow a small tubulin oligomer to become a microtubule.

The difference between nucleation intermediates and the growing plus end was highlighted by experiments showing a higher energetic barrier to tubulin addition to a nucleation template compared to an actively growing end (Wieczorek et al., 2015). Templated nucleation requires tubulin concentrations above the critical concentration for growth. As such, at low tubulin concentrations, no nucleation from templates is observed. However, if microtubules are grown at a high concentration of tubulin, and the buffer is rapidly exchanged for one with a low tubulin concentration, elongation can continue at this low concentration. In other words, a low concentration of tubulin can support continued growth from an already growing plus end, but it cannot overcome the kinetic barrier to nucleation. This data supports the idea that nucleation intermediates and growing ends must be structurally distinct. In addition, the work discussed in Chapter 3 suggests that DCX and EB3 recognize this difference in structure.

It may be the case that growing ends have a more tapered structure than nucleation intermediates, for example. In the *in vitro* experiments described in Wieczorek et al., 2015, the nucleation templates used all have a blunt ring shape (Wieczorek et al., 2015). In contrast, the growing microtubule end is often thought to have some level of tapering, in other words laterally joined protofilaments of different lengths (Brouhard & Rice, 2018; Chretien et al., 1995; Coombes et al., 2013; Gardner, Charlebois, et al., 2011). A tapered end structure would provide not only longitudinal binding sites, but lateral ones as well as “cozy corners” where an incoming tubulin dimer can form both a lateral and a longitudinal bond. In some models for microtubule growth, binding to corner sites is highlighted as an important and favourable step since two bindings sites lower the off-rate constant of incoming dimers, allowing longer dwell times at the tip of the microtubule and giving time for subsequent binding events that allow steady-state elongation

(Brouhard & Rice, 2018; Cleary & Hancock, 2021; Erickson & Pantaloni, 1981; Gardner, Charlebois, et al., 2011; Mickolajczyk et al., 2019; Rice et al., 2021).

Importantly, whether a soluble tubulin dimer is binding to a nucleation intermediate or a stably growing end, it must eventually straighten. The energetic penalty for tubulin straightening is an important factor for recent models of microtubule nucleation (Rice et al., 2021) as well as for growth and catastrophe (Alexandrova et al., 2022). The difference in structure between nucleation intermediates and growing ends may contribute to differences in the energetic penalty for straightening tubulin dimers. For example, growing ends may tend to have more stable lateral bonds between protofilaments, facilitating straightening (Igaev & Grubmüller, 2020; Rice et al., 2008)

4.4 The importance of stabilizing curved tubulin intermediates

To understand the underlying mechanisms of dynamic instability we need to understand the conformational changes occurring in tubulin during microtubule assembly, GTP hydrolysis, catastrophe, and shrinkage. The importance of tubulin's intrinsic curvature became apparent with the observation that both GTP and GDP tubulin are curved in solution (Ayaz et al., 2012; Nawrotek et al., 2011; Pecqueur et al., 2012; Rice et al., 2008). Tubulin must undergo conformational changes to straighten and become incorporated into a lattice, and later curve once again during shrinkage. MAPs recognize and regulate these different conformations of tubulin in order to control microtubule dynamics (Brouhard & Rice, 2014). Tubulin conformations of different curvatures are particularly interesting because they likely represent different intermediates

between growth and shrinkage. Here I list a few examples of MAPs that use tubulin curvature to slow or prevent catastrophe.

Members of the kinesin-4 family inhibit catastrophe despite slowing growth (Bieling et al., 2010; Taguchi et al., 2022; van der Vaart et al., 2013). These kinesins are thought to bind to the ends of growing microtubules, stabilizing the curved tubulin dimers there. Specifically, members of the kinesin-4 family are thought to stabilize an intermediate curved state (not quite as curved as a shrinking protofilament, but not as straight as tubulin in the lattice). Thus, these kinesins slow growth because they slow the transition from fully curved to fully straight, and they slow catastrophe because they slow the transition from partially curved to fully curved. Indeed, stabilizing a certain level of curvature in tubulin dimers at the growing end could promote the formation of lateral bonds, which ultimately help in longitudinal straightening of protofilaments (Rice et al., 2008).

A more recent example of catastrophe prevention through the stabilization of an intermediate curved state of tubulin comes from the cytoplasmic linker-associate proteins (CLASPs). CLASPs are known for their role in stabilizing microtubules during processes like cell polarization or division (reviewed in Lawrence et al., 2020). Specifically, CLASPs suppress catastrophes and promote rescues without modulating growth rate or increasing the size of the GTP-cap. Recent work has provided detail as to the molecular mechanism by which CLASPs regulates dynamic instability, proposing that CLASPs stabilize a curved intermediate state between growth and shrinkage (Lawrence et al., 2022). Work on CLASPs and on the kinesin-4 family highlights the importance of intermediate conformations of tubulin. During growth, tubulin dimers at the end of a microtubule must transition from their fully curved conformation a straight one. Stabilizing an

intermediate curvature state would therefore prevent catastrophe by slowing the outward curling of protofilaments and breaking of lateral bonds.

One interesting feature of CLASPs is that they slow catastrophe and promote rescue *without* changing either growth rates or shrinkage rates (Lawrence et al., 2018; Majumdar et al., 2018). This is not the case for the kinesin-4 family, mentioned above, which slows growth rates in addition to slowing catastrophe (Bieling et al., 2010; Taguchi et al., 2022; van der Vaart et al., 2013), or the nucleator DCX, which slows shrinkage rates in addition to slowing catastrophe (Manka & Moores, 2020; Moores et al., 2006). DCX has also been shown to bind preferentially to curved regions on the microtubule (Bechstet et al., 2014), allowing it to stabilize curved nucleation intermediates (Manka & Moores, 2018) and promote rescues (Manka & Moores, 2020).

However, the suppression of catastrophes and the promotion of rescues are not necessarily linked effects. For example, the centriolar protein CPAP slows growth rates, prevents catastrophes, and promotes rescues to regulate centriolar length (Campanacci et al., 2022; Ogunmolu et al., 2022; Sharma et al., 2016). The full-length protein is thought to prevent catastrophes by capping the ends of individual protofilaments (Campanacci et al., 2022; Cormier et al., 2009), with a tubulin-binding domain that recognizes the tip of β -tubulin, and a microtubule binding domain that binds to the lattice through electrostatic interactions (Sharma et al., 2016). Deletion of the tubulin-binding domain of CPAP disrupts its ability to recognize the microtubule end and prevent catastrophes. However, the deletion, leaving only the microtubule binding domain, does not change the ability of the protein to promote rescues. This observation suggests promotion of rescues and prevention of catastrophes involve separate conformational changes, or require stabilization of different tubulin conformations, since a single protein is able to affect one but not the other.

4.5 Lifetimes can be uncoupled from the GTP-cap size

The canonical link between microtubule stability and GTP-cap size was proposed even before dynamic instability was directly observed (Carlier & Pantaloni, 1981; Horio & Hotani, 1986; T. Mitchison & Kirschner, 1984b; Walker et al., 1988). This link was later supported by measurements of the size of EB comets on microtubules before and after tubulin washout (Duellberg, Cade, Holmes, et al., 2016). Microtubules with larger EB comets (and presumably larger GTP-caps) remained intact after tubulin washout for longer time lags than microtubules with smaller EB comets. In addition, in the moments right before the microtubules did eventually catastrophe, the intensity of the EB comets reduced to 20% of their original value. These experiments supported the notion that microtubule lifetime was tightly linked to GTP-cap size.

However, there are many situations where lifetimes are uncoupled from GTP-cap size, as highlighted in a recent review (V. J. Farmer & Zanic, 2022). Most of the work presented thus far focused on the dynamics of microtubule plus ends. However, minus ends also undergo dynamic instability (Walker et al., 1988), and their dynamics have recently been characterized in detail (Strothman et al., 2019). At any given tubulin concentration, minus ends grow more slowly than plus ends, and have smaller GTP-caps (as measured by EB-comet analysis). However, Strothman et al. showed that GTP-cap size scales with growth rate at either end, meaning that, at equivalent growth rates, a minus end would have a GTP-cap the same size as a plus end. Interestingly, minus ends have longer lifetimes than plus ends. In other words, at equivalent growth rates, with GTP-caps of the same size, minus ends undergo fewer catastrophes than plus ends. While GTP-cap size was shown to be determined by growth rate, lifetimes were shown to be determined by tubulin dissociation rate, which differ between the two ends.

Another example of lifetimes being uncoupled from GTP-cap size comes from the family of anti-catastrophe and rescue factors mentioned above, CLASPs (Lawrence et al., 2020). Indeed, CLASPs slow catastrophes without increasing the size of the GTP-cap (Lawrence et al., 2018; Majumdar et al., 2018). Instead, CLASPs are thought to stabilize incomplete lattices, perhaps at protofilaments with exposed terminal GDP-tubulin dimers, that would otherwise fall apart in a catastrophe (Aher et al., 2018; Mahserejian et al., 2022). When it comes to CLASPs, the size of the GTP-cap is far less important than the structure of the microtubule end, which can be maintained by stabilizing tubulin dimers in an intermediate state between growth and shrinkage (Lawrence et al., 2022).

We also see an uncoupling of lifetimes from GTP-cap size in our experiments growing microtubules in the presence of small viscosogens (Figure 2.4 and 2.8). As discussed above, as viscosity is increased with glycerol, lifetimes are increased without any measurable increase in GTP-cap size. Rather than stabilizing microtubules by slowing GTP hydrolysis rates, viscosity seems to be slowing the post-hydrolysis conformational changes at the end of the growing microtubule that eventually lead to catastrophe.

The importance of the microtubule end structure in determining catastrophe rates is also highlighted by work on the polymerase XMAP215, which also uncouples lifetimes and GTP-cap size (V. Farmer et al., 2021). As discussed previously (see sections 1.4.2 and 3.1.1), XMAP215 accelerates growth rates 5-fold on its own and up to 30-fold in the presence of EB1 (Brouhard et al., 2008; Zanic et al., 2013). In doing so, XMAP215 also increases the size of the GTP-cap. One could therefore hypothesize that XMAP215 increases lifetimes due to these larger GTP-caps. However, XMAP215 was actually shown to reduce lifetimes (V. Farmer et al., 2021). The proposed mechanism is that XMAP215 creates a “disorganized” end structure, with protruding

curved protofilaments that don't necessarily make lateral bonds with their neighbors. Thus, though XMAP215 accelerates the addition of tubulin onto each protofilament, it does so in an uncoordinated manner, creating an unstable end structure more prone to catastrophe.

4.6 Microtubules are sensitive to their environment

Most of the understanding of dynamic instability described thus far comes from *in vitro* experiments focused on a limited number of parameters, be it the viscosity of the environment or the action of one or two MAPs at a time. However, understanding the regulation of microtubule dynamics in cells is complicated by the combined action of many MAPs (Amos & Schlieper, 2005), along with the crowded and viscous nature of the cytoplasm (McGuffee & Elcock, 2010b), among other factors. Recent work has demonstrated the sensitivity of microtubules to the physical properties of cytoplasm *in vivo* (Molines et al., 2022). In both yeast and mammalian cells, microtubule dynamics change in response to cytoplasm concentration. More specifically, when cells are subjected to hyperosmotic shock, they shrink in volume, increasing cytoplasm density. As a result, microtubule growth rates and shrinkage rates both slow down, suggesting that increased cytoplasm density results in increased cytoplasm viscosity, the effects of which overcome any increase in macromolecular crowding (T. J. Mitchison, 2019; Molines et al., 2022; Wieczorek et al., 2013).

The effects of the viscosity of cytoplasm are particularly interesting when it comes to microtubule nucleation. As discussed in Chapter 2, small viscogens promoted spontaneous nucleation. Glycerol, specifically, lowered the critical concentration for spontaneous nucleation down to $\sim 4 \mu\text{M}$ at 3 cP. This result is especially interesting when comparing these experimental

conditions to conditions inside a cell. In fission yeast, for example, cytoplasm has a viscosity of around 10 cP, as measured by time-resolved fluorescence anisotropy imaging (Molines et al., 2022). In other words, cytoplasm viscosity is even higher than the experimental conditions we explored. In addition, the concentration of tubulin in the cytoplasm is estimated to be around 10 μM (Hiller & Weber, 1978; Parsons & Salmon, 1997). A critical concentration of 4 μM therefore implies that the energetic barrier to nucleation in cytoplasm is quite low, and that cells must keep the concentration of tubulin available for polymerisation in check. The action of MAPs throughout the cytoplasm is therefore essential for precise spatiotemporal control of nucleation (Wieczorek et al., 2015), especially as cells change their density of cytoplasm in response to environmental cues (Persson et al., 2020) or depending on phases of the cell cycle (Neurohr & Amon, 2020; Odermatt et al., 2021). In turn, microtubules themselves can contribute to modulating the physical properties of the environment, suggesting feedback loop between cytoplasm composition and microtubule dynamics (Carlini et al., 2020; Charras et al., 2009; Fakhri et al., 2014; Guo et al., 2018)

The physical properties of cytoplasm are of particular interest as they relate to questions of phase separation and liquid-like condensate formation (Ellis, 2001; Mitchison, 2019). Many MAPs have been shown to have disordered domains allowing them to form condensates. Proteins like Tau, TPX2, and several +TIP proteins, just to name a few, undergo liquid-liquid phase separation (King & Petry, 2020; Maan et al., 2023; Meier et al., 2023; Miesch et al., 2021; Song et al., 2023; Tan et al., 2019). This behavior allows some proteins to form a sheath around the microtubule, or a droplet at the growing end, or concentrate tubulin to promote fast nucleation.

The forces driving association reactions, be it the growth of cytoskeletal components or the formation of liquid-like condensates, are heavily dependent on the biophysical properties of cytoplasm (Ellis, 2001; T. J. Mitchison, 2019; Munishkina et al., 2004). Using viscosity and

viscogen size as a tool may provide insight into the formation of some condensates of interest. For example, a series of very recent papers support the notion that +TIP proteins form liquid-like condensates in cells, using multivalent interactions to concentrate various MAPs at microtubule ends (Maan et al., 2023; Meier et al., 2023; Miesch et al., 2021; Song et al., 2023). Viscogens of different sizes may differentially affect the range of conformations explored by unstructured protein domains that form such multivalent interactions. Thus, narrowing down the relevant size scale for the conformational space explored by these domains could help inform the mechanisms of action of these types of proteins.

4.7 Outlook

Dynamic instability is a fascinating behavior that makes microtubules very unique polymers. The development of the GTP-cap model provided a satisfying mechanism to explain stochastic switching between growing and shrinking (Carlier & Pantaloni, 1981; T. Mitchison & Kirschner, 1984b). Later, EBs provided molecular-level details about the size of the GTP-cap and strengthened the notion that catastrophe occurs as a result of loss of the GTP-cap, and that GTP-cap size correlates with microtubule stability and lifetime (Duellberg, Cade, Holmes, et al., 2016; Maurer et al., 2014).

Recent data however has challenged the textbook explanation for catastrophe. The GTP-cap model does not explain how small viscogens or anti-catastrophe factors like CLASP can increase lifetimes without changing the rate of GTP hydrolysis (Lawrence et al., 2018; Majumdar et al., 2018), or how minus ends have longer lifetimes than plus ends despite having smaller GTP-caps (Strothman et al., 2019). Conversely, the GTP-cap model does not explain how the polymerase

XMAP215 could increase GTP-cap size, yet shorten lifetimes (V. Farmer et al., 2021). The “loss of the GTP-cap” is no longer enough to explain why microtubules undergo catastrophe, and so our framework for understanding dynamic instability must go beyond the nucleotide state of tubulin.

The field is now turning towards the structure of the growing end and the relationship between protofilaments to explain catastrophe. Some MAPs like XMAP215 have been shown to cause catastrophe not by catalyzing GTP-hydrolysis, like EBs (Maurer et al., 2014), but rather by disrupting the coordination between growing protofilaments (V. Farmer et al., 2021). The relationship between protofilaments can be further studied by molecular dynamics simulations which can now include multiple protofilaments (Igaev & Grubmüller, 2020), or even a whole microtubule end structure (Igaev & Grubmüller, 2022). These types of simulations are revealing the importance of viscoelastic dynamics of protofilaments and the balance between the strain generated from GTP-hydrolysis and lateral interactions (Igaev & Grubmüller, 2022). The latest Monte Carlo models are also including strain between protofilaments, predicting catastrophe frequencies that are highly dependent on the structure of the growing end (Alexandrova et al., 2022). Such detailed simulations are made possible by recent cryo-EM and tomography structures of wild-type microtubules and, more recently, recombinant microtubules (Alexandrova et al., 2022; LaFrance et al., 2022; McIntosh et al., 2018). Altogether, these recent studies continue to offer molecular level detail to a conceptualization of catastrophes whereby the growing microtubule end is eventually destabilized by an unsustainable number of disrupted lateral contacts (Coombes et al., 2013; V. J. Farmer & Zanic, 2022; Li et al., 2014; Margolin et al., 2011; Rai et al., 2019).

The emergence of new tools and techniques is further propelling the field towards a more complete understanding of microtubules and their dynamic instability. For example, the

development of label-free microscopy techniques like IRM has opened the door to rapid imaging of dynamic microtubules over long timescales (Mahamdeh et al., 2018; Mahamdeh & Howard, 2019). Speed in image acquisition as well as improved image processing pipelines are already shedding light on the role of GTP-hydrolysis in the fluctuations seen during microtubule growth (Cleary et al., 2022). Improvements to imaging techniques also allow more precise tracking of microtubule ends during growth, allowing precise analysis of short pauses and moments of slow growth or shrinking throughout dynamic instability (Mahserejian et al., 2022).

Meanwhile, additional detail continues to be revealed from advances in electron microscopy. Among some of the most striking revelations has been the plasticity of the microtubule lattice. New reconstruction techniques revealed the possibility of multiple seams in the same microtubule, and other asymmetries or discontinuities throughout the lattice (Debs et al., 2020; Guyomar et al., 2022). These techniques will continue to provide useful insight, especially in the comparison of microtubule structure and function across species. Indeed, useful insight on the mechanisms underlying dynamic instability have come from studies of evolutionary divergence of the microtubule structure (Chaaban et al., 2018; Chaaban & Brouhard, 2017; Detrich et al., 2000; Hirst et al., 2020; Murray et al., 2022) (not to mention differences between tubulin isoforms and mutants (Hoff et al., 2022; Ti et al., 2016; Vemu et al., 2017)).

Overall, it will be important to continue to combine detailed, static, structural information with dynamic experiments to develop a framework for understanding dynamic instability that takes into account both the nucleotide state and conformation of the tubulin dimers at the microtubule end. The work presented in this thesis represents a small push on the dynamic side of things. My hope is that this thesis will help future budding researchers in the Brouhard Lab to kick-start their own projects armed with a better understanding of how our current models for dynamic instability

came to be, along with a few examples of how *in vitro* reconstitutions of complex processes can challenge canonical models and lead to a deeper understanding of everyone's favourite polymer.

References

- Aher, A., Kok, M., Sharma, A., Rai, A., Olieric, N., Rodriguez-Garcia, R., Katrukha, E. A., Weinert, T., Olieric, V., Kapitein, L. C., Steinmetz, M. O., Dogterom, M., & Akhmanova, A. (2018). CLASP Suppresses Microtubule Catastrophes through a Single TOG Domain. *Developmental Cell*, *46*(1), 40-58.e8.
<https://doi.org/10.1016/j.devcel.2018.05.032>
- Al-Bassam, J., van Breugel, M., Harrison, S. C., & Hyman, A. (2006). Stu2p binds tubulin and undergoes an open-to-closed conformational change. *The Journal of Cell Biology*, *172*(7), 1009–1022. <https://doi.org/10.1083/jcb.200511010>
- Alexandrova, V. V., Anisimov, M. N., Zaitsev, A. V., Mustyatsa, V. V., Popov, V. V., Ataulakhanov, F. I., & Gudimchuk, N. B. (2022). Theory of tip structure–dependent microtubule catastrophes and damage-induced microtubule rescues. *Proceedings of the National Academy of Sciences*, *119*(46), e2208294119.
<https://doi.org/10.1073/pnas.2208294119>
- Allen, M., Friedler, A., Schon, O., & Bycroft, M. (2002). The Structure of an FF Domain from Human HYPB/EBP1. *Journal of Molecular Biology*, *323*(3), 411–416.
[https://doi.org/10.1016/S0022-2836\(02\)00968-3](https://doi.org/10.1016/S0022-2836(02)00968-3)
- Alushin, G. M., Lander, G. C., Kellogg, E. H., Zhang, R., Baker, D., & Nogales, E. (2014). High-Resolution Microtubule Structures Reveal the Structural Transitions in $\alpha\beta$ -Tubulin upon GTP Hydrolysis. *Cell*, *157*(5), 1117–1129.
<https://doi.org/10.1016/j.cell.2014.03.053>
- Amos, L. A., & Schlieper, D. (2005). Microtubules and Maps. In *Advances in Protein Chemistry* (Vol. 71, pp. 257–298). Academic Press. [https://doi.org/10.1016/S0065-3233\(04\)71007-4](https://doi.org/10.1016/S0065-3233(04)71007-4)
- Ashford, A. J., & Hyman, A. A. (2006). Preparation of tubulin from porcine brain. In *Cell Biology, Four-Volume Set* (Vol. 2, pp. 155–160). Elsevier Inc.
<https://doi.org/10.1016/B978-012164730-8/50094-0>
- Aumeier, C., Schaedel, L., Gaillard, J., John, K., Blanchoin, L., & Théry, M. (2016). Self-repair promotes microtubule rescue. *Nature Cell Biology*, *18*(10), 1054–1064.
<https://doi.org/10.1038/ncb3406>

- Ayaz, P., Munyoki, S., Geyer, E. A., Piedra, F.-A., Vu, E. S., Bromberg, R., Otwinowski, Z., Grishin, N. V., Brautigam, C. A., & Rice, L. M. (2014). A tethered delivery mechanism explains the catalytic action of a microtubule polymerase. *eLife*, *3*, e03069.
<https://doi.org/10.7554/eLife.03069>
- Ayaz, P., Ye, X., Huddleston, P., Brautigam, C. A., & Rice, L. M. (2012). A TOG: $\alpha\beta$ -tubulin Complex Structure Reveals Conformation-Based Mechanisms for a Microtubule Polymerase. *Science*, *337*(6096), 857–860. <https://doi.org/10.1126/science.1221698>
- Bechstedt, S., & Brouhard, G. J. (2012). Doublecortin recognizes the 13-protofilament microtubule cooperatively and tracks microtubule ends. *Developmental Cell*, *23*(1), 181–192. <https://doi.org/10.1016/j.devcel.2012.05.006>
- Bechstedt, S., Lu, K., & Brouhard, G. J. (2014). Doublecortin recognizes the longitudinal curvature of the microtubule end and lattice. *Current Biology*, *24*(20), 2366–2375.
<https://doi.org/10.1016/j.cub.2014.08.039>
- Berg, O. G., & von Hippel, P. H. (1985). Diffusion-controlled macromolecular interactions. *Annual Review of Biophysics and Biophysical Chemistry*, *14*, 131–160.
<https://doi.org/10.1146/annurev.bb.14.060185.001023>
- Bieling, P., Laan, L., Schek, H., Munteanu, E. L., Sandblad, L., Dogterom, M., Brunner, D., & Surrey, T. (2007). Reconstitution of a microtubule plus-end tracking system in vitro. *Nature*, *450*(7172), Article 7172. <https://doi.org/10.1038/nature06386>
- Bieling, P., Telley, I. A., & Surrey, T. (2010). A Minimal Midzone Protein Module Controls Formation and Length of Antiparallel Microtubule Overlaps. *Cell*, *142*(3), 420–432.
<https://doi.org/10.1016/j.cell.2010.06.033>
- Bollinger, J. A., Imam, Z. I., Stevens, M. J., & Bachand, G. D. (2020). Tubulin islands containing slowly hydrolyzable GTP analogs regulate the mechanism and kinetics of microtubule depolymerization. *Scientific Reports*, *10*(1), 1–11.
<https://doi.org/10.1038/s41598-020-70602-0>
- Borisy, G. G., & Taylor, E. W. (1967). THE MECHANISM OF ACTION OF COLCHICINE. *The Journal of Cell Biology*, *34*(2), 525–533.
- Brouhard, G. J., & Rice, L. M. (2014). The contribution of $\alpha\beta$ -tubulin curvature to microtubule dynamics. *The Journal of Cell Biology*, *207*(3), 323–334.
<https://doi.org/10.1083/jcb.201407095>

- Brouhard, G. J., & Rice, L. M. (2018). Microtubule dynamics: An interplay of biochemistry and mechanics. *Nature Reviews Molecular Cell Biology*, *19*(7), 451–463.
<https://doi.org/10.1038/s41580-018-0009-y>
- Brouhard, G. J., Stear, J. H., Noetzel, T. L., Al-Bassam, J., Kinoshita, K., Harrison, S. C., Howard, J., & Hyman, A. A. (2008). XMAP215 is a processive microtubule polymerase. *Cell*, *132*(1), 79–88. <https://doi.org/10.1016/j.cell.2007.11.043>
- Carrier, M. F., & Pantaloni, D. (1981). Kinetic analysis of guanosine 5'-triphosphate hydrolysis associated with tubulin polymerization. *Biochemistry*, *20*(7), 1918–1924.
<https://doi.org/10.1021/bi00510a030>
- Carlini, L., Brittingham, G. P., Holt, L. J., & Kapoor, T. M. (2020). Microtubules Enhance Mesoscale Effective Diffusivity in the Crowded Metaphase Cytoplasm. *Developmental Cell*. <https://doi.org/10.1016/j.devcel.2020.07.020>
- Chaaban, S., & Brouhard, G. J. (2017). A microtubule bestiary: Structural diversity in tubulin polymers. *Molecular Biology of the Cell*, *28*(22), 2924–2931.
<https://doi.org/10.1091/mbc.e16-05-0271>
- Chaaban, S., Jariwala, S., Hsu, C. T., Redemann, S., Kollman, J. M., Müller-Reichert, T., Sept, D., Bui, K. H., & Brouhard, G. J. (2018). The Structure and Dynamics of *C. elegans* Tubulin Reveals the Mechanistic Basis of Microtubule Growth. *Developmental Cell*, *47*(2), 191-204.e8. <https://doi.org/10.1016/j.devcel.2018.08.023>
- Charras, G. T., Mitchison, T. J., & Mahadevan, L. (2009). Animal cell hydraulics. *Journal of Cell Science*, *122*(18), 3233–3241. <https://doi.org/10.1242/jcs.049262>
- Chretien, D., Fuller, S. D., & Karsenti, E. (1995). Structure of growing microtubule ends: Two-dimensional sheets close into tubes at variable rates. *Journal of Cell Biology*, *129*(5), 1311–1328. <https://doi.org/10.1083/jcb.129.5.1311>
- Cleary, J. M., & Hancock, W. O. (2021). Molecular mechanisms underlying microtubule growth dynamics. *Current Biology*, *31*(10), R560–R573.
<https://doi.org/10.1016/j.cub.2021.02.035>
- Cleary, J. M., Kim, T., Cook, A. S., McCormick, L. A., Hancock, W. O., & Rice, L. M. (2022). Measurements and simulations of microtubule growth imply strong longitudinal interactions and reveal a role for GDP on the elongating end. *eLife*, *11*, e75931.
<https://doi.org/10.7554/eLife.75931>

- Coombes, C. E., Yamamoto, A., Kenzie, M. R., Odde, D. J., & Gardner, M. K. (2013). Evolving Tip Structures Can Explain Age-Dependent Microtubule Catastrophe. *Current Biology*, 23(14), 1342–1348. <https://doi.org/10.1016/J.CUB.2013.05.059>
- David-Pfeuty, T., Erickson, H. P., & Pantaloni, D. (1977). Guanosinetriphosphatase activity of tubulin associated with microtubule assembly. *Proceedings of the National Academy of Sciences of the United States of America*, 74(12), 5372–5376.
- Debs, G. E., Cha, M., Liu, X., Huehn, A. R., & Sindelar, C. V. (2020). Dynamic and asymmetric fluctuations in the microtubule wall captured by high-resolution cryoelectron microscopy. *Proceedings of the National Academy of Sciences*, 117(29), 16976–16984. <https://doi.org/10.1073/pnas.2001546117>
- des Portes, V., Pinard, J. M., Billuart, P., Vinet, M. C., Koulakoff, A., Carrié, A., Gelot, A., Dupuis, E., Motte, J., Berwald-Netter, Y., Catala, M., Kahn, A., Beldjord, C., & Chelly, J. (1998). A novel CNS gene required for neuronal migration and involved in X-linked subcortical laminar heterotopia and lissencephaly syndrome. *Cell*, 92(1), 51–61. [https://doi.org/10.1016/s0092-8674\(00\)80898-3](https://doi.org/10.1016/s0092-8674(00)80898-3)
- Desai, A., & Mitchison, T. J. (1997). Microtubule polymerization dynamics. *Annual Review of Cell and Developmental Biology*, 13, 83–117. <https://doi.org/10.1146/annurev.cellbio.13.1.83>
- Detrich, H. W., Parker, S. K., Williams, R. C., Nogales, E., & Downing, K. H. (2000). Cold Adaptation of Microtubule Assembly and Dynamics: STRUCTURAL INTERPRETATION OF PRIMARY SEQUENCE CHANGES PRESENT IN THE α - AND β -TUBULINS OF ANTARCTIC FISHES*. *Journal of Biological Chemistry*, 275(47), 37038–37047. <https://doi.org/10.1074/jbc.M005699200>
- Dimitrov, A., Quesnoit, M., Moutel, S., Cantaloube, I., Poüs, C., & Perez, F. (2008). Detection of GTP-Tubulin Conformation in Vivo Reveals a Role for GTP Remnants in Microtubule Rescues. *Science*, 322(5906), 1353–1356. <https://doi.org/10.1126/science.1165401>
- Drechsel, D. N., Hyman, A. A., Cobb, M. H., & Kirschner, M. W. (1992). Modulation of the dynamic instability of tubulin assembly by the microtubule-associated protein tau. *Molecular Biology of the Cell*, 3(10), 1141–1154.

- Drenckhahn, D., & Pollard, T. D. (1986). Elongation of actin filaments is a diffusion-limited reaction at the barbed end and is accelerated by inert macromolecules. *The Journal of Biological Chemistry*, 261(27), 12754–12758.
- Duellberg, C., Cade, N. I., Holmes, D., & Surrey, T. (2016). The size of the EB cap determines instantaneous microtubule stability. *eLife*, 5. <https://doi.org/10.7554/eLife.13470>
- Duellberg, C., Cade, N. I., & Surrey, T. (2016). Microtubule aging probed by microfluidics-assisted tubulin washout. *Molecular Biology of the Cell*, 27(22), 3563–3573. <https://doi.org/10.1091/mbc.E16-07-0548>
- Dupuis, N. F., Holmstrom, E. D., & Nesbitt, D. J. (2018). Tests of Kramers' Theory at the Single-Molecule Level: Evidence for Folding of an Isolated RNA Tertiary Interaction at the Viscous Speed Limit. *The Journal of Physical Chemistry B*, 122(38), 8796–8804. <https://doi.org/10.1021/acs.jpcc.8b04014>
- Ellis, R. J. (2001). Macromolecular crowding: Obvious but underappreciated. *Trends in Biochemical Sciences*, 26(10), 597–604. [https://doi.org/10.1016/s0968-0004\(01\)01938-7](https://doi.org/10.1016/s0968-0004(01)01938-7)
- Erickson, H. P. (1974). Microtubule surface lattice and subunit structure and observations on reassembly. *The Journal of Cell Biology*, 60(1). <http://jcb.rupress.org/content/60/1/153.long>
- Erickson, H. P., & Pantaloni, D. (1981). The role of subunit entropy in cooperative assembly. Nucleation of microtubules and other two-dimensional polymers. *Biophysical Journal*, 34(2), 293–309. [https://doi.org/10.1016/S0006-3495\(81\)84850-3](https://doi.org/10.1016/S0006-3495(81)84850-3)
- Estévez-Gallego, J., Josa-Prado, F., Ku, S., Buey, R. M., Balaguer, F. A., Prota, A. E., Lucena-Agell, D., Kamma-Lorger, C., Yagi, T., Iwamoto, H., Duchesne, L., Barasoain, I., Steinmetz, M. O., Chrétien, D., Kamimura, S., Díaz, J. F., & Oliva, M. A. (2020). Structural model for differential cap maturation at growing microtubule ends. *eLife*, 9. <https://doi.org/10.7554/elife.50155>
- Fakhri, N., Wessel, A. D., Willms, C., Pasquali, M., Klopfenstein, D. R., MacKintosh, F. C., & Schmidt, C. F. (2014). High-resolution mapping of intracellular fluctuations using carbon nanotubes. *Science*, 344(6187), 1031–1035. <https://doi.org/10.1126/science.1250170>
- Farmer, V., Arpağ, G., Hall, S. L., & Zanic, M. (2021). XMAP215 promotes microtubule catastrophe by disrupting the growing microtubule end. *Journal of Cell Biology*, 220(10), e202012144. <https://doi.org/10.1083/jcb.202012144>

- Farmer, V. J., & Zanic, M. (2022). Beyond the GTP-cap: Elucidating the molecular mechanisms of microtubule catastrophe. *BioEssays*, *n/a(n/a)*, 2200081.
<https://doi.org/10.1002/bies.202200081>
- Fees, C. P., & Moore, J. K. (2019). A unified model for microtubule rescue. *Molecular Biology of the Cell*, *mbc.E18-08-0541*. <https://doi.org/10.1091/mbc.E18-08-0541>
- Flor-Parra, I., Iglesias-Romero, A. B., & Chang, F. (2018). The XMAP215 Ortholog Alp14 Promotes Microtubule Nucleation in Fission Yeast. *Current Biology*, *28(11)*, 1681-1691.e4. <https://doi.org/10.1016/j.cub.2018.04.008>
- Flyvbjerg, H., Jobs, E., & Leibler, S. (1996). *Kinetics of self-assembling microtubules: An “inverse problem” in biochemistry*. *93*, 5975–5979.
- Fourniol, F. J., Sindelar, C. V., Amigues, B., Clare, D. K., Thomas, G., Perderiset, M., Francis, F., Houdusse, A., & Moores, C. A. (2010). Template-free 13-protofilament microtubule-MAP assembly visualized at 8 Å resolution. *Journal of Cell Biology*, *191(3)*, 463–470.
<https://doi.org/10.1083/jcb.201007081>
- Fyngenson, D. K., Braun, E., & Libchaber, A. (1994). Phase diagram of microtubules. *Physical Review E*, *50(2)*, 1579–1588. <https://doi.org/10.1103/PhysRevE.50.1579>
- Gard, D. L., & Kirschner, M. W. (1987). A microtubule-associated protein from *Xenopus* eggs that specifically promotes assembly at the plus-end. *The Journal of Cell Biology*, *105(5)*, 2203–2215. <https://doi.org/10.1083/jcb.105.5.2203>
- Gardner, M. K., Charlebois, B. D., Jánosi, I. M., Howard, J., Hunt, A. J., & Odde, D. J. (2011). Rapid Microtubule Self-Assembly Kinetics. *Cell*, *146(4)*, 582–592.
<https://doi.org/10.1016/j.cell.2011.06.053>
- Gardner, M. K., Zanic, M., Gell, C., Bormuth, V., & Howard, J. (2011). Depolymerizing Kinesins Kip3 and MCAK Shape Cellular Microtubule Architecture by Differential Control of Catastrophe. *Cell*, *147(5)*, 1092–1103.
<https://doi.org/10.1016/J.CELL.2011.10.037>
- Gardner, M. K., Zanic, M., & Howard, J. (2013). Microtubule catastrophe and rescue. *Current Opinion in Cell Biology*, *25(1)*, 14–22. <https://doi.org/10.1016/j.ceb.2012.09.006>
- Gell, C., Bormuth, V., Brouhard, G. J., Cohen, D. N., Diez, S., Friel, C. T., Helenius, J., Nitsche, B., Petzold, H., Ribbe, J., Schäffer, E., Stear, J. H., Trushko, A., Varga, V., Widlund, P. O., Zanic, M., & Howard, J. (2010). Microtubule Dynamics Reconstituted In

- Vitro and Imaged by Single-Molecule Fluorescence Microscopy. *Methods in Cell Biology*, 95, 221–245. [https://doi.org/10.1016/S0091-679X\(10\)95013-9](https://doi.org/10.1016/S0091-679X(10)95013-9)
- Gell, C., Friel, C. T., Borgonovo, B., Drechsel, D. N., Hyman, A. A., & Howard, J. (2011). Purification of tubulin from porcine brain. *Methods Mol. Biol.*, 777, 15–28.
- Geyer, E. A., Burns, A., Lalonde, B. A., Ye, X., Piedra, F. A., Huffaker, T. C., & Rice, L. M. (2015). A mutation uncouples the tubulin conformational and GTPase cycles, revealing allosteric control of microtubule dynamics. *eLife*, 4(2015). <https://doi.org/10.7554/eLife.10113>
- Gigant, B., Curmi, P. A., Martin-Barbey, C., Charbaut, E., Lachkar, S., Lebeau, L., Siavoshian, S., Sobel, A., & Knossow, M. (2000). The 4 Å X-Ray Structure of a Tubulin:Stathmin-like Domain Complex. *Cell*, 102(6), 809–816. [https://doi.org/10.1016/S0092-8674\(00\)00069-6](https://doi.org/10.1016/S0092-8674(00)00069-6)
- Gleeson, J. G., Allen, K. M., Fox, J. W., Lamperti, E. D., Berkovic, S., Scheffer, I., Cooper, E. C., Dobyns, W. B., Minnerath, S. R., Ross, M. E., & Walsh, C. A. (1998). Doublecortin, a Brain-Specific Gene Mutated in Human X-Linked Lissencephaly and Double Cortex Syndrome, Encodes a Putative Signaling Protein. *Cell*, 92(1), 63–72. [https://doi.org/10.1016/S0092-8674\(00\)80899-5](https://doi.org/10.1016/S0092-8674(00)80899-5)
- Gonzalez, S. J., Goldblum, R. R., Vu, K. T., Shoemaker, R., Reid, T., McClellan, M., & Gardner, M. K. (2022). *Rapid binding to protofilament edge sites facilitates tip tracking of EB1 at growing microtubule plus-ends* [Preprint]. Cell Biology. <https://doi.org/10.1101/2022.06.07.495114>
- Guo, Y., Li, D., Zhang, S., Yang, Y., Liu, J.-J., Wang, X., Liu, C., Milkie, D. E., Moore, R. P., Tulu, U. S., Kiehart, D. P., Hu, J., Lippincott-Schwartz, J., Betzig, E., & Li, D. (2018). Visualizing Intracellular Organelle and Cytoskeletal Interactions at Nanoscale Resolution on Millisecond Timescales. *Cell*, 175(5), 1430-1442.e17. <https://doi.org/10.1016/j.cell.2018.09.057>
- Guyomar, C., Bousquet, C., Ku, S., Heumann, J. M., Guilloux, G., Gaillard, N., Heichette, C., Duchesne, L., Steinmetz, M. O., Gibeaux, R., & Chrétien, D. (2022). Changes in seam number and location induce holes within microtubules assembled from porcine brain tubulin and in *Xenopus* egg cytoplasmic extracts. *eLife*, 11, e83021. <https://doi.org/10.7554/eLife.83021>

- Hagen, S. J. (2010). Solvent viscosity and friction in protein folding dynamics. *Current Protein & Peptide Science*, *11*(5), 385–395. <https://doi.org/10.2174/138920310791330596>
- Helenius, J., Brouhard, G., Kalaidzidis, Y., Diez, S., & Howard, J. (2006). The depolymerizing kinesin MCAK uses lattice diffusion to rapidly target microtubule ends. *Nature*, *441*(1), 115–119. <https://doi.org/10.1038/nature04736>
- Hirst, W. G., Biswas, A., Mahalingan, K. K., & Reber, S. (2020). Differences in Intrinsic Tubulin Dynamic Properties Contribute to Spindle Length Control in *Xenopus* Species. *Current Biology*. <https://doi.org/10.1016/j.cub.2020.03.067>
- Hoff, K. J., Neumann, A. J., & Moore, J. K. (2022). The molecular biology of tubulinopathies: Understanding the impact of variants on tubulin structure and microtubule regulation. *Frontiers in Cellular Neuroscience*, *16*. <https://www.frontiersin.org/articles/10.3389/fncel.2022.1023267>
- Honnappa, S., Cutting, B., Jahnke, W., Seelig, J., & Steinmetz, M. O. (2003). Thermodynamics of the Op18/Stathmin-Tubulin Interaction*. *Journal of Biological Chemistry*, *278*(40), 38926–38934. <https://doi.org/10.1074/jbc.M305546200>
- Horio, T., & Hotani, H. (1986). Visualization of the dynamic instability of individual microtubules by dark-field microscopy. *Nature*, *321*(6070), 605–607. <https://doi.org/10.1038/321605a0>
- Howard, W. D., & Timasheff, S. N. (1986). GDP state of tubulin: Stabilization of double rings. *Biochemistry*, *25*(25), 8292–8300. <https://doi.org/10.1021/bi00373a025>
- Howes, S. C., Geyer, E. A., LaFrance, B., Zhang, R., Kellogg, E. H., Westermann, S., Rice, L. M., & Nogales, E. (2017). Structural differences between yeast and mammalian microtubules revealed by cryo-EM. *Journal of Cell Biology*, *216*(9), 2669–2677. <https://doi.org/10.1083/jcb.201612195>
- Hyman, A. A., Chrétien, D., Arnal, I., & Wade, R. H. (1995). Structural changes accompanying GTP hydrolysis in microtubules: Information from a slowly hydrolyzable analogue guanylyl-(alpha,beta)-methylene-diphosphonate. *Journal of Cell Biology*, *128*(1), 117–125. <https://doi.org/10.1083/jcb.128.1.117>
- Hyman, A. A., Salser, S., Drechsel, D. N., Unwin, N., & Mitchison, T. J. (1992). Role of GTP hydrolysis in microtubule dynamics: Information from a slowly hydrolyzable analogue,

- GMPCPP. *Molecular Biology of the Cell*, 3(10), 1155–1167.
<https://doi.org/10.1091/mbc.E12-03-0186>
- Igaev, M., & Grubmüller, H. (2020). Microtubule instability driven by longitudinal and lateral strain propagation. *PLOS Computational Biology*, 16(9), e1008132.
<https://doi.org/10.1371/journal.pcbi.1008132>
- Igaev, M., & Grubmüller, H. (2022). Bending-torsional elasticity and energetics of the plus-end microtubule tip. *Proceedings of the National Academy of Sciences*, 119(12), e2115516119. <https://doi.org/10.1073/pnas.2115516119>
- Ip, S. H., Johnson, M. L., & Ackers, G. K. (1976). Kinetics of deoxyhemoglobin subunit dissociation determined by haptoglobin binding: Estimation of the equilibrium constant from forward and reverse rates. *Biochemistry*, 15(3), 654–660.
<https://doi.org/10.1021/bi00648a032>
- Janson, M. E., de Dood, M. E., & Dogterom, M. (2003). Dynamic instability of microtubules is regulated by force. *The Journal of Cell Biology*, 161(6), 1029–1034.
<https://doi.org/10.1083/jcb.200301147>
- Jonasson, E. M., Mauro, A. J., Li, C., Labuz, E. C., Mahserejian, S. M., Scripture, J. P., Gregoret, I. V., Alber, M., & Goodson, H. V. (2019). Behaviors of individual microtubules and microtubule populations relative to critical concentrations: Dynamic instability occurs when critical concentrations are driven apart by nucleotide hydrolysis. *Molecular Biology of the Cell*, mbcE19020101. <https://doi.org/10.1091/mbc.E19-02-0101>
- Keates, R. A. B. (1980). Effects of glycerol on microtubule polymerization kinetics. *Biochemical and Biophysical Research Communications*, 97(3), 1163–1169.
[https://doi.org/10.1016/0006-291X\(80\)91497-7](https://doi.org/10.1016/0006-291X(80)91497-7)
- Keating, T. J., & Borisy, G. G. (2000). Immunostuctural evidence for the template mechanism of microtubule nucleation. *Nature Cell Biology*, 2(6), 352–357.
<https://doi.org/10.1038/35014045>
- Kellett, G. L., & Gutfreund, H. (1970). Reactions of haemoglobin dimers after ligand dissociation. *Nature*, 227(5261), 921–926. <https://doi.org/10.1038/227921a0>
- Kerssemakers, J. W. J., Munteanu, E. L., Laan, L., Noetzel, T. L., Janson, M. E., & Dogterom, M. (2006). Assembly dynamics of microtubules at molecular resolution. *Nature*, 442(7103), 709–712. <https://doi.org/10.1038/nature04928>

- King, M. R., & Petry, S. (2020). Phase separation of TPX2 enhances and spatially coordinates microtubule nucleation. *Nature Communications*, *11*(1), Article 1.
<https://doi.org/10.1038/s41467-019-14087-0>
- Koren, R., & Hammes, G. G. (1976). A kinetic study of protein-protein interactions. *Biochemistry*, *15*(5), 1165–1171. <https://doi.org/10.1021/bi00650a032>
- Kuchnir Fygenson, D., Flyvbjerg, H., Sneppen, K., Libchaber, A., & Leibler, S. (1995). Spontaneous nucleation of microtubules. *PHYSICAL REVIEW E*, *51*(5).
- Kueh, H. Y., & Mitchison, T. J. (2009). Structural Plasticity in Actin and Tubulin Polymer Dynamics. *Science (New York, N.Y.)*, *325*(5943), 960–963.
<https://doi.org/10.1126/science.1168823>
- LaFrance, B. J., Roostalu, J., Henkin, G., Greber, B. J., Zhang, R., Normanno, D., McCollum, C. O., Surrey, T., & Nogales, E. (2022). Structural transitions in the GTP cap visualized by cryo-electron microscopy of catalytically inactive microtubules. *Proceedings of the National Academy of Sciences*, *119*(2), e2114994119.
<https://doi.org/10.1073/pnas.2114994119>
- LaFrance, B. J., Roostalu, J., Henkin, G., Greber, B. J., Zhang, R., Normanno, D., McCollum, C., Surrey, T., & Nogales, E. (2021). *Structural transitions in the GTP cap visualized by cryo-EM of catalytically inactive microtubules* [Preprint]. Biophysics.
<https://doi.org/10.1101/2021.08.13.456308>
- Lawrence, E. J., Arpag˘, G., Norris, S. R., & Zanic, M. (2018). Human CLASP2 specifically regulates microtubule catastrophe and rescue. *Molecular Biology of the Cell*, *29*(10), 1168–1177. <https://doi.org/10.1091/mbc.E18-01-0016>
- Lawrence, E. J., Chatterjee, S., & Zanic, M. (2022). *CLASPs stabilize the intermediate state between microtubule growth and catastrophe* (p. 2022.12.03.518990). bioRxiv.
<https://doi.org/10.1101/2022.12.03.518990>
- Lawrence, E. J., Zanic, M., & Rice, L. M. (2020). CLASPs at a glance. *Journal of Cell Science*, *133*(8), jcs243097. <https://doi.org/10.1242/jcs.243097>
- Leano, J. B., Rogers, S. L., & Slep, K. C. (2013). A Cryptic TOG Domain with a Distinct Architecture Underlies CLASP-Dependent Bipolar Spindle Formation. *Structure*, *21*(6), 939–950. <https://doi.org/10.1016/j.str.2013.04.018>

- Li, C., Li, J., Goodson, H. V., & Alber, M. S. (2014). Microtubule dynamic instability: The role of cracks between protofilaments. *Soft Matter*, *10*(12), 2069–2080. <https://doi.org/10.1039/C3SM52892H>
- Maan, R., Reese, L., Volkov, V. A., King, M. R., van der Sluis, E. O., Andrea, N., Evers, W. H., Jakobi, A. J., & Dogterom, M. (2023). Multivalent interactions facilitate motor-dependent protein accumulation at growing microtubule plus-ends. *Nature Cell Biology*, *25*(1), Article 1. <https://doi.org/10.1038/s41556-022-01037-0>
- Mahamdeh, M., & Howard, J. (2019). Implementation of Interference Reflection Microscopy for Label-free, High-speed Imaging of Microtubules. *Journal of Visualized Experiments*, *150*. <https://doi.org/10.3791/59520>
- Mahamdeh, M., Simmert, S., Luchniak, A., Schäffer, E., & Howard, J. (2018). Label-free high-speed wide-field imaging of single microtubules using interference reflection microscopy. *Journal of Microscopy*, *272*(1), 60–66. <https://doi.org/10.1111/jmi.12744>
- Mahserejian, S. M., Scripture, J. P., Mauro, A. J., Lawrence, E. J., Jonasson, E. M., Murray, K. S., Li, J., Gardner, M., Alber, M., Zanic, M., & Goodson, H. V. (2022). Quantification of microtubule stutters: Dynamic instability behaviors that are strongly associated with catastrophe. *Molecular Biology of the Cell*, *33*(3), ar22. <https://doi.org/10.1091/mbc.E20-06-0348>
- Majumdar, S., Kim, T., Chen, Z., Munyoki, S., Tso, S.-C., Brautigam, C. A., & Rice, L. M. (2018). An isolated CLASP TOG domain suppresses microtubule catastrophe and promotes rescue. *Molecular Biology of the Cell*, *29*(11), 1359–1375. <https://doi.org/10.1091/mbc.E17-12-0748>
- Mandelkow, E. M., Mandelkow, E., & Milligan, R. A. (1991). Microtubule dynamics and microtubule caps: A time-resolved cryo-electron microscopy study. *Journal of Cell Biology*, *114*(5), 977–991. <https://doi.org/10.1083/jcb.114.5.977>
- Manka, S. W., & Moores, C. A. (2018). The role of tubulin–tubulin lattice contacts in the mechanism of microtubule dynamic instability. *Nature Structural & Molecular Biology*, *25*(7), 607–615. <https://doi.org/10.1038/s41594-018-0087-8>
- Manka, S. W., & Moores, C. A. (2020). Pseudo-repeats in doublecortin make distinct mechanistic contributions to microtubule regulation. *EMBO Reports*. <https://doi.org/10.15252/embr.202051534>

- Margolin, G., Goodson, H. V., & Alber, M. S. (2011). Mean-field study of the role of lateral cracks in microtubule dynamics. *Physical Review E*, 83(4), 041905. <https://doi.org/10.1103/PhysRevE.83.041905>
- Margolin, G., Gregoret, I. V., Cickovski, T. M., Li, C., Shi, W., Alber, M. S., & Goodson, H. V. (2012). The mechanisms of microtubule catastrophe and rescue: Implications from analysis of a dimer-scale computational model. *Molecular Biology of the Cell*, 23(4), 642–656. <https://doi.org/10.1091/mbc.e11-08-0688>
- Maurer, S. P., Bieling, P., Cope, J., Hoenger, A., & Surrey, T. (2011). GTP γ S microtubules mimic the growing microtubule end structure recognized by end-binding proteins (EBs). *Proceedings of the National Academy of Sciences*, 108(10), 3988–3993. <https://doi.org/10.1073/pnas.1014758108>
- Maurer, S. P., Cade, N. I., Bohner, G., Gustafsson, N., Boutant, E., & Surrey, T. (2014). EB1 Accelerates Two Conformational Transitions Important for Microtubule Maturation and Dynamics. *Current Biology*, 24(4), 372–384. <https://doi.org/10.1016/j.cub.2013.12.042>
- Maurer, S. P., Fourniol, F. J., Bohner, G., Moores, C. A., & Surrey, T. (2012). EBs Recognize a Nucleotide-Dependent Structural Cap at Growing Microtubule Ends. *Cell*, 149(2), 371–382. <https://doi.org/10.1016/j.cell.2012.02.049>
- McGuffee, S. R., & Elcock, A. H. (2010a). Diffusion, crowding & protein stability in a dynamic molecular model of the bacterial cytoplasm. *PLoS Computational Biology*, 6(3), e1000694. <https://doi.org/10.1371/journal.pcbi.1000694>
- McGuffee, S. R., & Elcock, A. H. (2010b). Diffusion, crowding & protein stability in a dynamic molecular model of the bacterial cytoplasm. *PLoS Computational Biology*, 6(3), e1000694. <https://doi.org/10.1371/journal.pcbi.1000694>
- McIntosh, J. R., O'Toole, E., Morgan, G., Austin, J., Ulyanov, E., Ataullakhanov, F., & Gudimchuk, N. (2018). Microtubules grow by the addition of bent guanosine triphosphate tubulin to the tips of curved protofilaments. *The Journal of Cell Biology*, jcb.201802138. <https://doi.org/10.1083/jcb.201802138>
- Meier, S. M., Farcas, A.-M., Kumar, A., Ijavi, M., Bill, R. T., Stelling, J., Dufresne, E. R., Steinmetz, M. O., & Barral, Y. (2023). Multivalency ensures persistence of a +TIP body at specialized microtubule ends. *Nature Cell Biology*, 25(1), Article 1. <https://doi.org/10.1038/s41556-022-01035-2>

- Melki, R., Carlier, M. F., Pantaloni, D., & Timasheff, S. N. (1989). Cold depolymerization of microtubules to double rings: Geometric stabilization of assemblies. *Biochemistry*, 28(23), 9143–9152. <https://doi.org/10.1021/bi00449a028>
- Mickolajczyk, K. J., Geyer, E. A., Kim, T., Rice, L. M., & Hancock, W. O. (2019). Direct observation of individual tubulin dimers binding to growing microtubules. *Proceedings of the National Academy of Sciences of the United States of America*, 116(15), 7314–7322. <https://doi.org/10.1073/pnas.1815823116>
- Miesch, J., Wimbish, R. T., Velluz, M.-C., & Aumeier, C. (2021). *A liquid +TIP-network drives microtubule dynamics through tubulin condensation* [Preprint]. *Cell Biology*. <https://doi.org/10.1101/2021.09.13.459419>
- Milo, R., & Phillips, R. (2015). *Cell Biology by the numbers* (1st ed.). Garland Science.
- Mitchison, T. J. (2019). Colloid osmotic parameterization and measurement of subcellular crowding. *Molecular Biology of the Cell*, 30(2), 173–180. <https://doi.org/10.1091/mbc.E18-09-0549>
- Mitchison, T., & Kirschner, M. (1984a). Microtubule assembly nucleated by isolated centrosomes. *Nature*, 312(5991), Article 5991. <https://doi.org/10.1038/312232a0>
- Mitchison, T., & Kirschner, M. (1984b). Dynamic instability of microtubule growth. *Nature*, 312(5991), 237–242. <https://doi.org/10.1038/312237a0>
- Mohan, R., Katrukha, E. A., Doodhi, H., Smal, I., Meijering, E., Kapitein, L. C., Steinmetz, M. O., & Akhmanova, A. (2013). End-binding proteins sensitize microtubules to the action of microtubule-targeting agents. *Proceedings of the National Academy of Sciences of the United States of America*, 110(22), 8900–8905. <https://doi.org/10.1073/pnas.1300395110>
- Molines, A. T., Lemièrè, J., Gazzola, M., Steinmark, I. E., Edrington, C. H., Hsu, C.-T., Real-Calderon, P., Suhling, K., Goshima, G., Holt, L. J., They, M., Brouhard, G. J., & Chang, F. (2022). Physical properties of the cytoplasm modulate the rates of microtubule polymerization and depolymerization. *Developmental Cell*, 57(4), 466-479.e6. <https://doi.org/10.1016/j.devcel.2022.02.001>
- Molines, A. T., Stoppin-Mellet, V., Arnal, I., Coquelle, F. M., & Coquelle, F. M. (2020). Plant and mouse EB1 proteins have opposite intrinsic properties on the dynamic instability of microtubules. *BMC Research Notes*, 13(1), 296. <https://doi.org/10.1186/s13104-020-05139-6>

- Moore, C. A., Perderiset, M., Francis, F., Chelly, J., Houdusse, A., & Milligan, R. A. (2004). Mechanism of microtubule stabilization by doublecortin. *Molecular Cell*, *14*(6), 833–839. <https://doi.org/10.1016/j.molcel.2004.06.009>
- Moore, C. A., Perderiset, M., Kappeler, C., Kain, S., Drummond, D., Perkins, S. J., Chelly, J., Cross, R., Houdusse, A., & Francis, F. (2006). Distinct roles of doublecortin modulating the microtubule cytoskeleton. *EMBO Journal*, *25*(19), 4448–4457. <https://doi.org/10.1038/sj.emboj.7601335>
- Munishkina, L. A., Cooper, E. M., Uversky, V. N., & Fink, A. L. (2004). The effect of macromolecular crowding on protein aggregation and amyloid fibril formation. *Journal of Molecular Recognition*, *17*(5), 456–464. <https://doi.org/10.1002/jmr.699>
- Murray, L. E., Kim, H., Rice, L. M., & Asbury, C. L. (2022). Working strokes produced by curling protofilaments at disassembling microtubule tips can be biochemically tuned and vary with species. *eLife*, *11*, e83225. <https://doi.org/10.7554/eLife.83225>
- Nawrotek, A., Knossow, M., & Gigant, B. (2011). The Determinants That Govern Microtubule Assembly from the Atomic Structure of GTP-Tubulin. *Journal of Molecular Biology*, *412*(1), 35–42. <https://doi.org/10.1016/j.jmb.2011.07.029>
- Nettesheim, G., Nabti, I., Murade, C. U., Jaffe, G. R., King, S. J., & Shubeita, G. T. (2020). Macromolecular crowding acts as a physical regulator of intracellular transport. *Nature Physics*, *16*(11), 1144–1151. <https://doi.org/10.1038/s41567-020-0957-y>
- Neurohr, G. E., & Amon, A. (2020). Relevance and Regulation of Cell Density. *Trends in Cell Biology*, *30*(3), 213–225. <https://doi.org/10.1016/j.tcb.2019.12.006>
- Noble, R. W., Reichlin, M., & Gibson, Q. H. (1969). The Reactions of Antibodies with Hemeprotein Antigens: The Measurement of Reaction Kinetics and Stoichiometry by Fluorescence Quenching. *Journal of Biological Chemistry*, *244*(9), 2403–2411. [https://doi.org/10.1016/S0021-9258\(19\)78238-6](https://doi.org/10.1016/S0021-9258(19)78238-6)
- Nogales, E. (1999). A structural view of microtubule dynamics. *Cellular and Molecular Life Sciences CMLS*, *56*(1), 133–142. <https://doi.org/10.1007/s000180050012>
- Nogales, E., Wolf, S. G., & Downing, K. H. (1998). Structure of the $\alpha\beta$ tubulin dimer by electron crystallography. *Nature*, *391*(6663), Article 6663. <https://doi.org/10.1038/34465>
- Northrup, S. H., & Erickson, H. P. (1992). Kinetics of protein-protein association explained by Brownian dynamics computer simulation. *Proceedings of the National Academy of*

- Sciences of the United States of America*, 89(8), 3338–3342.
<https://doi.org/10.1073/pnas.89.8.3338>
- Odde, D. J. (1997). Estimation of the diffusion-limited rate of microtubule assembly. *Biophysical Journal*, 73(1), 88–96.
- Odde, D. J., Cassimeris, L., & Buettner, H. M. (1995). Kinetics of microtubule catastrophe assessed by probabilistic analysis. *Biophysical Journal*, 69(3), 796–802.
[https://doi.org/10.1016/S0006-3495\(95\)79953-2](https://doi.org/10.1016/S0006-3495(95)79953-2)
- Odermatt, P. D., Miettinen, T. P., Lemièrre, J., Kang, J. H., Bostan, E., Manalis, S. R., Huang, K. C., & Chang, F. (2021). Variations of intracellular density during the cell cycle arise from tip-growth regulation in fission yeast. *eLife*, 10, e64901.
<https://doi.org/10.7554/eLife.64901>
- Olsson, C., & Swenson, J. (2020). Structural Comparison between Sucrose and Trehalose in Aqueous Solution. *The Journal of Physical Chemistry B*, 124(15), 3074–3082.
<https://doi.org/10.1021/acs.jpcc.9b09701>
- Oosawa, F., & Asakura, S. (1975). *Thermodynamics of the Polymerization of Protein*. Academic Press Inc.
- Oosawa, F., & Kasai, M. (1962). A theory of linear and helical aggregations of macromolecules. *Journal of Molecular Biology*, 4(1), 10–21. [https://doi.org/10.1016/S0022-2836\(62\)80112-0](https://doi.org/10.1016/S0022-2836(62)80112-0)
- Passani, L. A., Bedford, M. T., Faber, P. W., McGinnis, K. M., Sharp, A. H., Gusella, J. F., Vonsattel, J. P., & MacDonald, M. E. (2000). Huntingtin's WW domain partners in Huntington's disease post-mortem brain fulfill genetic criteria for direct involvement in Huntington's disease pathogenesis. *Human Molecular Genetics*, 9(14), 2175–2182.
<https://doi.org/10.1093/hmg/9.14.2175>
- Pecqueur, L., Duellberg, C., Dreier, B., Jiang, Q., Wang, C., Plückthun, A., Surrey, T., Gigant, B., & Knossow, M. (2012). A designed ankyrin repeat protein selected to bind to tubulin caps the microtubule plus end. *Proceedings of the National Academy of Sciences of the United States of America*, 109(30), 12011–12016.
<https://doi.org/10.1073/pnas.1204129109>

- Persson, L. B., Ambati, V. S., & Brandman, O. (2020). Cellular Control of Viscosity Counters Changes in Temperature and Energy Availability. *Cell*.
<https://doi.org/10.1016/j.cell.2020.10.017>
- Petry, S., Groen, A. C., Ishihara, K., Mitchison, T. J., & Vale, R. D. (2013). Branching microtubule nucleation in xenopus egg extracts mediated by augmin and TPX2. *Cell*, *152*(4), 768–777. <https://doi.org/10.1016/j.cell.2012.12.044>
- Pierson, G. B., Burton, P. R., & Himes, R. H. (1978). Alterations in number of protofilaments in microtubules assembled in vitro. *Journal of Cell Biology*, *76*(1), 223–228.
<https://doi.org/10.1083/jcb.76.1.223>
- Pollard, T. D., & Cooper, J. A. (1986). Actin and actin-binding proteins. A critical evaluation of mechanisms and functions. *Annual Review of Biochemistry*, *55*, 987–1035.
<https://doi.org/10.1146/annurev.bi.55.070186.005011>
- Popov, A. V., Severin, F., & Karsenti, E. (2002). XMAP215 is required for the microtubule-nucleating activity of centrosomes. *Current Biology : CB*, *12*(15), 1326–1330.
[https://doi.org/10.1016/s0960-9822\(02\)01033-3](https://doi.org/10.1016/s0960-9822(02)01033-3)
- Rai, A., Liu, T., Glauser, S., Katrukha, E. A., Estévez-Gallego, J., Rodríguez-García, R., Fang, W. S., Díaz, J. F., Steinmetz, M. O., Altmann, K. H., Kapitein, L. C., Moores, C. A., & Akhmanova, A. (2019). Taxanes convert regions of perturbed microtubule growth into rescue sites. *Nature Materials*, *19*(3), 355–365. <https://doi.org/10.1038/s41563-019-0546-6>
- Rai, A., Liu, T., Katrukha, E. A., Estévez-Gallego, J., Manka, S. W., Paterson, I., Díaz, J. F., Kapitein, L. C., Moores, C. A., & Akhmanova, A. (2021). Lattice defects induced by microtubule-stabilizing agents exert a long-range effect on microtubule growth by promoting catastrophes. *Proceedings of the National Academy of Sciences of the United States of America*, *118*(51), e2112261118. <https://doi.org/10.1073/pnas.2112261118>
- Ravelli, R. B. G., Gigant, B., Curmi, P. A., Jourdain, I., Lachkar, S., Sobel, A., & Knossow, M. (2004). Insight into tubulin regulation from a complex with colchicine and a stathmin-like domain. *Nature*, *428*(6979), Article 6979. <https://doi.org/10.1038/nature02393>
- Rice, L. M., Montabana, E. A., & Agard, D. A. (2008). The lattice as allosteric effector: Structural studies of alpha-beta- and gamma-tubulin clarify the role of GTP in microtubule

- assembly. *Proceedings of the National Academy of Sciences of the United States of America*, 105(14), 5378–5383. <https://doi.org/10.1073/pnas.0801155105>
- Rice, L. M., Moritz, M., & Agard, D. A. (2021). Microtubules form by progressively faster tubulin accretion, not by nucleation–elongation. *Journal of Cell Biology*, 220(5), e202012079. <https://doi.org/10.1083/jcb.202012079>
- Roostalu, J., & Surrey, T. (2017). Microtubule nucleation: Beyond the template. *Nature Reviews Molecular Cell Biology*, 18(11), 702–710. <https://doi.org/10.1038/nrm.2017.75>
- Roostalu, J., Thomas, C., Cade, N. I., Kunzelmann, S., Taylor, I. A., & Surrey, T. (2020). The speed of GTP hydrolysis determines GTP cap size and controls microtubule stability. *eLife*, 9. <https://doi.org/10.7554/eLife.51992>
- Roth, D., Fitton, B. P., Chmel, N. P., Wasiluk, N., & Straube, A. (2018). Spatial positioning of EB family proteins at microtubule tips involves distinct nucleotide-dependent binding properties. *Journal of Cell Science*, jcs.219550. <https://doi.org/10.1242/jcs.219550>
- Salmon, E. D., Saxton, W. M., Leslie, R. J., Karow, M. L., & McIntosh, J. R. (1984). Diffusion coefficient of fluorescein-labeled tubulin in the cytoplasm of embryonic cells of a sea urchin: Video image analysis of fluorescence redistribution after photobleaching. *Journal of Cell Biology*, 99(6), 2157–2164. <https://doi.org/10.1083/jcb.99.6.2157>
- Schaedel, L., Triclin, S., Chrétien, D., Abrieu, A., Aumeier, C., Gaillard, J., Blanchoin, L., Théry, M., & John, K. (2019). Lattice defects induce microtubule self-renewal. *Nature Physics*, 15(8), 830–838. <https://doi.org/10.1038/s41567-019-0542-4>
- Schindelin, J., Arganda-Carreras, I., Frise, E., Kaynig, V., Longair, M., Pietzsch, T., Preibisch, S., Rueden, C., Saalfeld, S., Schmid, B., Tinevez, J.-Y., White, D. J., Hartenstein, V., Eliceiri, K., Tomancak, P., & Cardona, A. (2012). Fiji: An open-source platform for biological-image analysis. *Nature Methods*, 9(7), 676–682. <https://doi.org/10.1038/nmeth.2019>
- Schultz, S. G., & Solomon, A. K. (1961). Determination of the effective hydrodynamic radii of small molecules by viscometry. *The Journal of General Physiology*, 44, 1189–1199. <https://doi.org/10.1085/jgp.44.6.1189>
- Sekhar, A., Latham, M. P., Vallurupalli, P., & Kay, L. E. (2014). Viscosity-Dependent Kinetics of Protein Conformational Exchange: Microviscosity Effects and the Need for a Small

- Viscogen. *The Journal of Physical Chemistry B*, 118(17), 4546–4551.
<https://doi.org/10.1021/jp501583t>
- Sekhar, A., Vallurupalli, P., & Kay, L. E. (2012). Folding of the four-helix bundle FF domain from a compact on-pathway intermediate state is governed predominantly by water motion. *Proceedings of the National Academy of Sciences*, 109(47), 19268–19273.
<https://doi.org/10.1073/pnas.1212036109>
- Sekhar, A., Vallurupalli, P., & Kaya, L. E. (2013). Defining a length scale for millisecond-timescale protein conformational exchange. *Proceedings of the National Academy of Sciences of the United States of America*, 110(28), 11391–11396.
<https://doi.org/10.1073/pnas.1303273110>
- Shahid, S., Hassan, M. I., Islam, A., & Ahmad, F. (2017). Size-dependent studies of macromolecular crowding on the thermodynamic stability, structure and functional activity of proteins: In vitro and in silico approaches. *Biochimica Et Biophysica Acta. General Subjects*, 1861(2), 178–197. <https://doi.org/10.1016/j.bbagen.2016.11.014>
- Shearwin, K. E., Timasheff, S. N., & Perez-Ramirez, B. (1994). Linkages between the dissociation of .alpha..beta. tubulin into subunits and ligand binding: The ground state of tubulin is the GDP conformation. *Biochemistry*, 33(4), 885–893.
<https://doi.org/10.1021/bi00170a006>
- Slep, K. C., & Vale, R. D. (2007). Structural basis of microtubule plus end tracking by XMAP215, CLIP-170, and EB1. *Molecular Cell*, 27(6), 976–991.
<https://doi.org/10.1016/j.molcel.2007.07.023>
- Song, X., Yang, F., Yang, T., Wang, Y., Ding, M., Li, L., Xu, P., Liu, S., Dai, M., Chi, C., Xiang, S., Xu, C., Li, D., Wang, Z., Li, L., Hill, D. L., Fu, C., Yuan, K., Li, P., ... Yao, X. (2023). Phase separation of EB1 guides microtubule plus-end dynamics. *Nature Cell Biology*, 25(1), Article 1. <https://doi.org/10.1038/s41556-022-01033-4>
- Strothman, C., Farmer, V., Arpağ, G., Rodgers, N., Podolski, M., Norris, S., Ohi, R., & Zanic, M. (2019). Microtubule minus-end stability is dictated by the tubulin off-rate. *The Journal of Cell Biology*, 218(9), 2841–2853. <https://doi.org/10.1083/jcb.201905019>
- Taguchi, S., Nakano, J., Imasaki, T., Kita, T., Saijo-Hamano, Y., Sakai, N., Shigematsu, H., Okuma, H., Shimizu, T., Nitta, E., Kikkawa, S., Mizobuchi, S., Niwa, S., & Nitta, R. (2022). Structural model of microtubule dynamics inhibition by kinesin-4 from the

- crystal structure of KLP-12 –tubulin complex. *eLife*, *11*, e77877.
<https://doi.org/10.7554/eLife.77877>
- Tan, R., Lam, A. J., Tan, T., Han, J., Nowakowski, D. W., Vershinin, M., Simó, S., Ori-McKenney, K. M., & McKenney, R. J. (2019). Microtubules gate tau condensation to spatially regulate microtubule functions. *Nature Cell Biology*, *21*(9), Article 9.
<https://doi.org/10.1038/s41556-019-0375-5>
- Thawani, A., Kadzik, R. S., & Petry, S. (2018). XMAP215 is a microtubule nucleation factor that functions synergistically with the γ -tubulin ring complex. *Nature Cell Biology*, *20*(5), 575–585. <https://doi.org/10.1038/s41556-018-0091-6>
- Ti, S.-C., Pamula, M. C., Howes, S. C., Duellberg, C., Cade, N. I., Kleiner, R. E., Forth, S., Surrey, T., Nogales, E., & Kapoor, T. M. (2016). Mutations in Human Tubulin Proximal to the Kinesin-Binding Site Alter Dynamic Instability at Microtubule Plus- and Minus-Ends. *Developmental Cell*, *37*(1), 72–84. <https://doi.org/10.1016/j.devcel.2016.03.003>
- Tilney, L. G., Bryan, J., Bush, D. J., Fujiwara, K., Mooseker, M. S., Murphy, D. B., & Snyder, D. H. (1973). Microtubules: Evidence for 13 protofilaments. *Journal of Cell Biology*, *59*(2), 267–275. <https://doi.org/10.1083/jcb.59.2.267>
- Triclin, S., Inoue, D., Gaillard, J., Htet, Z. M., DeSantis, M. E., Portran, D., Derivery, E., Aumeier, C., Schaedel, L., John, K., Letierrier, C., Reck-Peterson, S. L., Blanchoin, L., & Théry, M. (2021). Self-repair protects microtubules from destruction by molecular motors. *Nature Materials*, 1–9. <https://doi.org/10.1038/s41563-020-00905-0>
- Tropini, C., Roth, E. A., Zanic, M., Gardner, M. K., & Howard, J. (2012). Islands containing slowly hydrolyzable GTP analogs promote microtubule rescues. *PLoS ONE*, *7*(1).
<https://doi.org/10.1371/journal.pone.0030103>
- van der Vaart, B., van Riel, W. E., Doodhi, H., Kevenaer, J. T., Katrukha, E. A., Gumy, L., Bouchet, B. P., Grigoriev, I., Spangler, S. A., Yu, K. L., Wulf, P. S., Wu, J., Lansbergen, G., van Battum, E. Y., Pasterkamp, R. J., Mimori-Kiyosue, Y., Demmers, J., Olieric, N., Maly, I. V., ... Akhmanova, A. (2013). CFEOM1-Associated Kinesin KIF21A Is a Cortical Microtubule Growth Inhibitor. *Developmental Cell*, *27*(2), 145–160.
<https://doi.org/10.1016/j.devcel.2013.09.010>

- Vasquez, R. J., Gard, D. L., & Cassimeris, L. (1994). XMAP from *Xenopus* eggs promotes rapid plus end assembly of microtubules and rapid microtubule polymer turnover. *The Journal of Cell Biology*, *127*(4), 985–993. <https://doi.org/10.1083/jcb.127.4.985>
- Vemu, A., Atherton, J., Spector, J. O., Moores, C. A., & Roll-Mecak, A. (2017). Tubulin isoform composition tunes microtubule dynamics. *Molecular Biology of the Cell*, *28*(25), 3564–3572. <https://doi.org/10.1091/mbc.E17-02-0124>
- Verma, V., & Maresca, T. J. (2019). Direct observation of branching MT nucleation in living animal cells. *The Journal of Cell Biology*, *218*(9), 2829–2840. <https://doi.org/10.1083/jcb.201904114>
- Vitre, B., Coquelle, F. M., Heichette, C., Garnier, C., Chrétien, D., & Arnal, I. (2008). EB1 regulates microtubule dynamics and tubulin sheet closure in vitro. *Nature Cell Biology*, *10*(4), Article 4. <https://doi.org/10.1038/ncb1703>
- von Loeffelholz, O., Venables, N. A., Drummond, D. R., Katsuki, M., Cross, R., & Moores, C. A. (2017). Nucleotide- and Mal3-dependent changes in fission yeast microtubules suggest a structural plasticity view of dynamics. *Nature Communications*, *8*(1), Article 1. <https://doi.org/10.1038/s41467-017-02241-5>
- Voter, W. A., & Erickson, H. P. (1984). The kinetics of microtubule assembly. Evidence for a two-stage nucleation mechanism. *The Journal of Biological Chemistry*, *259*(16), 10430–10438.
- Voter, W. A., O'Brien, E. T., & Erickson, H. P. (1991). Dilution-induced disassembly of microtubules: Relation to dynamic instability and the GTP cap. *Cell Motility*, *18*(1), 55–62. <https://doi.org/10.1002/cm.970180106>
- Wagstaff, J. M., Planelles-Herrero, V. J., Sharov, G., Alnami, A., Kozielski, F., Derivery, E., & Löwe, J. (2022). *Cytomotive actins and tubulins share a polymerisation switch mechanism conferring robust dynamics* [Preprint]. *Molecular Biology*. <https://doi.org/10.1101/2022.09.08.507146>
- Walker, R. A., O'Brien, E. T., Pryer, N. K., Soboeiro, M. F., Voter, W. A., Erickson, H. P., & Salmon, E. D. (1988). Dynamic instability of individual microtubules analyzed by video light microscopy: Rate constants and transition frequencies. *Journal of Cell Biology*, *107*(4), 1437–1448. <https://doi.org/10.1083/jcb.107.4.1437>

- Walker, R. A., Pryer, N. K., & Salmon, E. D. (1991). Dilution of individual microtubules observed in real time in vitro: Evidence that cap size is small and independent of elongation rate. *Journal of Cell Biology*, *114*(1), 73–81.
<https://doi.org/10.1083/jcb.114.1.73>
- Ward, E. S., Güssow, D., Griffiths, A. D., Jones, P. T., & Winter, G. (1989). Binding activities of a repertoire of single immunoglobulin variable domains secreted from *Escherichia coli*. *Nature*, *341*(6242), Article 6242. <https://doi.org/10.1038/341544a0>
- Weisenberg, R. C., Broisy, G. G., & Taylor, E. William. (1968). Colchicine-binding protein of mammalian brain and its relation to microtubules. *Biochemistry*, *7*(12), 4466–4479.
<https://doi.org/10.1021/bi00852a043>
- Weisenberg, R. C., & Deery, W. J. (1976). Role of nucleotide hydrolysis in microtubule assembly. *Nature*, *263*(5580), 792–793. <https://doi.org/10.1038/263792a0>
- Wieczorek, M., Bechstedt, S., Chaaban, S., & Brouhard, G. J. (2015). Microtubule-associated proteins control the kinetics of microtubule nucleation. *Nature Cell Biology*, *17*(7), 907–916. <https://doi.org/10.1038/ncb3188>
- Wieczorek, M., Chaaban, S., & Brouhard, G. J. (2013). Macromolecular crowding pushes catalyzed microtubule growth to near the theoretical limit. *Cellular and Molecular Bioengineering*, *6*(4), 383–392. <https://doi.org/10.1007/s12195-013-0292-9>
- Yedgar, S., Tetreau, C., Gavish, B., & Lavalette, D. (1995). Viscosity dependence of O₂ escape from respiratory proteins as a function of cosolvent molecular weight. *Biophysical Journal*, *68*(2), 665–670.
- Zanic, M., Stear, J. H., Hyman, A. A., & Howard, J. (2009). EB1 Recognizes the Nucleotide State of Tubulin in the Microtubule Lattice. *PLoS ONE*, *4*(10), e7585.
<https://doi.org/10.1371/journal.pone.0007585>
- Zanic, M., Widlund, P. O., Hyman, A. A., & Howard, J. (2013). Synergy between XMAP215 and EB1 increases microtubule growth rates to physiological levels. *Nature Cell Biology*, *15*(6), Article 6. <https://doi.org/10.1038/ncb2744>
- Zhang, R., Alushin, G. M., Brown, A., & Nogales, E. (2015). Mechanistic Origin of Microtubule Dynamic Instability and Its Modulation by EB Proteins. *Cell*, *162*(4), 849–859.
<https://doi.org/10.1016/j.cell.2015.07.012>

- Zhang, R., LaFrance, B., & Nogales, E. (2018). Separating the effects of nucleotide and EB binding on microtubule structure. *Proceedings of the National Academy of Sciences*, *115*(27), E6191–E6200. <https://doi.org/10.1073/pnas.1802637115>
- Zhang, X., Poniewierski, A., Hou, S., Sozański, K., Wisniewska, A., Wiczorek, S. A., Kalwarczyk, T., Sun, L., & Hołyst, R. (2015). Tracking structural transitions of bovine serum albumin in surfactant solutions by fluorescence correlation spectroscopy and fluorescence lifetime analysis. *Soft Matter*, *11*(12), 2512–2518. <https://doi.org/10.1039/C5SM00101C>
- Zheng, Y., Wong, M. L., Alberts, B., & Mitchison, T. (1995). Nucleation of microtubule assembly by a γ -tubulin-containing ring complex. *Nature*, *378*(6557), 578–583. <https://doi.org/10.1038/378578a0>